Self-Sealing Barriers of Sand/Bentonite-Mixtures in a Clay Repository

SB-Experiment in the Mont Terri Rock Laboratory

Final Report

GRS - 302

Gesellschaft für Anlagen-
und Reaktorsicherheit
(GRS) mbH

Self-Sealing Barriers of Sand/Bentonite-Mixtures in a Clay Repository

SB-Experiment in the Mont Terri Rock Laboratory

Final Report

Tilmann Rothfuchs
Oliver Czaikowski
Lothar Hartwig
Karsten Hellwald
Michael Komischke
Rüdiger Miehe
Chun-Liang Zhang

October 2012

Acknowledgement:

This report was prepared under contract No. 02E9894 with the Bundesministerium für Wirtschaft und Technologie (BMWi) as part of the Mont Terri Project TR 2009-03.

The work was conducted by the Gesellschaft für Anlagen- und Reaktorsicherheit (GRS) mbH.

The authors are responsible for the content of this report.

GRS - 302
ISBN 978-3-939355-81-6

Keywords:
Gas Entry Pressure, Mont Terri Rock Laboratory, Permeability, Sand/Bentonite Mixture, Self-sealing Barriers, Swelling Pressure

Zusammenfassung

Viele Konzepte zur Endlagerung hochradioaktiver Abfälle in geologischen Formationen sehen im Hinblick auf den sicheren Einschluss der Abfälle die Verwendung von hoch kompaktiertem Bentonit als Puffermaterial (Buffer) zwischen Abfallbehälter und Wirtsgestein vor. Im Jahre 2000 begann die GRS ergänzend hierzu moderat kompaktierte Sand/Bentonit-Mischungen als alternatives Verschlussmaterial zu untersuchen, da derartige Materialmischungen möglicherweise eine geeignete Alternative insbesondere für den Verschluss gasführender Endlagerbereiche darstellen können.

Im Vergleich zu hoch kompaktiertem Dichtmaterial weisen Sand/Bentonit-Mischungen im ungesättigten Zustand eine hohe Gaspermeabilität und einen vergleichsweise niedrigen Gaseintrittsdruck im gesättigten Zustand auf, wobei gleichzeitig ein ausreichendes Selbstabdichtungspotenzial aufgrund der Quellung des Tons bedingt durch die Wasseraufnahme aus dem Wirtsgestein gegeben ist. Durch die Auswahl optimierter Materialmischungen kann eine unerwünschte Ausbildung hoher Gasdrücke im Nahfeld des Einlagerungsbereichs infolge Korrosionsgasbildung vermieden werden. Die mögliche Migration von Radionukliden aus der Abfallmatrix in der flüssigen Phase durch den aufgesättigten Buffer wird, wie auch im Wirtsgestein, diffusionsgesteuert und damit vergleichsweise langsam erfolgen.

Zur Bestimmung geeigneter Materialmischungen wurden zunächst Untersuchungen im geowissenschaftlichen Labor der GRS in Braunschweig durchgeführt. Seit 2004 wurden weitere Untersuchungen zur Verifizierung des Materialverhaltens unter In-situ-Bedingungen im Mont Terri Untertagelabor (MTRL) in der Schweiz im Rahmen des SB-Experiments (**S**elfsealing **B**arriers of Clay/Sand Mixtures) vorgenommen.

In Endlagern in Tonformationen kann das körnige Dichtmaterial als Buffer und/oder als abdichtender Versatz in Einlagerungsbohrlöchern wie auch in Strecken eingesetzt werden, wobei das Material mit geringer Verdichtung eingebaut wird.

Ziel des SB-Experiments

Das Ziel des SB-Experiments bestand darin zu belegen, dass die Dichteigenschaften von Sand/Bentonit-Gemischen, die zuvor im GRS-Labor untersucht wurden, auch unter endlagerrelevanten In-situ-Bedingungen technisch realisiert und nachgewiesen werden

können. Die wichtigsten Materialeigenschaften, die zur Sicherstellung der geforderten Dichteigenschaften erfüllt sein müssen, sind im Folgenden aufgeführt:

Das Dichtmaterial sollte eine **hohe Gaspermeabilität** ($> 10^{-18}$ m^2) aufweisen, um die Entwicklung hoher Gasdrücke aufgrund von Korroisonsgasbildung im Endlagernahfeld durch Migration der Gase durch das Dichtmaterial zu verhindern.

Die **Wasserpermeabilität** des Dichtmaterials sollte niedrig sein ($< 10^{-18}$ m^2). Durch Wasseraufnahme aus dem Gebirge verringert sich die Wasserpermeabilität aufgrund von Quellung, wobei von einer weiteren Reduzierung bedingt durch das Kriechen des Gebirges mit einer Verheilung der Auflockerungszone ausgegangen werden kann.

Damit das Dichtmaterial als eine Art Ventil wirkt, muss der **Gaseintrittsdruck** niedriger als der des Wirtsgesteins sein, um eine bevorzugte Gasmigration über die Dichtung zu provozieren.

Zur Gewährleistung der Abdichtung gegenüber zufließendem Formationswasser ist ein ausreichender **Quelldruck** bei Zutritt von Wasser notwendig. Da der Gasfluss bevorzugt über die Dichtung und nicht in das Wirtsgestein hinein erfolgen soll, darf der Gaseintrittsdruck der Dichtung den des Gebirges nicht überschreiten. Eine Voraussetzung dafür ist, dass der Quelldruck der Dichtung den Gaseintrittsdruck des Gebirges nicht übersteigt.

Untersuchungsprogramm des SB-Experiments

Die Durchführung des SB-Vorhabens umfasste drei Phasen:

1. Laboruntersuchungen zur Festlegung geeigneter Materialmischungen und Installationstechniken zur Erzielung der erforderlichen Einbaudichte

2. Großmaßstäbliche Laboruntersuchungen (Technikumsversuche) zur Entwicklung der Einbautechnik und zur Ermittlung der Aufsättigungsdauer unter Laborbedingungen.

3. In-situ-Untersuchungen in Bohrlöchern im Untertagelabor Mont Terri unter repräsentativen Endlagerbedingungen.

Laboruntersuchungen

Die Dichteigenschaften von Sand/Bentonit-Mischungen wurden zunächst in den Vorhaben „Zweiphasenfluss-Projekt“ /JOC 00/ und KENTON /MIE 03/ untersucht, wobei der Schwerpunkt auf den Ein- und Zweiphasenfluss-Eigenschaften lag.

Aufbauend auf den beiden Vorgängerprojekten wurde im SB-Vorhaben ein Laborprogramm zur Optimierung der Dichtmaterialien durchgeführt, welches zeigte, dass die Mischungen mit 35 % Tonanteil und 50 % Tonanteil die Anforderungen am besten erfüllen. Aus diesem Grund wurden für die In-situ-Untersuchungen im MTRL Mischungen mit den Mischungsverhältnissen 65 %-Sand/35 %-Bentonit und 50 %-Sand/50 %-Bentonit ausgewählt.

Großmaßstäblicher Laborversuch (Technikumsversuch)

Vor Beginn der In-situ-Experimente wurden aufbauend auf den Labormessungen zunächst Untersuchungen im Maßstab 1:1 (s. Abb. 4.1) im GRS-Labor in Braunschweig in Stahlrohren vorgenommen. Die Versuche entsprachen im Wesentlichen den Abmessungen der In-situ-Versuche im MTRL (s. Abb. 5.2).

Das wesentlichen Ergebnisse lassen sich wie folgt zusammenfassen:

- Die Materialverdichtung mit einem Elektrovibrator ergab optimale Einbaudichten. Für die als am besten geeignet befunden Materialmischung 65 %-Sand/35 %-Bentonit wurde eine maximale Einbaudichte von 2,07 g/cm^3 erzielt.

- Die in Prognoserechnungen ermittelte Aufsättigungsdauer der 1 m langen und 0,3 m durchmessenden Dichtung im Technikumsversuch wurde um mehr als das 5-fache überschritten. Ein Grund könnte in der zu gering angesetzten Materialporosität liegen, da die Menge des aufgenommenen Wassers diejenige, die sich aus der Anfangsporosität berechnet, um mehr als 80 % überstieg.

- Insbesondere die Dichteigenschaften der Materialmischung 65 %-Sand/35 %-Bentonit wurden mit nachfolgenden Werten (s. auch Tab. 4.2) exzellent bestätigt:

  - Gaspermeabilität im frühen Einbauzustand: $6{,}4 \cdot 10^{-14}$ m^2
  - Wasserpermeabilität im Sättigungszustand: $1{,}5 \cdot 10^{-18}$ m^2

- Quelldruck im Sättigungszustand: 0,4 MPa
- Gaseintrittsdruck im Sättigungszustand: ~0,25 MPa
- Gaspermeabilität nach Gasdurchbruch: $3{,}7 \cdot 10^{-17}$ m^2

In-situ-Untersuchungen

Für die In-situ-Untersuchungen im MTRL wurden in einer Versuchsnische (Abb. 5.2) vier Bohrungen mit einem Durchmesser von 0,31 m und einer Tiefe von 3 m erstellt. Zwei Bohrlöcher wurden mit einer 65 %-Sand/35 %-Bentonit-Mischung, ein Bohrloch mit einer 50 %-Sand/50 %-Bentonit-Mischung und eine Bohrung mit gebrochenen Pellets der NAGRA aus reinem Bentonit zum unmittelbaren Vergleich mit den Sand/Bentonit-Mischungen befüllt. und bis zur erforderlichen Einbaudichte von rd. 1,9 bzw. 1,7 g/cm^3 verdichtet (s. Tabelle 5.1). Die Druckaufgabe mit synthetischem Formationswasser bzw. Gas erfolgte über eine Schrägbohrung, die wie im Mock-up-Test zu einer mit einem porösen Medium gefüllten Druckkammer, hier im untersten Teil des Bohrlochs, führte. Oberhalb des Dichtelements wurde die Bohrung mit einem Packer abgedichtet und der verbleibende obere Teil der Bohrung mit Beton verfüllt. An der Packerunterseite, am oberen Ende der Dichtung, waren zwei Quelldruckaufnehmer installiert. Zwischen der Druckkammer und der Dichtung war eine Filterfritte eingebaut, um eine homogene Verteilung des jeweiligen Fließmediums über den ganzen Querschnitt der Dichtung sicherzustellen. Eine weitere Filterfritte befand sich zwischen der Dichtung und dem Packer, um das durch die Dichtung transportierte Fluid ebenfalls über den gesamten Querschnitt der Dichtung aufzufangen. Im Gegensatz hierzu waren im Dichtungsbereich entlang der Bohrlochwand keine weiteren Druckaufnehmer installiert, um das System nicht durch Fließwege entlang von Messkabeln zu beeinflussen. Es wurde davon ausgegangen, dass der Druckverlauf im In-situ-Versuch grundsätzlich dem des Technikumsversuchs entspricht.

Die Länge der Dichtungen mit 65 %-Sand/35 %-Bentonit betrug 1 m. Da davon ausgegangen wurde, dass die Aufsättigungsdauer bei höheren Tonanteilen deutlich länger andauern würde, wurde die Länge der Dichtungen 50 %-Sand/50 %-Bentonit sowie die aus gebrochenen Bentonitpellets auf 0,5 m ausgelegt.

Die Aufsättigung der Dichtungen im In-situ-Versuch wurde beim Versuch SB2 am 8. Februar 2006, sowie bei den nachfolgenden Versuchen SB1, SB13 und SB15 am

1. November 2006 gestartet. Die wesentlichen Ergebnisse der In-situ-Versuche lassen sich wie folgt zusammenfassen:

- Bei den Versuchen SB1 und SB15 im südlichen Teil der Versuchsnische zeigte sich bereits im frühen Versuchsstadium ein gewisser Wasseraustritt an der oberen Ausgangsseite, der möglicherweise auf vergleichsweise hoch wirksame Auflockerungen entlang der Bohrlochwand zurückgeführt werden muss. Beide Versuche wurden daraufhin an der Ausgangsseite verschlossen, woraufhin sich mehr oder weniger konstante Druckverhältnisse im Dichtsystem bis zum Versuchsende Ende 2011 anhaltend ausbildeten. Die Versuche konnten demgemäß nur auf der Grundlage von Nachuntersuchungen an Probematerial, das nach Versuchsende gewonnen wurde, ausgewertet werden. Quell- und Gaseintrittsdruck konnten bei diesen Versuchen nicht ermittelt werden. Die jeweils bei Versuchsende bestimmten Wassergehalte betrugen bei SB1 24,5 %, was bei Berücksichtigung der hier erzielten Einbaudichte in etwa der Vollsättigung entspricht und bei SB15 rd. 30 %, was zwar die geringe Einbaudichte von 1,69 g/cm^3 und die zugehörige Porosität von 41 % widerspiegelt, nicht aber dem sich aus diesem Porositätswert errechnenden Wassergehalt von 26 % entspricht. Wegen der ungünstigen vor-Ort-Bedingungen konnten die günstigen Dichteigenschaften der Sand/Bentonit-Dichtungen in diesen beiden Versuchen nicht nachgewiesen werden.

- Beim Versuch SB13 mit reinem Bentonit wurde während der gesamten Versuchsdauer von rd. 5 Jahren kein Wasserdurchbruch erreicht. Das Material weist der beeindruckenden Quelldruckentwicklung zufolge ein hohes Dichtvermögen bzw. eine sehr geringe Gasdurchlässigkeit auf. Die bei Versuchsende durchgeführte Messung zur Bestimmung des Gaseintrittsdrucks scheiterte daran, dass die Gebirgsdurchlässigkeit im zur Verfügung stehenden Versuchszeitraum bis Ende März 2012 immer noch deutlich höher war, als der im Dichtmaterial herrschende Quelldruck (Abb. 5.6). Die Auswertung des bei Versuchsende gewonnen Probematerials aus der Dichtung wies einen Wassergehalt von rd. 30 % auf, was in etwa der Vollsättigung entspricht und belegt, dass der Versuch bei Versuchsende kurz vor der Vollsättigung gestanden haben dürfte. Mit dem Versuch wurde vergleichend belegt, dass die günstigen Dichteigenschaften von Sand/Bentonit-Dichtungen gegenüber Gasen mit reinem Bentonit nicht erreicht werden.

- Beim Versuch SB2 wurde wie beim Technikumsversuch die Sättigung nicht nach der ursprünglich erwarteten Aufsättigungsdauer von rd. 170 Tagen erzielt. Nachdem

eine Aufsättigungsdauer von etwa 5 Jahren, wie sie beim Technikumsversuch beoabachtet worden war, abgewartet worden war und immer noch kein Wasserdurchbruch bzw. eine Aufsättigung zu beobachten war, wurde eine modelltheoretische Analyse der im Versuch und im umliegenden Gebirge herrschenden Versuchsbedingungen vorgenommen mit dem Ergebnis, dass die Aufsättigung zwar vermutlich bereits nach ca. 4 Jahren erreicht wurde, aber ein Wasseraustritt an der Ausgangsseite der Dichtung wegen eines zu geringen Injektionsdrucks nicht stattfinden konnte. Die Analyseergebnisse zeigten zudem, dass eine Anhebung des Injektionsdrucks auf einen Wert von rd. 11 MPa, wie im Technikumsversuch angewendet, zu dem gewünschten Wasseraustritt führen und die ausstehenden Bestimmungen der Wasserpermeabilität und des Gaseintrittsdrucks der aufgesättigten Dichtung möglich machen müsste.

Diese Vorgehensweise umsetzend, konnten die zu bestimmenden Materialdaten nachfolgend wie folgt bestimmt werden:

- Gaspermeabilität im frühen Einbauzustand: $3{,}29 \cdot 10^{-14}$ m^2
- Wasserpermeabilität im Sättigungszustand: $4{,}2 \cdot 10^{-18}$ m^2
- Quelldruck im Sättigungszustand: 0,15 – 0,19 MPa
- Gaseintrittsdruck im Sättigungszustand: ~0,45 MPa
- Gaspermeabilität nach Gasdurchbruch: $9{,}3 \cdot 10^{-17}$ – $4{,}1 \cdot 10^{-16}$ m^2

Mit den vorgenannten Daten werden sowohl die erwarteten optimierten Materialdichteigenschaften von Sand/Bentonit-Dichtungen als auch ihre Übertragbarkeit von kleineren Laborproben auf Technikums- und reale In-situ-Verhältnisse gut bestätigt und die Projektziele erreicht. Eine vergleichende Zusammenfassung der Labor- und In-situ-Ergebnisse ist der Tab. 6.1 auf Seite 128 zu entnehmen.

Foreword

Several years ago, GRS performed laboratory investigations on the suitability of clay/mineral mixtures as optimized sealing materials in underground repositories for radioactive wastes /JOC 00/ /MIE 03/.

The investigations yielded promising results so that plans were developed for testing the sealing properties of those materials under representative in-situ conditions in the Mont Terri Rock Laboratory (MTRL). The project was proposed to the "Projektträger Wassertechnologie und Entsorgung (PtWT+E)", and finally launched in January 2003 under the name SB-project ("**S**elf-sealing **B**arriers of Clay/Mineral Mixtures in a Clay Repository").

The project was divided in two parts, a pre-project running from January 2003 until June 2004 under contract No. 02E9713 /ROT 04/ and the main project running from January 2004 until June2012 under contract No. 02E9894 with originally PtWT+E, later renamed as PTKA-WTE.

In the course of the pre-project it was decided to incorporate the SB main project as a cost shared action of PtWT+E and the European Commission (contract No. FI6W-CT-2004-508851) into the EC Integrated Project ESDRED (Engineering Studies and Demonstrations of Repository Designs) performed by 11 European project partners within the 6th European framework programme. The ESDRED project was terminated prior to the termination of the SB project. Interim results were reported by mid 2009 in two ESDRED reports /DEB09/ /SEI 09/.

This report presents the results achieved in the whole SB-project comprising preceding laboratory investigations for the final selection of suited material mixtures, the conduction of mock-up tests in the geotechnical laboratory of GRS in Braunschweig and the execution of in-situ experiments at the MTRL.

Table of Contents

1 Introduction

1.1 Background

For about two decades geological clay formations have been investigated with regard to their suitability to host a repository for high-level radioactive waste. Underground research laboratories (URL) in clay formations are currently operated in the plastic Boom clay formation near Mol in Belgium, the consolidated Callovo-Oxfordian clay formation at Bure in France, and in the consolidated Opalinus clay formation at Mont Terri in Switzerland.

Gas generated by anaerobic corrosion of waste containers or by radiolysis of water in the host formation may lead to the development of gas pressures in the repository which in turn can lead to fracturing of the host rock if the gas pressure exceeds the least principal stress (σ_3) in the rock. The integrity of the host formation would be disturbed and the release of radioactive material from the disposal rooms would be possible.

However, the gas pressure build-up in a repository is controlled by the gas production rate as well as the storativity and the gas transport properties of both, the host rock and the engineered barriers. Important transport mechanisms are advection/diffusion, two-phase flow, dilatancy controlled gas flow and fracture flow. These processes are controlled by the gas and porewater pressure. At low gas generation rates, all gas can be transported by advection/diffusion and two phase flow through the host rock. Fracturing will only occur in case of high gas production rates.

Although there are good reasons to assume that gas pressure in a repository is limited due to the intrinsic properties of the host rock, engineering measures can be used to make the system even more robust. Two technical possibilities can be considered:

1. Provide an adequate gas storage volume in the backfill of the disposal rooms whereby the gas can be kept at a comparably low pressure. According to Rübel et al. /RÜB 04/, clay formations like the Opalinus clay provide enough water to completely corrode the vitrified HLW canisters in a disposal borehole. Up to 481 m^3 of hydrogen gas would be produced per canister by its complete corrosion. Depending on the depth of the repository, 7 to 14 m^3 backfill would be required per

canister to maintain the gas pressure at an acceptable level, e. g., below the gas entry pressure of the host rock.

2. Seal the disposal rooms with an optimized sealing material which allows the gases to migrate continuously out of the disposal room thereby keeping the gas pressure at a safe low level. Sand/bentonite mixtures may be suited in this regard. Optimized material mixtures have a high gas permeability in the unsaturated state, allowing the gases to migrate out of the repository. Even after water uptake from the host rock and compaction due to rock creep, these materials exhibit a comparably low gas entry pressure to gas and thus, high gas pressures will not build up in the repository, neither in the unsaturated nor in the saturated state. On the contrary, after water uptake and swelling of the clay minerals, the permeability to water reduces to very low values and hence, transportation of leached radionuclides out of the disposal areas is diffusion controlled as is in the host rock.

The extraordinary sealing properties of sand/bentonite mixtures were therefore investigated in detail in the geotechnical laboratory of GRS within two projects, the “Two-Phase Flow” Project /JOC 00/ and the KENTON project /MIE 03/. Seal properties such as permeability to water and gas, gas entry/break-through pressure, and swelling pressure were determined for different mixing ratios and different degrees of compaction in order to provide a data basis for the planning of further large-scale laboratory mock-up test and in-situ experiments. The results of both projects were quite promising and it was thus concluded to continue with further work, aiming at the qualification of sand/bentonite sealing materials under repository representative in-situ conditions.

Hence, in January 2003, GRS started the SB (Self-sealing Barriers) project which consists of the following three major project phases:

1. Preceding laboratory investigations for selection of suited material mixtures and development of installation/emplacement techniques;

2. Large-scale laboratory mock-up testing for the development of suited material installation techniques, testing of measuring instrumentation and determination of time needed to reach full seal saturation;

3. In-situ testing in boreholes under representative conditions in the Mont Terri Rock Laboratory.

1.2 Project objectives and rationale

The overall objective of the project was to test and demonstrate that the sealing properties of sand/bentonite mixtures determined in the laboratory can technically be realized and maintained in situ under repository relevant conditions (e. g., installation density, saturation, swelling pressure).

The most important material properties that need to be met in a repository are listed in the following:

Permeability to gas

The SB-buffer should have a high permeability to gas. One way to avoid the development of a high gas pressure in the disposal rooms is to allow the generated gases to migrate through the seal. Right after material installation, the permeability to gas in the unsaturated state ranges between 10^{-15} m^2 – 10^{-13} m^2. According to lab investigations, it remains above 10^{-17} m^2 after gas break-through in the saturated state.

Permeability to water

The SB-buffer should have a low permeability to water. After water uptake from the host rock, the water permeability of the material reduces because of the swelling of the clay minerals. An initial value of about 10^{-18} m^2 – 10^{-17} m^2 is considered sufficient in analogy to the permeability of 10^{-16} m^2 – 10^{-14} m^2 of the excavation disturbed zone (EDZ) in the host rock /BOS 02/. It is expected that the permeability to water will reduce further as a result of ongoing rock creep with healing of the EDZ and compaction of the sealing material.

Gas entry pressure

As the buffer material is designed to act as a gas vent the gas entry/break-through pressure of the sealing material must be low enough in comparison to the gas entry pressure of the host rock to ensure gas migration through the seal. According to NAGRA /NAG 02/, the gas entry pressure in the undisturbed Opalinus clay at 600 m depth below ground amounts to about 5 MPa and thus the gas entry pressure of the seal in such a situation should be lower than 5 MPa. The conditions at the MTRL differ

significantly from these conditions. According to Thury et al. /THU 99/, the overburden pressure at Mont Terri yields a vertical stress of only 7.25 MPa with a horizontal minor stress component of about 2 MPa. Also the porewater pressure amounts to only about 2 MPa so that the gas entry/break-through pressure of the seal in the envisaged SB-experiment was to be kept at a Mont Terri specific level of well below 2 MPa which can be considered a conservative design value if the necessary sealing effectiveness can be demonstrated even for this condition.

Swelling characteristics of the buffer

Adequate swelling pressure to obtain the desired sealing effectiveness against formation water inflow. The sealing material will seal itself by swelling when taking up water. The material fills the entire space between the waste canister and the drift wall and any gap remaining from seal construction. Adequate swelling pressure and the capacity for large volumetric strains under free swelling conditions are considered very advantageous /PEL 99/. On the other hand, laboratory experiments suggest that gas penetration of an initially water-saturated clay buffer occurs only when the gas pressure slightly exceeds the sum of the swelling pressure and the groundwater pressure /ROD 99/. Consequently, in order to cause the gas to flow preferentially through the seal and not into the host rock, the swelling pressure should not exceed the gas entry pressure of the host rock.

1.3 Overview of the work programme

The envisaged strategy for a successful execution of the project was set up as follows:

- Test plan development

  A test plan was developed on basis of information available from the preceding projects and the literature as well as of intensive discussion with potential project partners or expert organizations. The test plan represents a guideline for the project relevant R&D work.

- Preceding investigations at GRS's Geoscientific Laboratory in Braunschweig

  1. Selection of suited sand/bentonite mixtures

In preceding laboratory investigations the material mixtures exhibiting the desired material properties with regard to installation density, swelling pressure, permeability to gas and water, and gas entry/break-through pressure were to be determined first. Then, the saturation behaviour of the selected material mixtures was to be determined with special respect to the time needed for achieving full saturation of the seal in the mock-up- and the in-situ experiments. These first investigations were done on small samples of about 5 cm diameter and 10 cm length. The laboratory investigations are is described in Section 2.

2. Material parameter determination and calibration and scoping calculations for the design and conduction of the envisaged mock-up and in-situ experiments.

   This work package was mostly concerned with the determination of material parameters needed for the model calculations to predict the large-scale mock-up tests and the field experiments. Modelling was done by GRS using the code CODE_BRIGHT /OLI 96/ which requires the determination of a series of material parameters for the selected seal materials and the host rock. The respective works and data are outlined in Sections 2 and 3.

3. Scoping calculations for the design of the mock-up tests and the in-situ experiments (the respective work is described in more detail in Section 3.5)

- Large-scale laboratory mock-up tests at the GRS laboratory in Braunschweig for development and testing of suitable material installation techniques and adequate instrumentation (see Section 4) and for testing the transferability of the results obtained on small samples in earlier lab tests.

- Execution of in-situ experiments

  The realization of the required installation density, the water saturation in interaction with the surrounding host rock, the resulting swelling pressure and the gas entry/break-through pressure of the actually selected and used material mixtures was to be demonstrated in up to four test boreholes in a specially excavated test niche at the MTRL (see Section 5 for further details).

  After termination of the in-situ experiments, samples were to be extracted from the seal and the surrounding host rock for post-test analyses of the results achieved in

the demonstration tests (saturation, homogeneity of the saturation, porosity etc., see Section 5.4).

- Finally, the whole project was to be evaluated and all project data and experiences were to be documented in this final project report. On basis of the results obtained from the project, proposals were to be made for the sealing of disposal boreholes, drifts and rooms in a clay repository (summary and conclusions see Section 6).

1.4 Principle design of experimental set-ups

The SB experiments were planned to be performed in vertical test boreholes in a test niche at the Mont Terri Rock Laboratory (MTRL). The principle design of an experiment is shown in Fig. 1.1.

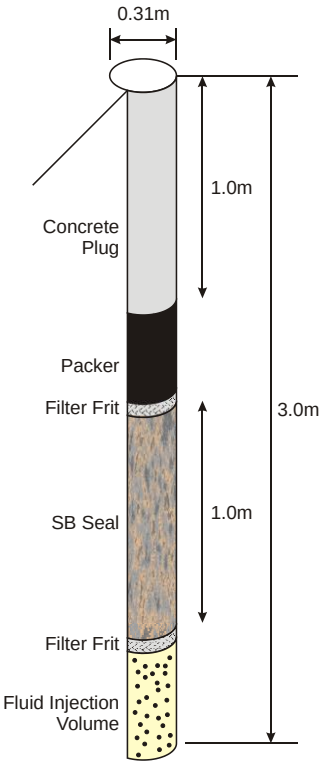

Fig. 1.1 Principle design of a borehole sealing test (mock-up and in situ)

The test borehole has a diameter of about 0.31 m and a depth of about 5 m to enable placing of the seal below the excavation disturbed zone (EDZ) in the floor of the test niche.

The lower part of the boreholes, the injection volume, is filled with a porous material (e. g., alumina beads or sand). At top of the porous medium a filter frit is placed for

ensuring a homogeneous distribution of the injected water over the entire borehole cross section. Above the filter frit, the sand/bentonite seal is installed in several layers to a height of 1 m. On top of the seal a further filter frit is installed for water and gas collection. The whole borehole is sealed against the ambient atmosphere by a gastight packer. The most upper part of the test borehole is grouted for keeping the packer in place at higher swelling pressure of the SB seal.

Synthetic formation water is injected to the bottom of the seal from an injection tube running from a valve panel in the test room via an inclined borehole. After full saturation, the water injection is terminated and followed subsequently by injecting nitrogen gas to the bottom of the seal.

The water or gas flowing through the seal is collected in the upper collection volume by a further tube running back to the control valve panel where gas and water flow rates and pressures will be controlled and measured.

Each experiment is conducted in four stages:

1. determination of the initial installation density of granular sand/bentonite mixture,
2. determination of the initial gas permeability
3. water injection to simulate the groundwater flow to the seals,
4. gas injection to simulate the gas generation in the boreholes with determination of the remaining gas permeability.

The mock-up tests (compare Sections 3.5.1 and 4) were planned as a full-scale replica of the in the in-situ experiments in order to provide adequate experimental data and experiences for the successful designing and conduction of the in-situ experiments at the MTRL.

1.5 Time schedule

The time schedule of the SB-project is depicted in Fig. 1.2. It presents an overview of the timing of all activities performed during the whole project duration including the pre-project and all relevant work done within the national project and the European Commission co-sponsored project ESDRED.

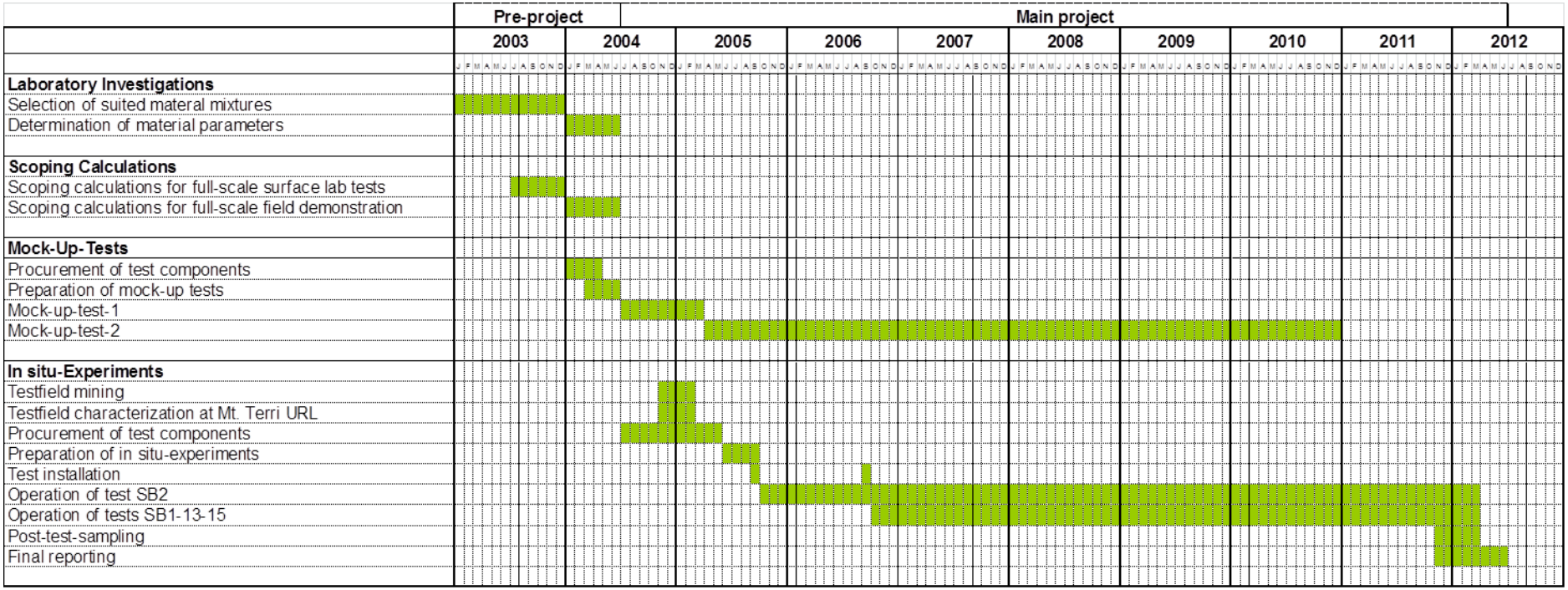

Fig. 1.2 Time schedule of the SB-project

2 Laboratory programme

The laboratory programme of the SB-project was subdivided into the following three major parts:

- Selection of suitable sealing material mixtures,
- Determination of material parameters for modelling,
- Post-tests on the samples taken from the seal and the surrounding rock after the in-situ experiment.

2.1 Selection of suitable material mixtures

To select suitable material mixtures that fulfil the various requirements for a successful demonstration of the sealing effectiveness of the sand/bentonite mixtures under representative in-situ conditions some laboratory investigations were performed in addition to those already reported by Miehe et al. /MIE 03/ and Jockwer et al. /JOC 00/. The criteria mentioned in Section 1.2 were considered with regard to the qualification of the material mixtures used in the SB in-situ experiment in the MTRL:

- permeability to the Opalinus clay solution of about 10^{-18} m^2 to 10^{-17} m^2,
- gas entry/break-through pressure lower than 2 MPa,
- swelling pressure close to or less than 2 MPa.

Since the hydro-mechanical properties are strongly dependent on the material density, the installation density that can be achieved in situ was to be considered first. It is dependent on the material composition, e. g., the bentonite content, the grain distribution, the water content, and the installation technique.

A natural Ca-Bentonite Calcigel produced by Süd-Chemie AG in Germany and pure quartz sand was used in the laboratory and in-situ experiments. In the first part of the laboratory programme, three mixtures with sand/bentonite ratios of 65/35, 50/50 and 30/70 was tested. On basis of the results, optimised mixtures were selected for the mock-up test and the in-situ experiment.

The following parameters were determined:

- grain and bulk density (installation density)
- gas permeability
- water permeability
- gas entry/break-through pressure and gas permeability after break-through
- swelling pressure
- time of saturation
- water retention.

2.1.1 Density

First, the installation density of the sealing materials was investigated in tubes with diameters similar to the planned boreholes. The bentonite and the sand will be prepared by a mixer (Fig. 2.1a).

a) Preparation by a mixer

b) Electric vibrator and funnel

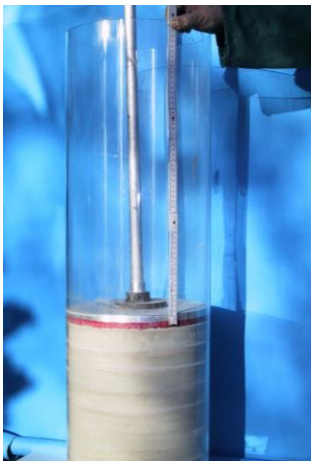

c) compaction by layers in a plexiglass tube

Fig. 2.1 Preparation of the sand/bentonite mixtures

The prepared sand/bentonite mixtures were emplaced in a plexiglass tube by layers and compacted by a vibrator (Fig. 2.1b and Fig. 2.1c). According to the installed mass and volume of the material, the installation density was determined. The grain density was measured with helium using an air comparison pycnometer after Beckmann. From

the results, the other state parameters of the compacted material such as grain density, water content and porosity can be determined.

2.1.2 Permeability, gas entry/break-through pressure, swelling pressure

The permeability and gas entry/break-through pressure of sand/bentonite mixtures were examined in two newly constructed oedometer cells, as shown in Fig. 2.2 /ZHA 04/. The cell allowed a normal sample size of 50 mm diameter and 50 mm length.

The following general testing procedure was applied:

1. Installation: The prepared sand/bentonite mixture is emplaced in the cell and compacted to the similar density achieved in the large tube by vibrating-compaction.

2. Gas injection: Under the installed conditions, gas is injected into the sample for the determination of **permeability to gas**.

3. Water injection: After the measurement of the gas permeability, synthetic Opalinus clay solution is injected to the sample for the measurement of **permeability to water**. The composition of the Opalinus clay solution is listed in Tab. 2.1.

4. Gas injection again: After water injection, gas was injected again to the saturated sample by stepwise increasing the gas pressure to determine the **gas entry/break-through pressure** and to measure the **gas permeability after the break-through**.

5. Compaction and repeating points 3 and 4: The sample was further compacted at 5 MPa to a higher density possibly achieved in boreholes and drifts. Under these conditions, points 3 and 4 were repeated to measure the **permeability to water and to gas**, and the **gas entry/break-through pressure** at higher density.

Due to water uptake and swelling of the clay minerals a reduction of porosity and permeability takes place. For interpretation of the results, the swelling pressure was measured, too.

Tab. 2.1 Composition of the used Opalinus clay solution (ph value: 7.6)

Na [mmol/l]	**K** [mmol/l]	**Ca** [mmol/l]	**Mg** [mmol/l]	**Cl** [mmol/l]	**SO_4** [mmol/l]
235	1.7	25	16	287	14

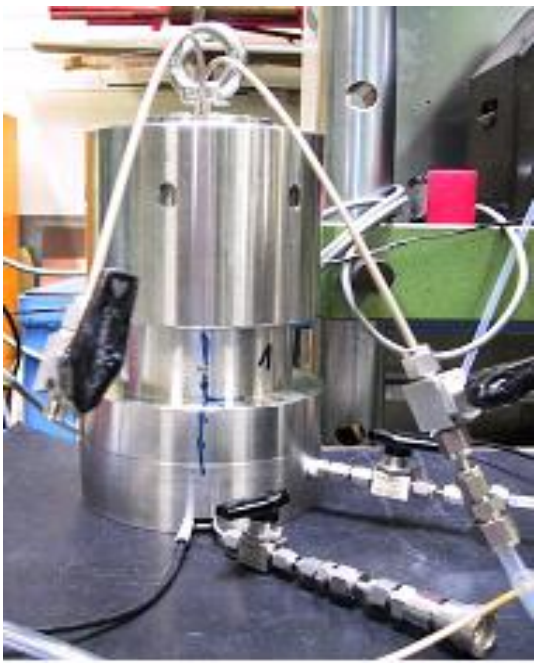

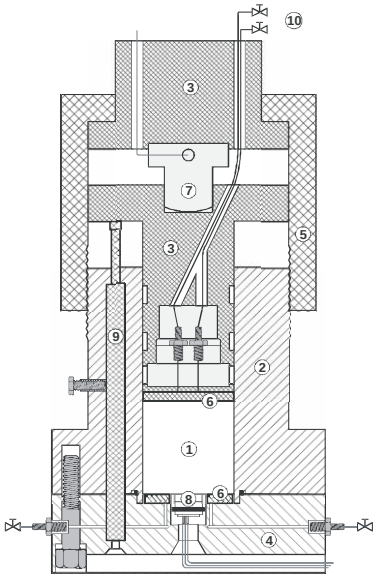

1 = sample, 2 = oedometer, 3 = pressure stamp, 4 = base plate, 5 = annular nut, 6 = sintered stainless steel filter, 7 = load sensor, 8 = pressure transducer, 9 = inductive displacement transducer, 10 = shutoff valve

Fig. 2.2 GRS oedometer cell

2.1.3 Saturation

For prediction of the time needed to achieve full saturation of the mock-up and in-situ experiments, a series of saturation tests was conducted on the sand/bentonite mixtures in steel cylinders of 50 mm diameter and 100 mm length (Fig. 2.3).

In a first group of the tests, the samples were saturated with the Opalinus clay solution at atmospheric pressure. In a second group, the samples were saturated at an injection pressure of about 1 MPa. For each sand/bentonite mixture, the tests lasted for two time intervals of one and three months. After the saturation phase, the samples were cut in

small discs. The water contents and densities of the discs were measured and their distributions along the sample length were determined.

Fig. 2.3 Experimental set-up for saturation tests

2.2 Preliminary results of laboratory investigations

2.2.1 Installation density and porosity

The seal materials consist of bentonite powder (Calcigel) and ordinary sand. The grain size distribution of the sand is shown in Fig. 2.4.

The sand is available at every commercial sand pit. The bentonite (Calcigel) is a product of the Süd-Chemie AG (Germany). The place of origin is Bavaria (Germany). The mineralogical composition (Tab. 2.2) is described in the “Product information of Calcigel” /SÜD 01/.

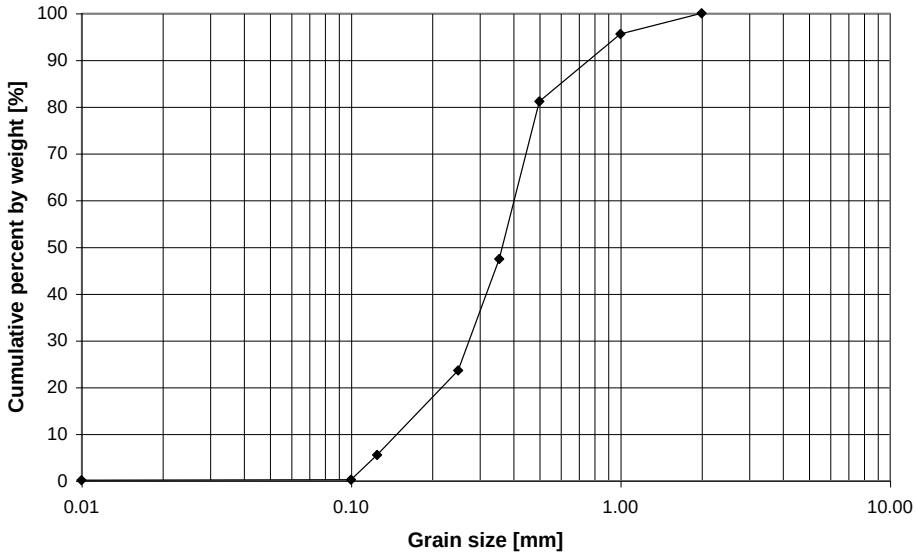

Fig. 2.4 Grain size distribution of the sand

Tab. 2.2 Mineralogical composition after Süd-Chemie AG /SÜD 01/

Mineralogical component	Percentage
Montmorillonite	60 – 70 %
Quartz	6 – 9 %
Feldspar	1 – 4 %
Kaolinite	1 – 2 %
Mica	1 – 6 %
other minerals	5 – 10 %

The grain densities of the sand, the bentonite, and of the mixtures were determined at the state of delivery as well as after drying at 105 °C until constancy of weight. The results are summarized in Tab. 2.3 and Tab. 2.4. Considering the water content of the bentonite and the sand, the bulk (or installation) densities and porosities were calculated for the state of delivery and at the dry state as well.

Tab. 2.3 Results of the investigations on installation densities, compacted by hand

Sample Sand/bentonite ratio	**Grain density (dry)** ρ_g [g/cm³]	**Grain density (state of delivery)** ρ_{go} [g/cm³]	**Bulk density (dry)** ρ_{bd} [g/cm³]	**Bulk density (state of delivery)** ρ_b [g/cm³]	**Porosity (dry)** Φ_d [%]	**Porosity (state of delivery)** Φ [%]
65/35	2.672	2.578	1.816	1.869	32.0	27.5
50/50	2.676	2.572	1.756	1.821	34.4	29.2
30/70	2.696 *	2.573	1.603	1.680	40.5	34.7
Calcigel	2.706	2.491	n. d.	n. d.	n. d.	n. d.
Sand	2.672	2.65	n. d.	n. d.	n. d.	n. d.

* calculated by the grain densities of the pure sand and Calcigel

n. d.: not determined

Tab. 2.4 Results of investigations on installation densities, compacted by vibrator

Sample Sand/bentonite ratio	**Grain density (dry)** ρ_g [g/cm³]	**Grain density (state of delivery)** ρ_{go} [g/cm³]	**Bulk density (dry)** ρ_b [g/cm³]	**Bulk density (state of delivery)** ρ_b [g/cm³]	**Porosity (dry)** Φ [%]	**Porosity (state of delivery)** Φ [%]
65/35	2.672	2.578	1.876	1.930	29.8	25.1
50/50	2.676	2.572	1.668	1.73	37.7	32.7
30/70	2.696 *	2.573	1.394	1.461	48.0	42.4
Calcigel	2.706	2.491	n. d.	n. d.	n. d.	n. d.
Sand	2.672	2.65	n. d.	n. d.	n. d.	n. d.

* calculated by the grain densities of the pure sand and Calcigel

n. d.: not determined

A comparison of the samples compacted by hand and by vibration shows that the densities of the mixtures with 35 % and 50 % bentonite content are in a similar order of magnitude. The densities of the samples with the highest bentonite content of 70 % were lower which may be explainable by the higher bentonite content, which possibly acts as a buffer and hinders further compaction.

2.2.2 Permeability, gas entry/break-through pressure, swelling pressure

For the determination of the hydraulic parameters, the sand/bentonite mixtures were installed in the oedometer cells. The installation densities corresponded to the densities described in Section 2.2.1. The water contents of the materials were determined by drying in an oven according to DIN 18121-1.

Under the installed conditions of the sealing material compacted by hand, the gas permeabilities were measured. After the measurement of the gas permeability, the samples were saturated with bentonite solution and the swelling pressures as well as the water permeabilities were determined. For the measurement of the gas break-through pressure, gas was injected by increasing the gas pressure to the saturated samples. The results of the hydraulic measurements as well as the swelling pressures as measured in the oedometer cell (Fig. 2.2) are summarized in Tab. 2.5.

With respect to the requirements described in Section 1.2 and under consideration of an acceptable saturation time the sand/bentonite mixtures 65/35 and 50/50 were found to be the most suited material mixtures for the envisaged in-situ experiments.

For the investigation of the hydraulic properties at higher densities the same sand/bentonite samples as described above, were compacted at 5 MPa at wet condition. After determination of the water permeability, the gas break-through pressure was measured and the gas permeability after the gas break-through was calculated (Tab. 2.6).

In order to confirm previous results and to complete the data especially with respect to swelling pressure and gas break-through pressure, further investigations in the oedometer were performed on samples with mixing ratios of 65/35 and 50/50 compacted by hand. The pressure history during the saturation is depicted in Fig. 2.5. The figure shows the injection pressures and the resulting pressure response at the sensors installed outside the cells.

Tab. 2.5 Parameters of SB samples compacted by hand (sample size: 50 mm diameter, 50 mm length)

Sample Sand/bentonite ratio	**Bulk density (state of delivery)** ρ_b [g/cm^3]	**Gas permeability** k_g [m^2]	**Water permeability** k_w [m^2]	**Gas break-through pressure** p_{bth} [MPa]	**Swelling pressure** p_s [MPa]	**Water content** w [wt%]
65/35	1.869	$1.23 \cdot 10^{-13}$	$9.02 \cdot 10^{-18}$	0.4	0.2 – 0.4	2.9
50/50	1.821	$7.48 \cdot 10^{-14}$	$1.79 \cdot 10^{-18}$	0.4	0.3 – 0.5	3.7
30/70	1.680	$1.16 \cdot 10^{-15}$	$5.50 \cdot 10^{-19}$	1	0.4 – ?	4.8
Calcigel	n. d.	n. d.	n. d.	n. d.	n. d.	6.07
Sand	n. d.	n. d.	n. d.	n. d.	n. d.	1.11

n. d.: not determined

Tab. 2.6 Hydraulic parameters after compaction of the wet mixtures at 5 MPa (sample size: 50 mm diameter, 50 mm length)

Sample Sand/bentonite ratio	**Water permeability** k_w [m^2]	**Gas break-through pressure** p_{bth} [MPa]	**Gas permeability (after break-through)** k_g [m^2]
65/35	$1.50 \cdot 10^{-17}$	2.36	$6.70 \cdot 10^{-17}$
50/50	$3.08 \cdot 10^{-20}$	n. d.	n. d.
30/70	$6.45 \cdot 10^{-20}$	ca. 10	$7.26 \cdot 10^{-19}$

n. d.: not determined

In order to confirm previous results and to complete the data especially with respect to swelling pressure and gas break-through pressure, further investigations in the oedometer were performed on samples with mixing ratios of 65/35 and 50/50

compacted by hand. The pressure history during the saturation is depicted in Fig. 2.5. The figure shows the injection pressures and the resulting pressure response at the sensors installed outside the cells.

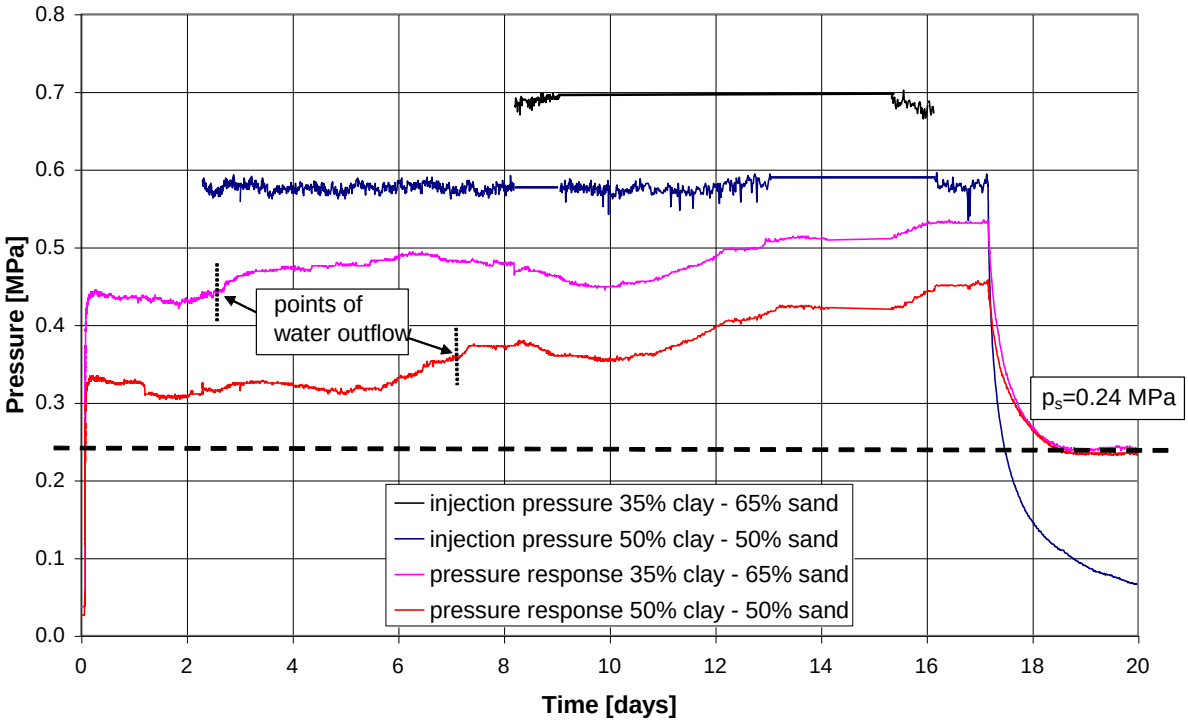

Fig. 2.5 Pressure history of sand/bentonite samples 65/35 and 50/50 in the saturation phase for determination of the swelling pressure

The remaining pressure (after disconnecting and reducing the injection pressure down to atmospheric conditions) is assumed to represent the swelling pressure, which is marked in Fig. 2.5 by the horizontal broken line. The vertical dotted lines mark the points of water outflow of the samples. After saturation, the water permeabilities were measured. The results are summarized in Tab. 2.7.

Tab. 2.7 Results of the second oedometer tests (sample size: 100 mm diameter, 100 mm length)

Sample Sand/bentonite ratio	**Bulk density (state at delivery)** [g/cm^3]	**Water permeability** [m^2]	**Swelling pressure** [MPa]
65/35	1.903	$4.73 \cdot 10^{-18}$	0.24
50/50	1.703	$4.26 \cdot 10^{-18}$	0.24

2.2.3 Saturation

All investigation on saturation were performed on samples compacted by hand. In a first group, samples were saturated with Opalinus clay solution at atmospheric pressure.

The investigations show, that saturation increases somewhat with increasing bentonite content. Furthermore, a dependence on time of the distribution of the saturation along the samples is observed. It is trivial that highest saturations were measured near the contact of the water with the samples. The results are plotted in Fig. 2.6. The saturations > 100 % is a principal problem of bentonite and can be explained by the method of determination of the densities and preparation of the samples and a deposition of water between the intermediate layers of the mica minerals as well. The saturation was calculated by the water content and the grain and bulk densities, both determined after drying at 105 °C. Depending on the degree of dryness, a changing of the grain densities and the bulk densities can be observed. With increasing dryness, the grain density increases too, and the bulk density decreases (see Tab. 2.4). The saturation, however, increases up to values above 100 %.

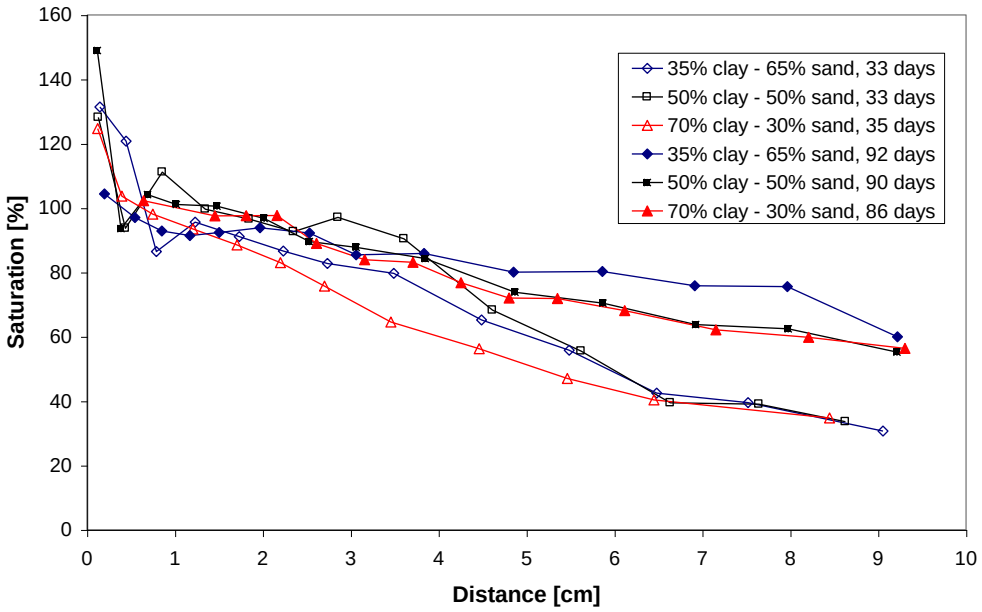

Fig. 2.6 Distribution of saturation along the samples

The evolution of the dry density is presented in Fig. 2.7. The investigations show a decrease of the dry densities with increasing bentonite content. This result might be explained by the higher bentonite content, which possibly acts as a buffer and hinders further compaction during the preparation procedure. At the front of the samples, where the sample contacts the water, a slight increase of density was determined for the samples with lower bentonite contents of 35 % and 50 %. This increase was not observed at the samples with the highest bentonite content of 70 %. A significant dependence on time was not observed. The variations of the density along the samples might be explained by inhomogeneities due to the preparation procedure.

In a second group, samples with a sand/bentonite ratio of 65/35 and 50/50 were saturated with an Opalinus Clay solution at increased injection pressures of 1 MPa. The measurements were performed to investigate the influence of pressure on the saturation process and to determine the water permeability as well as the gas entry/break-through pressure.

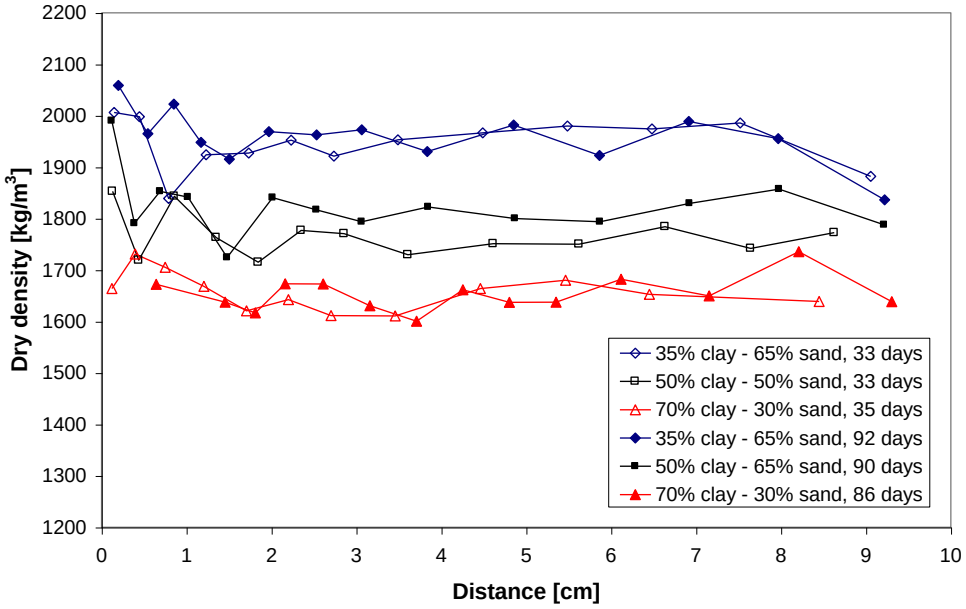

Fig. 2.7 Distribution of the densities along the samples

After saturation, the water permeability (for the Opalinus Clay solution) was measured. The results, summarized in Tab. 2.8, show, that the permeability of the samples with the lower bentonite content of 35 % was somewhat higher than the permeability with the bentonite content of 50 %.

Tab. 2.8 Results of the saturation experiments at increased water injection pressure

Sample Sand/bento-nite ratio	**Bulk density (state of delivery)** [g/cm^3]	**Water permeability** [m^2]	**Gas break-through pressure** [MPa]	**Gas permeability after break-through** [m^2]	**Water content after break-through** [%]
65/35 (1)	1.901	$3.3 \cdot 10^{-18}$	n. d.	$1.6 \cdot 10^{-17}$	n. d.
65/35 (2)	1.900	$3.9 \cdot 10^{-18}$	1.1	$1.1 \cdot 10^{-17}$	16
50/50 (1)	1.704	$1.1 \cdot 10^{-18}$	2.3	$5.5 \cdot 10^{-18}$	n. d.
50/50 (2)	1.703	$1.8 \cdot 10^{-18}$	2.8	$6.2 \cdot 10^{-18}$	21.4

n. d.: not determined

The investigations of the gas entry/break-through pressure were performed on a sample with 65 % of sand and 35 % of bentonite and two further samples with a sand/bentonite ratio of 50/50, reducing the flow rate of the HPLC pump to 0.2 ml/min. The results are plotted in Fig. 2.8 to Fig. 2.10. At the point of gas break-through, marked by a dotted line, the gas flow rate at the outlet side of the samples increases rapidly. This effect was very distinct, especially at the samples with the higher bentonite content of 50 %. At saturated state, the higher bentonite content causes a higher swelling capacity and thus leads to an increased flow resistance and to a higher capillary entry pressure as well. This process hinders the continuous inflow of the gas. Anyway, immediately after the pressure reaches the point of break-through, the gas flows into the sample. The determined gas break-through pressures are summarized in Tab. 2.8.

In comparison to the sample 65/35 with a gas break-through pressure of 1.1 MPa, the gas break-through pressure of the samples 50/50 clearly increased with values ranging between 2.3 MPa and 2.8 MPa, which can be explained by the higher swelling capacity due to the higher bentonite content.

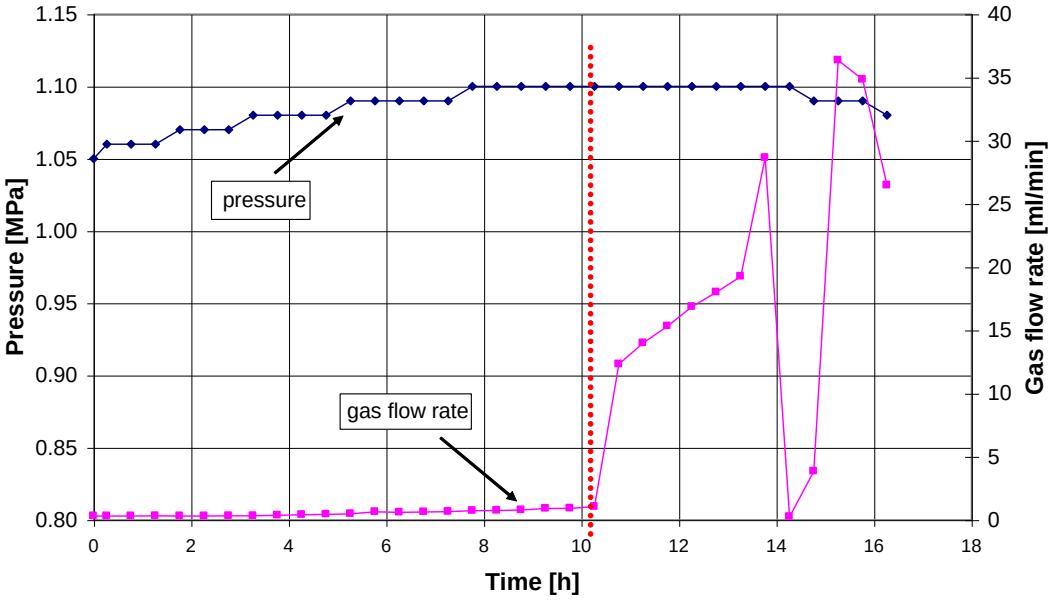

Fig. 2.8 Development of pressure and gas flow rate at the outlet of the sample with a sand/bentonite ratio of 65/35 (dotted line: point of gas break-through, rate of HPLC pump: 0.2 ml/min)

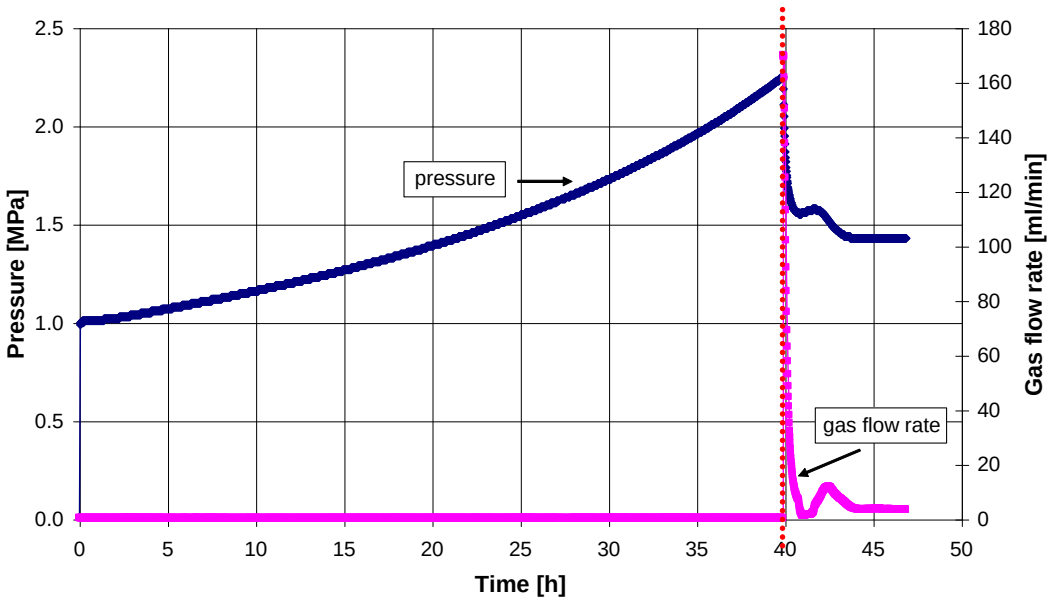

Fig. 2.9 Development of pressure and gas flow rate at the outlet of the first sample with a sand/bentonite ratio of 50/50 (1) (dotted line: point of gas break-through, rate of HPLC pump: 0.2 ml/min)

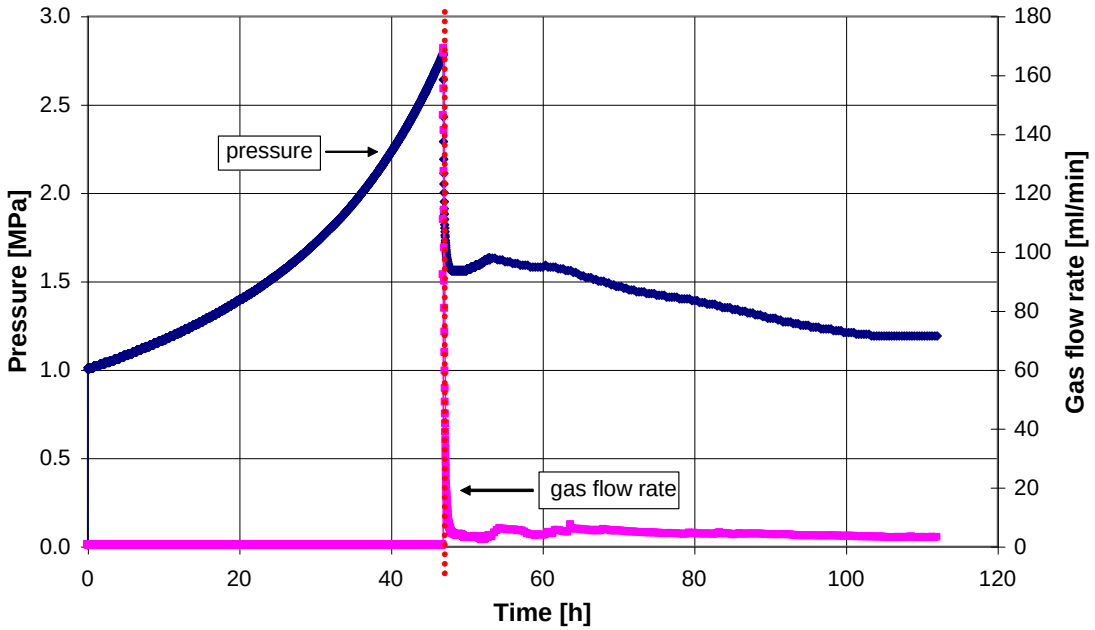

Fig. 2.10 Development of pressure and gas flow rate at the outlet of the second sample with a sand/bentonite ratio of 50/50 (2) (dotted line: point of gas break-through, rate of HPLC pump: 0.2 ml/min)

After gas break-through, the gas permeability was measured and the corresponding water content of one sample of both sand/bentonite mixtures was determined (Tab. 2.8). Due to the higher bentonite content, a lower permeability of the samples with a sand/bentonite ratio of 50/50 was measured. The remaining water content of the sample with 65 % of sand and 35 % of bentonite was 16 %, while the mixture with 50 % of both components contained 21.4 % of water. The higher water content of this mixture can be explained by a better absorption of water due to the higher bentonite content.

2.2.4 Summary and conclusions drawn from the laboratory investigations

Investigations for the determination of the petrophysical parameters were performed on sand/bentonite mixtures containing 35 %, 50 % and 70 % of bentonite.

Tab. 2.9 summarizes the parameter values determined in the laboratory and compares them to the requirements described in Section 1.2. The averaged value of each parameter is given in parentheses.

Tab. 2.9 Comparison of the measured parameters to the requirements (averages in parentheses)

Measured parameters at installation conditions					
Sand/ bent. ratio	**Gas permeability at dry cond.** [m^2]	**Water permeability at full saturation** [m^2]	**Gas entry pressure** [MPa]	**Gas permeability after gas break-through** [m^2]	**Swelling pressure** [MPa]
65/35	$1.2 \cdot 10^{-13}$	$9 \cdot 10^{-18} – 3.3 \cdot 10^{-17}$ ($5.2 \cdot 10^{-18}$)	0.4 – 1.1 (0.75)	$1.1 \cdot 10^{-17} – 1.6 \cdot 10^{-17}$ ($1.4 \cdot 10^{-17}$)	0.2 – 0.4 (0.28)
50/50	$7.5 \cdot 10^{-14}$	$1.1 \cdot 10^{-18} – 4.3 \cdot 10^{-18}$ ($2.2 \cdot 10^{-18}$)	0.4 – 2.8 (1.83)	$5.5 \cdot 10^{-18} – 6.2 \cdot 10^{-18}$ ($5.9 \cdot 10^{-18}$)	0.3 – 0.5 (0.35)
30/70	$1.2 \cdot 10^{-15}$	$5.5 \cdot 10^{-19}$	1	n. d.	0.4 – ?
Requirements					
	Gas permeability	**Water permeability**	**Gas entry pressure**	**Gas permeability after gas break-through**	**Swelling pressure**
	high	$1 \cdot 10^{-18} – 1 \cdot 10^{-17}$	< 2	high	< 2

n. d.: not determined

From Tab. 2.9 can be taken that the mixtures with sand/bentonite ratios of 65/35 and 50/50 meet the requirements. It can be expected that the gas entry pressure may reduce further in the case of significantly lower gas generation rates which are expected in a real repository. The extrapolation of the test results suggests that the mixture with 30 % of sand and 70 % of bentonite may have higher swelling and gas entry pressure than the given upper limit.

Based on these results, mixtures with sand/bentonite ratios of 65/35 and 50/50 were selected for the mock-up tests (Section 4) and in-situ experiments (Section 5).

3 Modelling

The project related modelling was performed by using the code CODE_BRIGHT developed by the Technical University of Catalonia (UPC) in Barcelona (note that Version 2.3 of the code was used for the scoping calculations and Version 3.0 for the post test calculations presented in Chapter 6). A general and detailed description is given in /OLI 96/ and in the code manual /UPC 02/, according to the aforementioned literature only a brief description is given in the following section.

The theoretical framework of the computer programme CODE_BRIGHT is composed of three main parts: balance equations, constitutive equations and equilibrium restrictions. The subscripts identify the phase ('s' for solid, 'l' for liquid and 'g' for gas). The superscripts indicate the species ('h' for mineral, 'w' for water and 'a' for air). The liquid phase may contain water and dissolved air, and the gas phase may be a mixture of dry air and water vapour. Thermal equilibrium between phases is assumed. This means that the three phases are at the same temperature.

3.1 Balance equations

The balance equations are established for the porous medium as a whole. The compositional approach is adopted to establish the mass balance equations. It consists of balancing the species rather than the phases. The mass balance of solid present in the medium is written as:

$$\frac{\partial}{\partial t}\left(\rho_s(1-n)\right) + \nabla \cdot (\mathbf{j}_s) = 0 \qquad (3.1)$$

where ρ_s is the mass of solid per unit volume of solid, j_s is the flux of solid, t is time and ∇ is the divergence operator.

Water is present in liquid and gas phases. The total mass balance of water is expressed as:

$$\frac{\partial}{\partial t}(\theta_l^w S_l n + \theta_g^w S_g n) + \nabla \cdot \left(\mathbf{j}_l^w + \mathbf{j}_g^w\right) = f^w \qquad (3.2)$$

where θ_l^w and θ_g^w are the masses of water per unit volume of liquid and gas, respectively. S_α is the volumetric fraction of pore volume, occupied by the alpha phase

$(\alpha = l, g)$. j_l^w and j_g^w denote the total mass fluxes of water in the liquid and gas phases (water vapour), with respect to a fixed reference system. f^w is an external supply of water per unit volume of medium.

Dry air is present in liquid and gas phases. The total mass balance of dry air is expressed as:

$$\frac{\partial}{\partial t}(\theta_l^a S_l n + \theta_g^a S_g n) + \nabla \cdot \left(\mathbf{j}_l^a + \mathbf{j}_g^a\right) = f^a \qquad (3.3)$$

where θ_l^a and θ_g^a are the masses of dry air per unit volume of liquid and gas, respectively. S_α is the volumetric fraction of pore volume, occupied by the alpha phase $(\alpha = l, g)$. j_l^a and j_g^a denote the total mass fluxes of dry air in the liquid and gas phases (water vapour), with respect to a fixed reference system. f^a is an external supply of dry air per unit volume of medium.

Thermal equilibrium between phases is assumed. This means that the three phases are at the same temperature. Consequently, the total internal energy, per unit volume of porous media, is obtained adding the internal energy of each phase. Applying the balance equation to this quantity, the following equation is obtained:

$$\frac{\partial}{\partial t}\left(E_s \rho_s (1-\phi) + E_l \rho_l S_l \phi + E_g \rho_g S_g \phi\right) + \nabla \cdot \left(\mathbf{j}_c + \mathbf{j}_{Es} + \mathbf{j}_{El} + \mathbf{j}_{Eg}\right) = f^E \qquad (3.4)$$

where E_s is the solid specific internal energy; E_l and E_g are specific internal energies corresponding to liquid and gas phase, respectively, ρ_s is the solid density; ρ_l and ρ_g are the liquid and gas phase densities; j_c is the conductive heat flux; j_{Es} is the advective energy flux of solid phase with respect to a fixed reference system; j_{El} and j_{Eg} are the advective energy flux of liquid and gas phases, respectively, with respect to a fixed reference system; f^E is the energy supply per unit volume of medium.

The balance of momentum for the porous medium reduces to the equilibrium equation in total stresses:

$$\nabla \cdot \sigma + \mathbf{b} = 0 \qquad (3.5)$$

where σ is the stress tensor and b is the vector of body forces.

3.2 Equilibrium restrictions

Equilibrium restrictions are given for the concentration of water vapour in gas and of dissolved air in water. The mass of water vapour per unit volume of gas $\left(\theta_g^w\right)$ is determined via the psychrometric law:

$$\theta_g^w = \left(\theta_g^w\right)^0 \exp\left[\frac{-(P_g - P_l)M_w}{R(273.15+T)\rho_l}\right] \tag{3.6}$$

where P_l and P_g are liquid and gas pressures, respectively, $\left(\theta_g^w\right)^0$ is the vapour density in the gaseous phase in contact with a planar surface (i. e., when $P_g - P_l = 0$), M_w is the molecular mass of water (0.018 kg/mol), R is the gas constant (8.314 J/mol·K) and T is the temperature (in degree Celsius). $\left(\theta_g^w\right)^0$ is depending on temperature. The vapour partial pressure is computed by means of the ideal gas law.

The solubility of air in water is controlled by Henry's law:

$$\omega_l^g = \frac{P_a}{H} \cdot \frac{M_a}{M_w} \tag{3.7}$$

where ω_l^g is the mass fraction of air in the liquid, P_a is the partial pressure of air, M_a is the molecular mass of air (0.02895 kg/mol) and H = 10000 MPa is Henry's constant. According to the definition of partial density, $\theta_l^w = \omega_l^g \cdot \rho_l$.

3.3 Constitutive equations

The constitutive equations establish the link between the independent variables and the dependent variables. Concerning the hydraulic problem it is assumed that the liquid and gas flows follow Darcy's law:

$$q_\alpha = -\mathbf{K}_\alpha(\nabla P_\alpha - \rho_\alpha \mathbf{g}) \tag{3.8}$$

where $K_\alpha = k\, k_{r\alpha}/\mu_\alpha$ is the permeability tensor. The intrinsic permeability tensor (k) depends on the pore structure of the porous medium. $k_{r\alpha}$ is the value of relative permeability that controls the variation of permeability in the unsaturated regime and μ_α denotes the dynamic viscosity. α stands either for l or g depending on whether liquid or gas flow is considered. g is the gravity vector.

The variation of intrinsic permeability with porosity is given by:

$$k = \mathbf{k}_0 \cdot \frac{\phi^3}{(1-\phi)^2} \cdot \frac{(1-\phi_0)^2}{\phi_0^3} \tag{3.9}$$

where ϕ_0 is a reference porosity. The relative permeabilities of the liquid and gaseous phases are dependent on the degree of liquid saturation according to:

$$S_e = \frac{S_l - S_{lr}}{S_{ls} - S_{lr}} \tag{3.10}$$

and

$$k_{rl} = A \cdot S_e^{\lambda} \tag{3.11a}$$

$$k_{rg} = 1 - k_{rl} \tag{3.11b}$$

where S_l, S_{lr}, S_{ls}, S_e are the actual, residual, maximum and effective saturation of liquid, respectively, and A and λ are parameters.

It is necessary to define the retention curve of the materials relating to the degree of saturation to suction $(P_g - P_l)$. The expression of Van Genuchten is selected:

$$S_e = \left[1 + \left(\frac{P_g - P_l}{P}\right)^{1/(1-\beta)}\right]^{-\beta} \tag{3.12}$$

where $P_g - P_l \geq 0$ and $P = P_0 \cdot \frac{\sigma}{\sigma_0}$; P_0 is a material parameter.

The molecular diffusion of vapour is governed by Fick's law:

$$\mathbf{i}_g^w = -\mathbf{D}_g^w \nabla \omega_g^w = -\left(\phi \rho_g S_g \tau \mathbf{D}_m^w I + \rho_g \mathbf{D}_g'\right) \cdot \nabla \omega_g^w \tag{3.13}$$

where i_g^w is the non-advective mass flux of water in gas, D_g^w is the dispersion tensor, ω_g^w is the mass fraction of water in gas, τ is the tortuosity and D_g' is the mechanical dispersion tensor. Usually, a constant dispersion coefficient corresponding to the molecular diffusion of vapour in air is assumed:

$$D_m^w = \tau D \left(\frac{(273.15+T)^n}{P_g}\right) \tag{3.14}$$

where P_g is given in MPa. For τ a value equal to 0.8, for n a value of 2.3 and for D a value of 5.9E-12 has been adopted. D_g' can be neglected if air flow is insignificant.

In saturated porous materials, mechanical behaviour is best understood in terms of effective stress $\sigma' = \sigma - P_l m$, where m^T is an auxiliary vector [1,1,1,0,0,0]. For unsaturated materials it is necessary to consider two independent stress variables: net stresses $(\sigma - P_l m)$ and capillary suction $s = (P_g - P_l)$. The net stress is the excess of total stress over gas pressure. If full saturation is achieved, net stress becomes effective stress. The mechanical constitutive equation takes the incremental form:

$$d\boldsymbol{\sigma}' = \mathbf{D} d\varepsilon + \mathbf{h} ds \tag{3.15}$$

where σ' is now used for net stresses, ε is the strain sensor. D is the constitutive stiffness matrix, defined by Young's modulus E_i, shear modulus G and Poisson's ratio υ_i through the classical orthotropic linear elasticity with i depending on bedding plane orientation and h is a constitutive vector relating changes of suction to changes in net stress.

For the Barcelona Basic Model (BBM) as the yield function a classical Modified Cam-Clay model is taken:

$$q^2 - M^2 (p' + p_s)(p_o - p') = 0 \tag{3.16}$$

where M is a constant value characterising the critical failure state line

$$q = Mp' \tag{3.17}$$

where q is the deviatoric stress.

It is assumed that the apparent cohesion increases with suction by

$$p_s = p_{so} + k \cdot s \tag{3.18}$$

where p_{so} is the tensile strength in saturated conditions, κ and p are parameters.

The net isotropic yield stress p_o is considered to be dependent on suction through

$$p_o = p^c \left(\frac{p_o^*}{p^c} \right)^{\frac{\lambda(o) - k_{io}}{\lambda(s) - k_{io}}} \tag{3.19a}$$

with

$$\lambda(s) = \lambda(o)\left[(1-r)\exp(-\beta s) + r\right] \tag{3.19b}$$

where p*o is the net yield stress for saturated conditions, $\lambda(o)$, $\lambda(s)$ are the slopes of the virgin compression lines for saturated and unsaturated conditions, r is a constant related to the matrix stiffness, β provides the rate of change of $\lambda(s)$ with suction, kio is the initial slope of the isotropic unloading-reloading paths for saturated conditions, p^c is a reference stress.

Hardening depends on plastic strain according to

$$\frac{dp_o^*}{p_o^*} = \frac{v}{\lambda(o) - k_{io}} d\varepsilon_v^p \tag{3.20}$$

where v = 1+e is the specific volume, e is the void ratio.

Volumetric elastic strains induced by changes of net mean stress and suction are given by

$$d\varepsilon_v^e = d\varepsilon_{vp}^e + d\varepsilon_{vs}^e \tag{3.21a}$$

with

$$d\varepsilon_{vp}^e = \frac{k_i}{\mathbf{v}} \frac{dp'}{p'} \tag{3.21b}$$

$$k_i = k_{io}(1 + \alpha_i s) \tag{3.21c}$$

$$d\varepsilon_{vs}^e = \frac{k_s}{v} \frac{ds}{s + p_{at}} \tag{3.21d}$$

$$k_s = k_{so}\left(1 + \alpha_{sp} \ln\left(\frac{p'}{p_{ref}}\right)\right)\exp(\alpha_{ss} s) \tag{3.21e}$$

where k_{io}, k_i are the slopes of the isotropic unloading-reloading paths for saturated and unsaturated conditions, respectively, k_{so}, k_s are the slopes of the wetting-drying paths for saturated and unsaturated conditions at a given stress p' in the elastic domain, pat,

pref are the atmospheric pressure and the reference pressure, α_i, α_{sp}, α_{ss} are parameters.

Deviatoric elastic deformations are computed through shear modulus G and the Poisson ratio ν:

$$d\varepsilon_q^e = \frac{G}{3} dq \tag{3.22a}$$

with

$$G = \frac{3(1-2\nu)}{2(1+\nu)} \frac{(1+e)}{k_i} p' \tag{3.22b}$$

3.4 Material parameters

A number of parameters associated with the above equations are material specific parameters which were to be determined by laboratory and in-situ experiments. For the scoping calculations presented here, the buffer material parameters were firstly estimated from a few limited tests on the sand-bentonite mixtures and the parameters for the Opalinus clay were taken from /ZHA 04/. The values of the physical properties are shown in Tab. 3.1.

The hydraulic parameters for the sand/bentonite mixtures and the Opalinus clay are shown Tab. 3.2. The retention curves for the mixtures with bentonite contents of 35 %, 50 % and 70 % were established by extrapolation of the two-phase flow data obtained on the compacted sand/bentonite mixtures with bentonite contents of 10 % and 25 % in the KENTON project /JOC 00/ /MIE 03/ as shown in Fig. 3.1. The test data obtained on a mixture with 20 % of bentonite and 80 % of sand by Alonso et al. /ALO 02/ vary in the range between the curves of mixtures with bentonite contents of 10 % and 25 %. Application of the extrapolated retention curves to the simulation of a saturation test on sand/bentonite mixtures in a cylinder of 50 mm diameter and 100 mm length at an injection pressure of 1 MPa led to a reasonable saturation time of about 2 days for the sand/bentonite ratio 65/35 and 6 days for the sand/bentonite ratio 50/50, which is in good agreement with the actually observed times of 2 – 5 days and 5 – 13 days, respectively.

Tab. 3.1 Physical properties determined for sand/bentonite mixtures and Opalinus clay

Property	Symbol	Unit	Opalinus Clay	Sand/ bentonite 65/35	Sand/ bentonite 50/50	Sand/ bentonite 30/70
Grain density	ρ_s	[kg/m^3]	2710	2672	2676	2680
Dry density	ρ_d	[kg/m^3]	2340	1900	1700	1450
Void ratio	e_o	[-]	0.190	0.406	0.574	0.848
Porosity	ϕ_0	[-]	0.160	0.289	0.365	0.459
Water content	w_0	[%]	7.2	2.9	3.7	4.8
Initial suction	s_0	[MPa]	0	1.2	1.8	3.6
Degree of saturation	S_{l0}	[%]	100	17	17	17

Tab. 3.2 Hydraulic parameters determined for sand/bentonite mixtures and Opalinus clay, associated with the constitutive equations

Parameter in equation	Symbol	Unit	Opalinus clay	Sand/ bentonite 65/35	Sand/ bentonite 50/50	Sand/ bentonite 30/70
(3.9)	ϕ_0	[-]	0.16	0.274	0.331	0.384
(3.9)	k_o	[m^2]	$2\cdot10^{-20}$	$4\cdot10^{-18}$	$1\cdot10^{-18}$	$5\cdot10^{-19}$
(3.10)	S_{lr}	[-]	0.01	0.01	0.01	0.01
(3.10)	S_{ls}	[-]	1.0	1.0	1.0	1.0
(3.11a)	A	[-]	1			
(3.11a)	λ	[-]	5			
(3.12)	β	[-]	0.4	0.9	0.9	0.9
(3.12)	P_o	[MPa]	20	1.0	1.5	3
(3.14)	τ	[-]	0.8	1	1	1

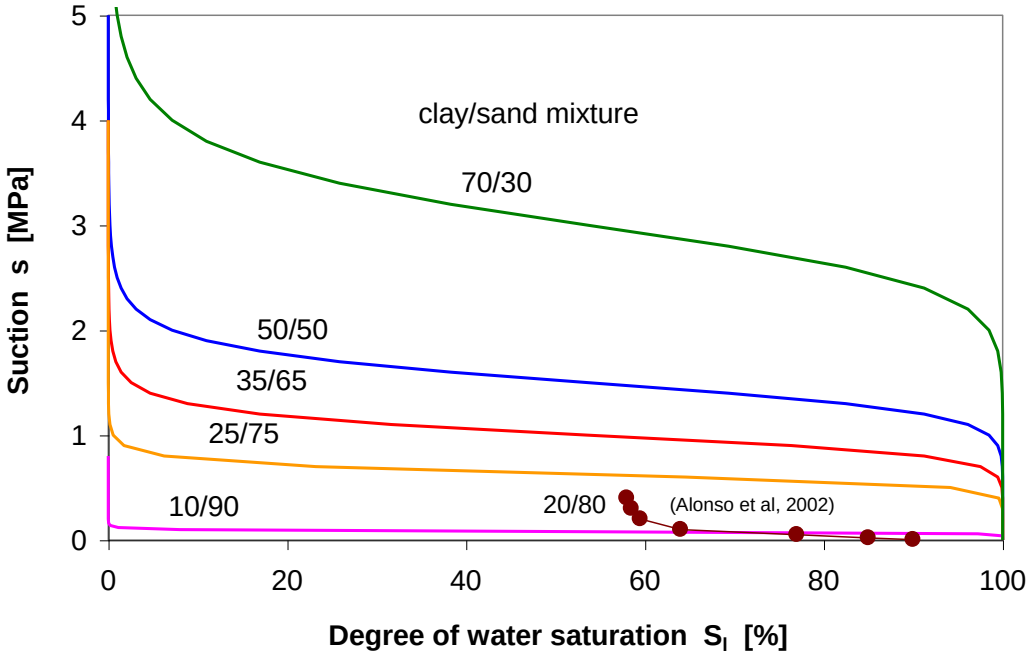

Fig. 3.1 Retention curves for different sand/bentonite mixtures

The retention curve of the Opalinus clay is taken from /ZHA 04/ and presented in Fig. 3.2. The intrinsic permeability of the sand/bentonite mixtures was measured using the Opalinus clay solution.

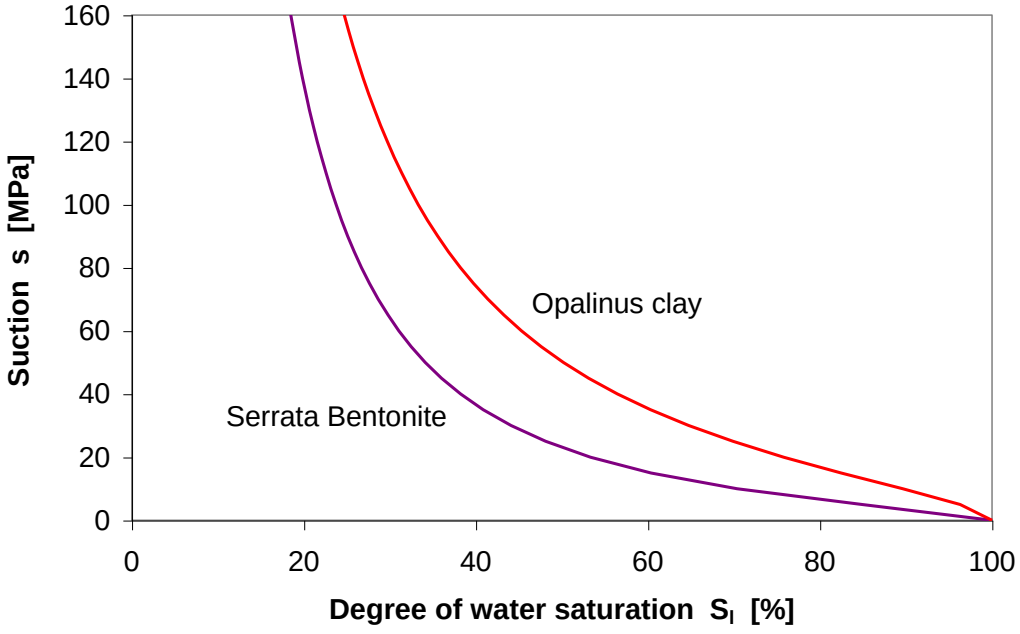

Fig. 3.2 Retention curves for the Opalinus clay and Serrata bentonite /ZHA 04/

Fig. 3.3 shows the relationship between intrinsic permeability and porosity for the mixtures and the Opalinus clay. The permeability decreases with decreasing porosity. In the tests, it was found that sand/bentonite mixtures with bentonite contents higher than 50 % after compaction at 5 MPa exhibit very low permeability of 10^{-20} m^2 which is comparable to that of the intact clay rock. The relative liquid and gas permeability for the mixtures are given as a function of degree of water saturation in Fig. 3.4. First, they are assumed equal for all mixtures because of a lack of test data. Fig. 3.5 compares the relative permeability of the Opalinus clay and the Serrata bentonite.

Fig. 3.6 compares the compaction results obtained on sand/bentonite mixtures with the modelling curves, whereas Fig. 3.7 illustrates the swelling behaviour of sand/bentonite mixtures. The mixtures swell with increasing water saturation due to the existence of clay minerals. However, the assumed swelling capacity seems to be low. The maximum swelling strain of Δe = 0.0003 to 0.0007 is reached after saturation.

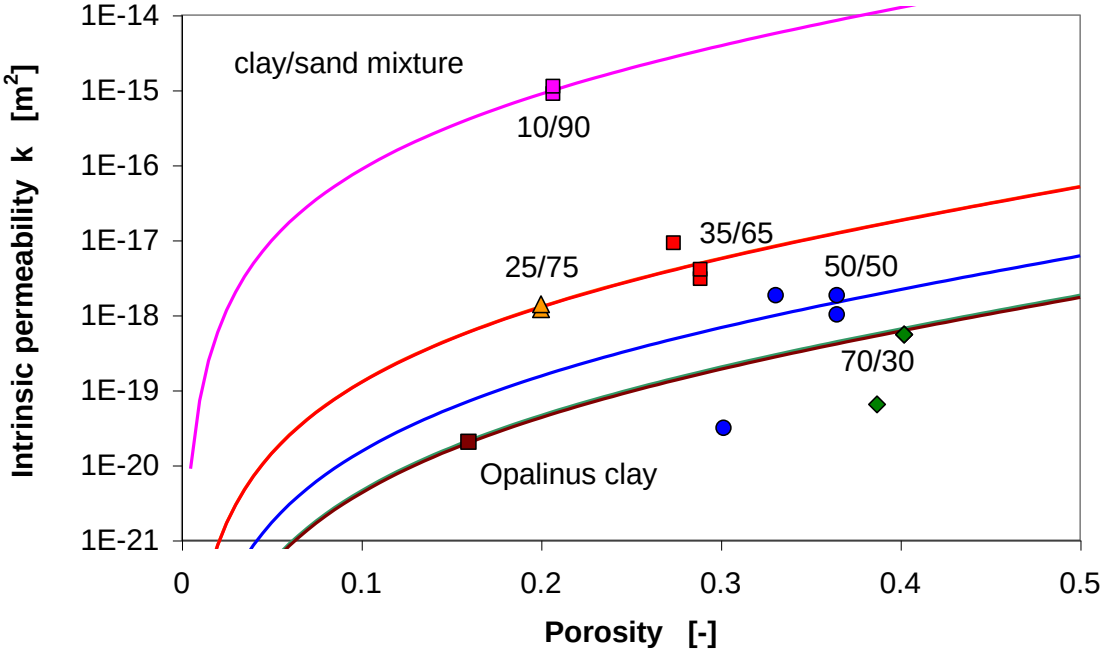

Fig. 3.3 Intrinsic permeability as a function of porosity for different sand/bentonite mixtures and the Opalinus clay

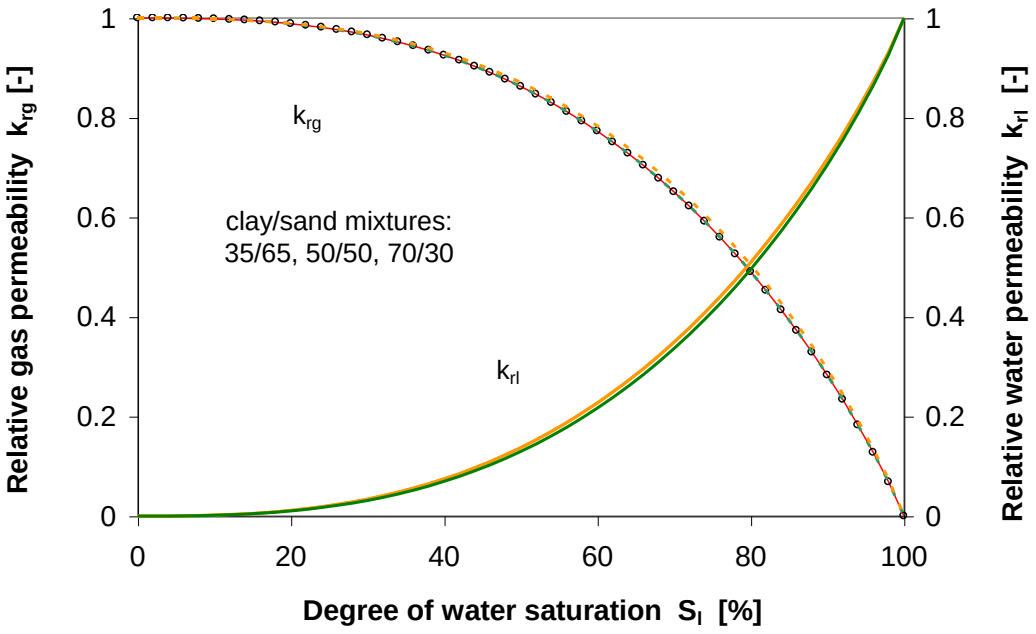

Fig. 3.4 Relative water and gas permeability as a function of saturation for the sand/bentonite mixtures

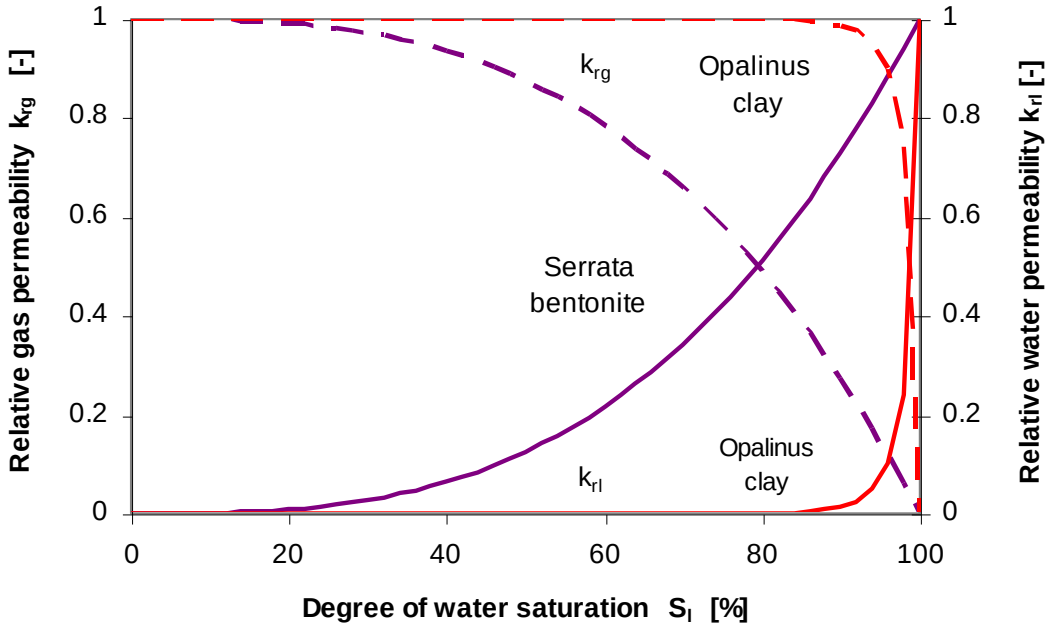

Fig. 3.5 Relative water and gas permeability as a function of saturation for Opalinus clay and Serrata bentonite /ZHA 04/

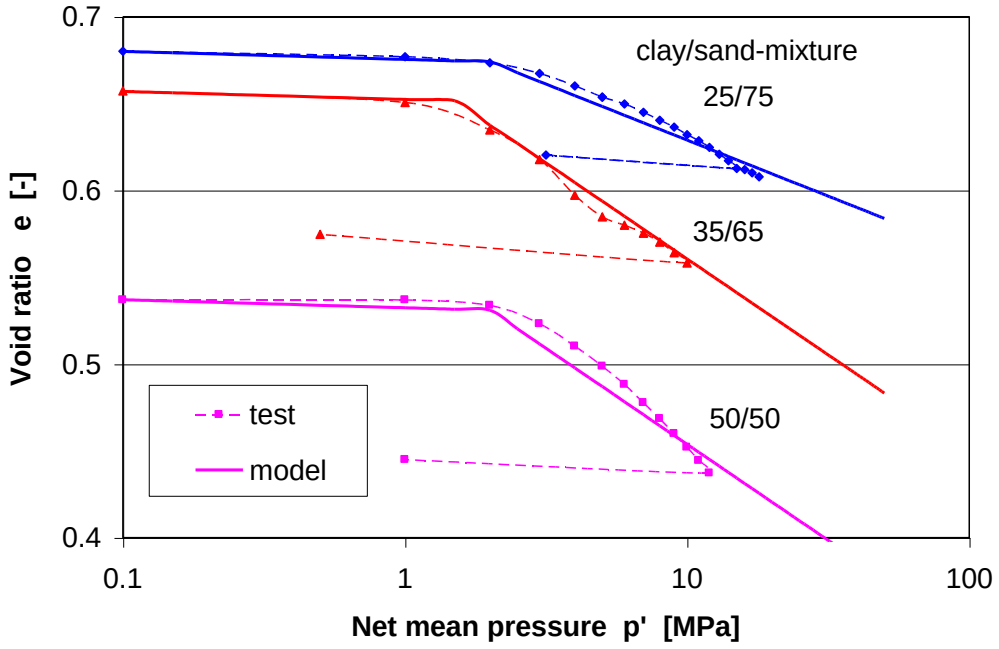

Fig. 3.6 Compaction behaviour of sand/bentonite mixtures

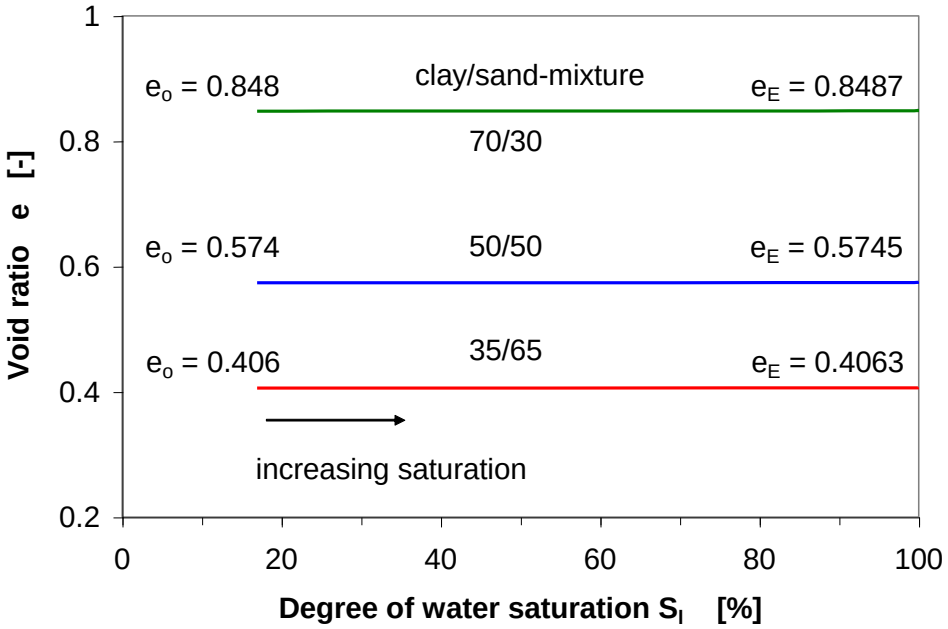

Fig. 3.7 Swelling of sand/bentonite mixtures due to water saturation

Mean values of the mechanical parameters are given in Tab. 3.3. They were determined from a few limited compaction tests on the sand/bentonite mixtures in oedometer cells and the parameters for the Opalinus clay were taken from /ZHA 04/.

Tab. 3.3 Mechanical parameters determined for sand/bentonite mixtures and Opalinus clay, associated with the constitutive equations

Parameter in equation	**Symbol**	**Unit**	**Opalinus clay**	**Sand/ bentonite 65/35**	**Sand/ bentonite 50/50**	**Sand/ bentonite 30/70**
(3.21c)	k_{io}	[-]	0.0035	0.002	0.002	0.002
(3.21c)	α_i	[-]	0	0	0	0
(3.21e)	k_{so}	[-]	$4 \cdot 10^{-5}$	0.0005	0.0007	0.001
(3.21e)	α_{sp}	[-]		0	0	0
(3.21e)	α_{ss}	[MPa^{-1}]		0	0	0
(3.21e)	p_{ref}	[MPa]		-	-	-
(3.22b)	v	[-]	0.33	0.35	0.35	0.35
Bulk modulus	K	[MPa]	3500	80	80	80
Shear modulus	G	[MPa]	1340	27	27	27
Young's modulus	E	[MPa]	3570	40	40	40
(3.17)	M	[-]	1.5	1.5	1.5	1.5
(3.18)	k	[-]	-0.007	-0.1	-0.1	-0.1
(3.19a)	p^c	[MPa]	0.1	0.1	0.1	0.1
(3.19a)	p_o^*	[MPa]	20.0	1.5	2.0	2.5
(3.19a)	$\lambda(o)$	[-]	0.027	0.05	0.05	0.05
(3.19b)	r	[-]	0.6	0.75	0.75	0.75
(3.19b)	ß	[MPa^{-1}]	0.015	0.05	0.05	0.05

3.5 Scoping calculations

Preceding both the above-mentioned mock-up- and in-situ experiments were scoping calculations performed to enable proper design of the experiments and to qualify, at a later stage, the used THM models by comparing modelling and test results.

As already mentioned the Barcelona Basic Model (BBM) was used for the assessment of the mechanical behaviour of the sealing materials and the Opalinus clay. Gas and water flow was modelled according to Darcy's law and the molecular diffusion of water vapour is governed by Fick's law. The mass of water vapour per unit volume of gas is determined via the psychrometric law and the solubility of air in water is controlled by Henry's law. The hydraulic parameters for the sand/bentonite mixtures such as relative permeability and capillary pressure as functions of saturation were established by extrapolation of the two-phase flow data obtained in the KENTON project and additionally validated through special laboratory saturation tests on small samples.

The scoping calculations for designing the tests were performed by using material parameters described in Section 3.4 and parameter values for the Opalinus Clay were taken from the literature /ZHA 04/.

The calculations focused on prediction of testing conditions such as adequate injection pressures for water and gas, duration of water saturation, ranges of measuring parameters (gas and water flux, swelling pressure, total pressure etc.), and determination of initial and boundary conditions in the in-situ test field. In the scoping calculations, the materials installed in the mock-up test and the in-situ experiments were assumed as homogeneous and isotropic. Processes prevailing in the materials during the tests were considered as coupled THM processes, so that the balance equations given in Section 3.1 were to be solved.

The numerical models and the modelling results are presented in the following sections.

3.5.1 Mock-up tests

Scoping calculations for the mock-up tests were mainly done to predict the time needed to achieve full saturation of the SB seals of 1 m length as originally foreseen for both the mock-up and in-situ experiments.

3.5.1.1 Numerical model

The mock-up tests (see also Section 4) were to be designed as a full-scale replica of the envisaged in the in-situ experiments (Fig. 1.1 below). The length of the tube used in the laboratory should have a length of 2.5 m in order to accept a test seal length of 1 m together with a gravel-filled fluid injection chamber of 0.5 m length. As in the in-situ experiments, the gas permeability, the time required to achieve saturation, the water permeability, the gas entry/break-through pressures, and the gas permeability after the break-through were to be determined in the course of the test in order to provide adequate experimental data and experiences for the successful conduction of the in-situ experiments at the MTRL.

Regarding the conclusions drawn from the preceding laboratory experiments (Section 2.2.4), the selected sand/bentonite mixtures with bentonite contents of 35 % and 50 % were considered in the calculations. The selected materials are installed in steel tubes of 0.31 m diameter and 1.0 m length. Due to the symmetry of the steel tubes, only half of the construction (injection chamber, seal, and filter) was considered in the used axisymmetric model shown in Fig. 3.8.

According to the envisaged test procedure (see Section 1.4), the following steps were considered in the calculations:

Step 1: Water injection at constant water pressure to determine evolution of water saturation and time needed for full saturation;

Step 2: Water flow through the saturated seal at constant injection pressure and measurement of water outflow;

Step 3: Reduction of the water pressure down to atmospheric pressure to examine the swelling pressure (remaining total stress) in the seal;

Step 4: Gas injection into the saturated seal at constant flow rate to determine gas break-through pressure and gas outflow.

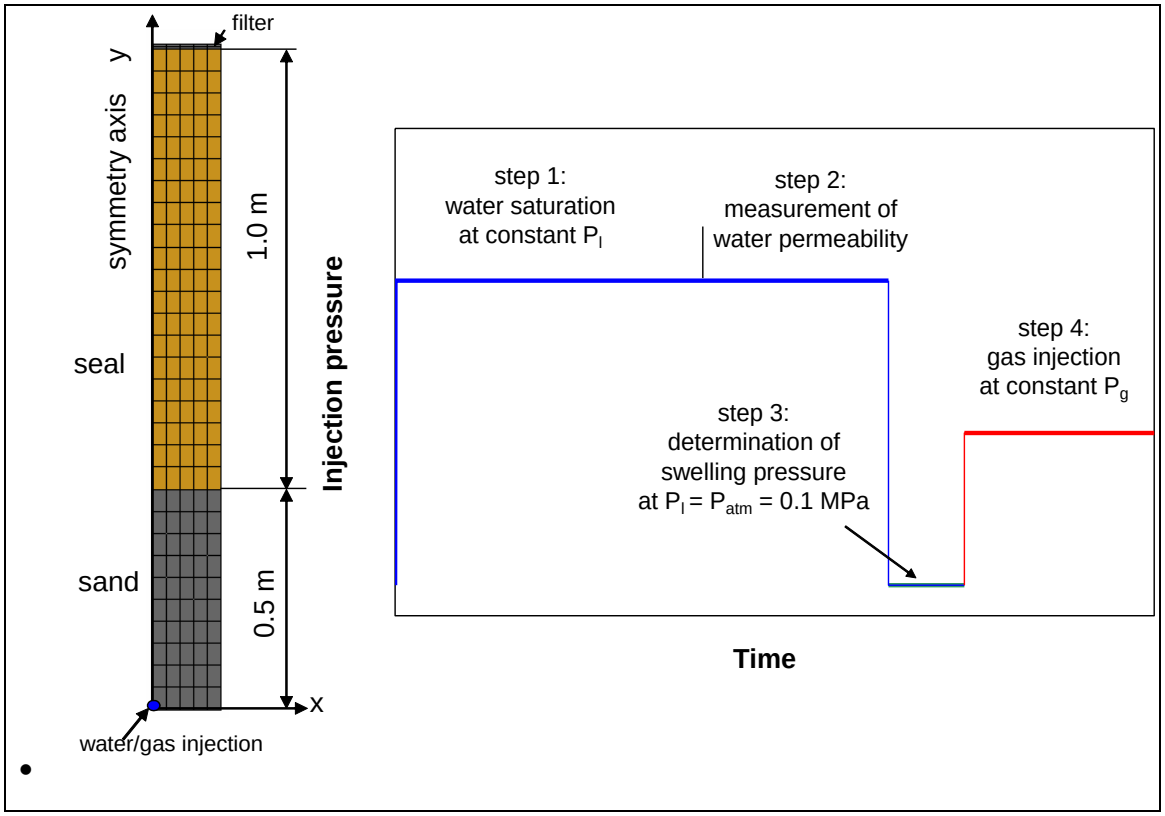

Fig. 3.8 Numerical model and calculation steps

The following initial and boundary conditions were prescribed in the calculations:

- The initial stress in the seal $\sigma_{10} = \sigma_{20} = \sigma_{30}$ = 0.1 MPa induced by compacting the seal material in the steel tube;
- No displacement of all boundaries ΔU = 0 due to confinement of the seal in the stiff tube;
- No water and gas outflow through the circumferential surface $Q_w = Q_g = 0$, because of the tight steel tube;
- Water injection at the bottom of the seal at given pressure P_l;
- Gas injection at the bottom of the seal at given flow rate $\dot{Q}_g$;
- Atmospheric pressure $P_g = P_{atm}$ = 0.1 MPa at top boundary of the seal.

In the calculations, the water injection pressure and the gas injection rate are varied as follows: P_l = 0, 0.2, 0.5, 1.0 MPa; $\dot{Q}_g$ = 0.02, 0.2 ml/min.

Note that real values (gauge values) of water and gas pressure as well as stress are equal to the calculated values minus the atmospheric pressure P_{atm} = 0.1 MPa.

3.5.1.2 Modelling results

Water saturation and flow

Water saturation and flow was calculated for both selected mixtures under different injection pressures between 0 and 1 MPa. Fig. 3.9 and Fig. 3.10 show the distribution and evolution of water saturation in the seal with sand/bentonite ratio 65/35 at an injection pressure of 1 MPa, whereas the calculation results for the seal with ratio 50/50 at the same injection pressure of 1 MPa are illustrated in Fig. 3.11 and Fig. 3.12. The seals are saturated from the bottom to the top. The time needed to reach a full saturation at 1 MPa injection pressure is about 6 month for the seal with ratio 35/65 and 19 month for the ratio 50/50.

Tab. 3.4 summarizes the saturation times for both seals at different pressures.

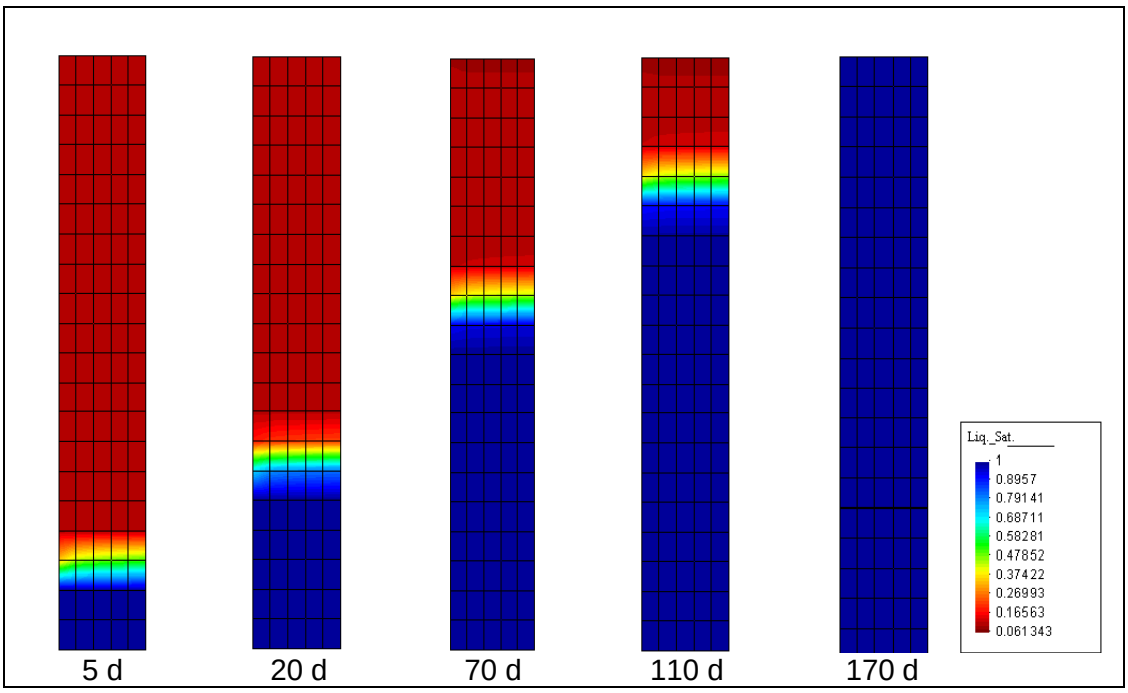

Fig. 3.9 Distribution of water saturation in the seal with 65/35 sand/bentonite ratio at an injection pressure of 1 MPa

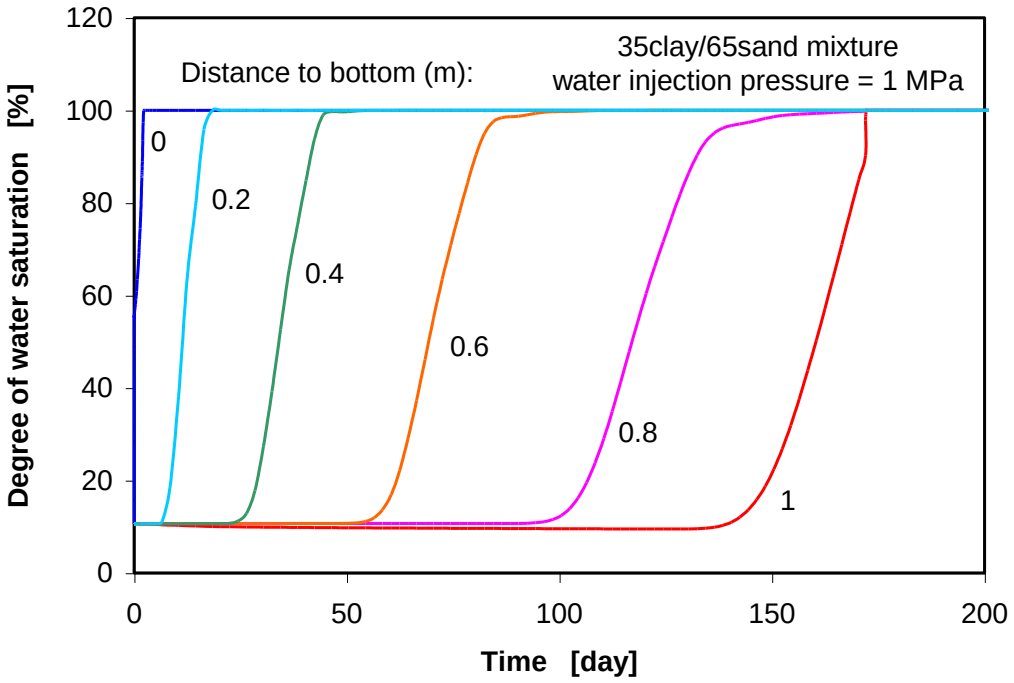

Fig. 3.10 Evolution of water saturation in the seal with 65/35 sand/bentonite ratio at an injection pressure of 1 MPa

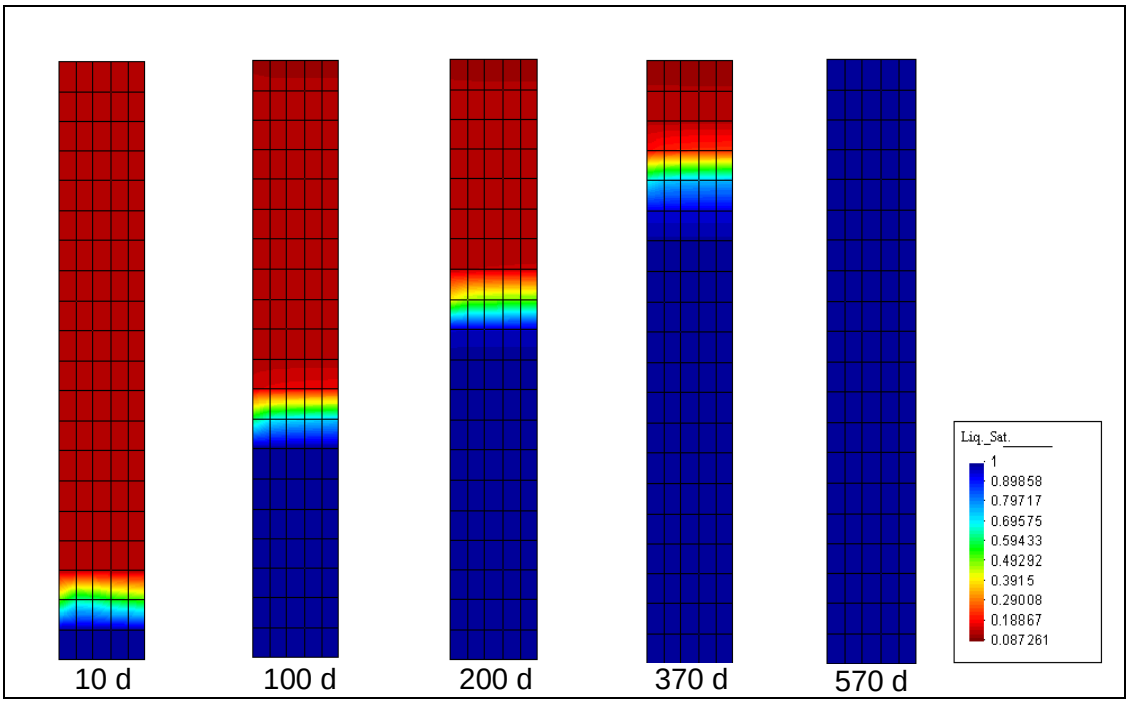

Fig. 3.11 Distribution of water saturation in the seal with 50/50 sand/bentonite ratio at an injection pressure of 1 MPa

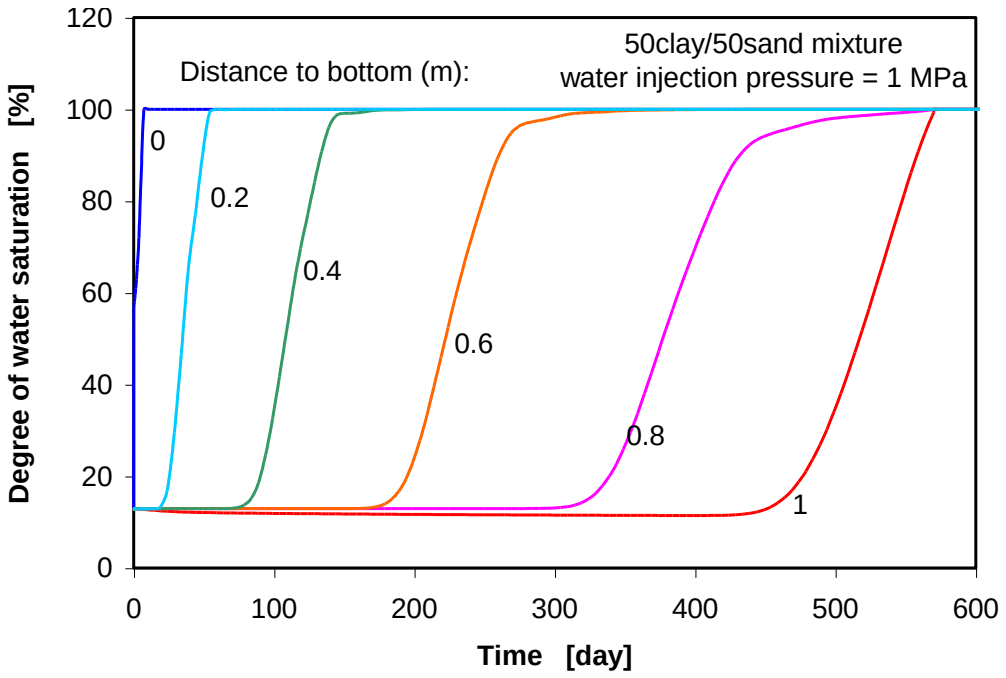

Fig. 3.12 Evolution of water saturation in the seal with 50/50 sand/bentonite ratio at an injection pressure of 1 MPa

Tab. 3.4 Time needed for a full saturation of the seals at different pressure

Sand/bentonite seal	**Injection pressure**	**[MPa]**	**0.0**	**0.2**	**0.5**	**1.0**
65/35	Time	[day]	380	300	240	170
50/50	Time	[day]	900	840	700	570

Fig. 3.13 and Fig. 3.14 show the evolution of pore water pressures at different locations in the seals. After full saturation, the water flux at the outlet was predicted for both seals at 1 MPa injection pressure to $\dot{Q}_w = 2.9 \cdot 10^{-4}$ ml/min for the seal with 35 % bentonite and to $\dot{Q}_w = 9.0 \cdot 10^{-5}$ ml/min for the sela with 50 % bentonite. To collect a water volume of 10 ml in a steady flow state, the time needed is about 25 days for the 35 % bentonite seal and 80 days for the 50 % bentonite seal.

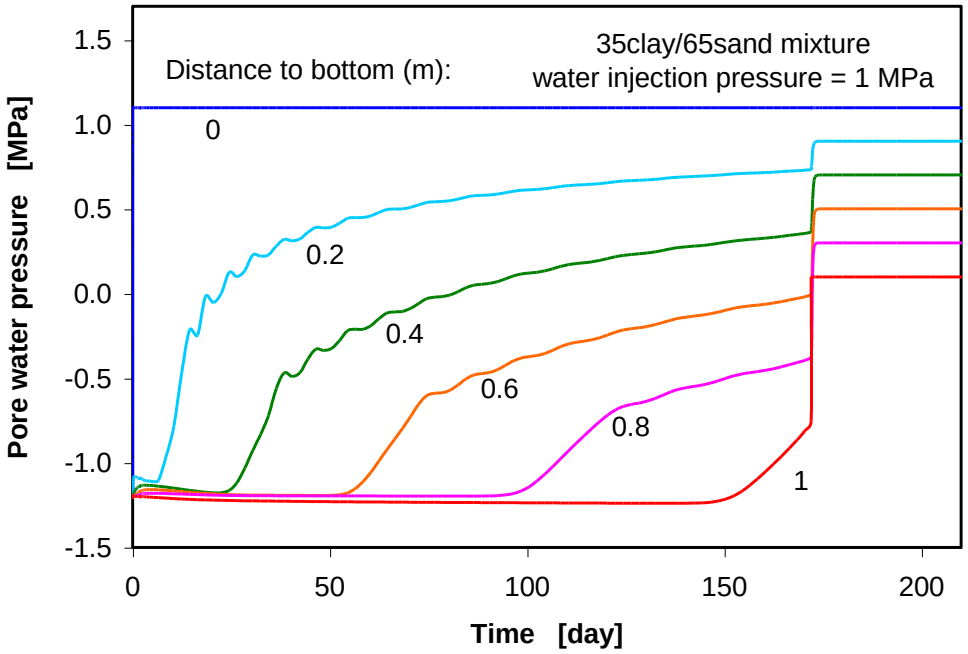

Fig. 3.13 Evolution of pore water pressure in the seal with 65/35 sand/bentonite ratio at an injection pressure of 1 MPa

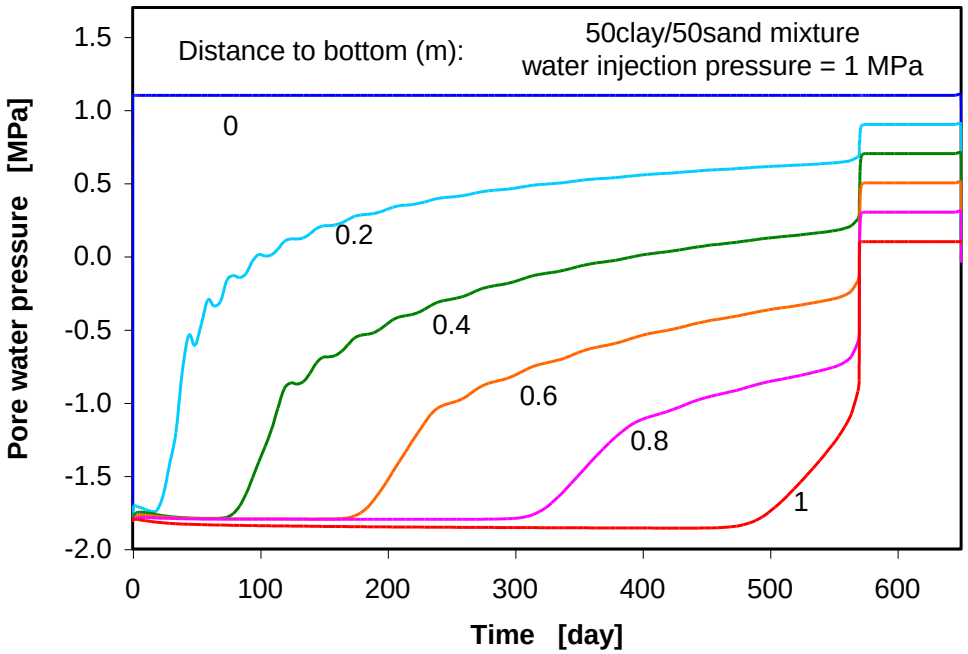

Fig. 3.14 Evolution of pore water pressure in the seal with 50/50 sand/bentonite ratio at an injection pressure of 1 MPa

Gas flow and gas break-through

Gas flow through the fully saturated seals was simulated by injecting dry gas at constant rate of 0.02 and 0.2 ml/min. Fig. 3.15 and Fig. 3.16 show the development of pore gas pressures in the seal with 65/35 sand/bentonite ratio during the gas injection with the constant injection rates, while the evolution of pore gas pressures in the seal with 50/50 sand/bentonite ratio is depicted in Fig. 3.17 and Fig. 3.18. It is obvious that the gas pressure at the bottom of the seals builds up rapidly and then more or less keeps constant until gas breaks through the initially saturated seals. The maximum gas pressure observed at the bottom is defined here as the gas break-through pressure. Slow gas injection generates a low gas entry/break-through pressure. The gas outflow after the gas break-through was predicted as well. Tab. 3.5 summarises the modelled results of gas break-through pressure, gas outflow rate, time needed until breaking and time needed for collecting a normal gas volume of 100 ml at the outlet after the gas break-through.

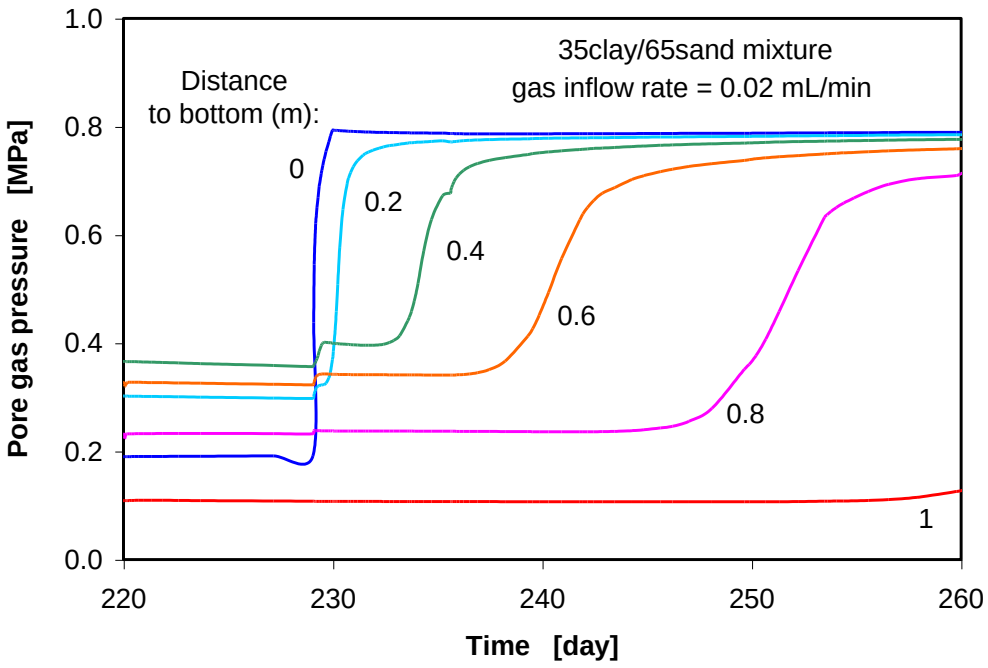

Fig. 3.15 Evolution of pore gas pressure in the seal with 65/35 sand/bentonite ratio during gas injection at an injection rate of 0.02 ml/min

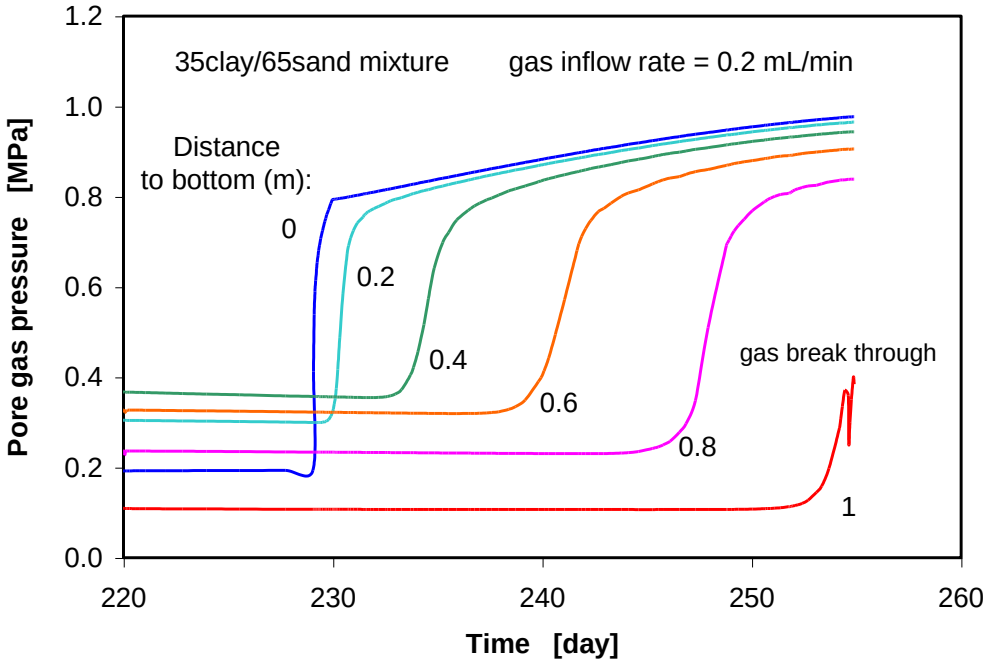

Fig. 3.16 Evolution of pore gas pressure in the seal with 65/35 sand/bentonite ratio during gas injection at an injection rate of 0.2 ml/min

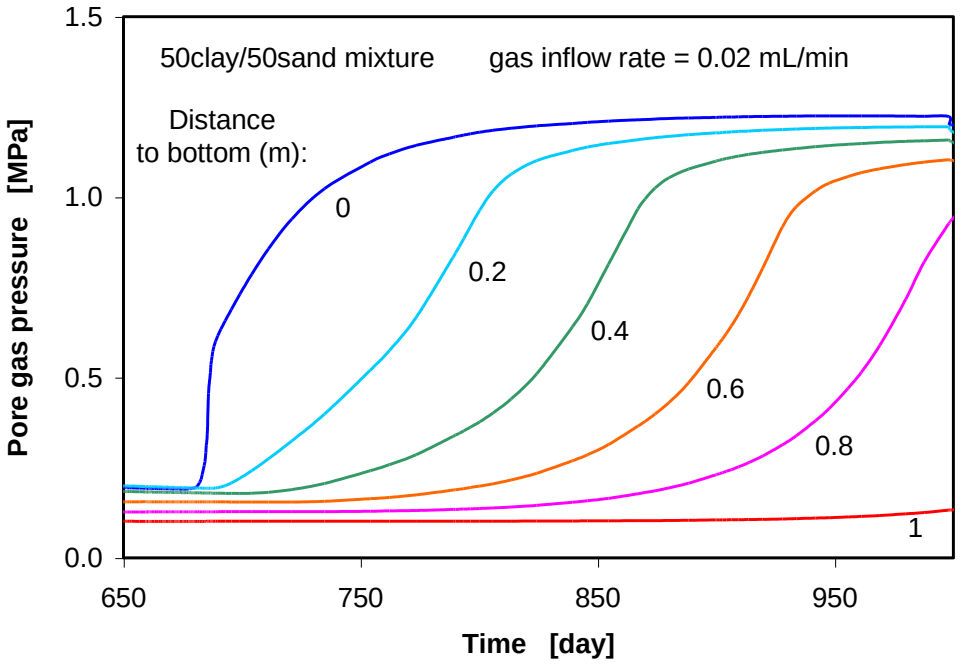

Fig. 3.17 Evolution of pore gas pressure in the seal with 50/50 sand/bentonite ratio during gas injection at an injection rate of 0.02 ml/min

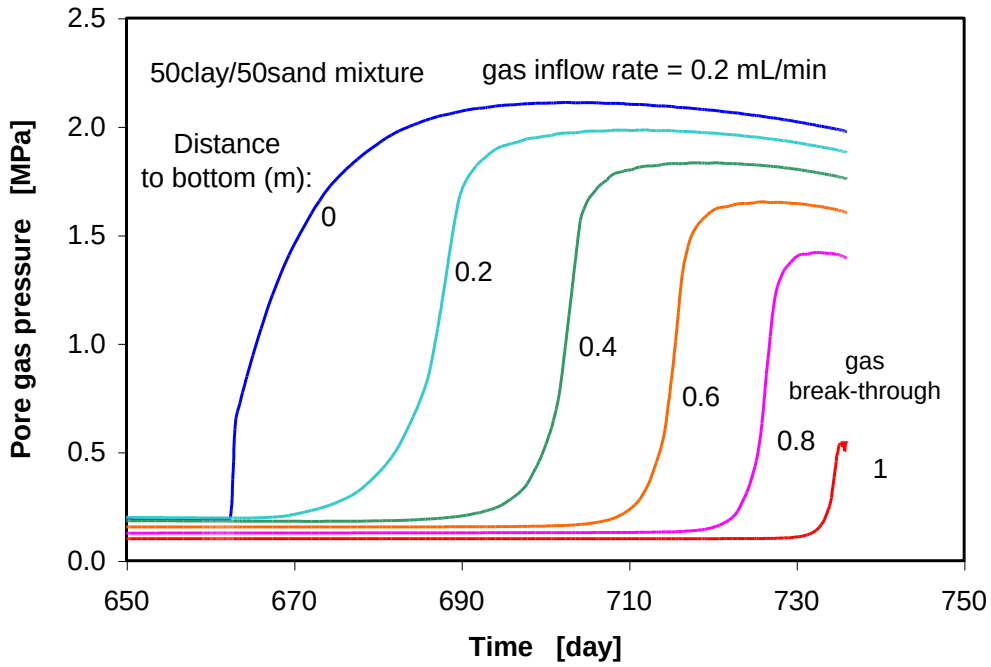

Fig. 3.18 Evolution of pore gas pressure in the seal with 50/50 sand/bentonite ratio during gas injection at an injection rate of 0.2 ml/min

Tab. 3.5 Gas break-through pressure and outflow rate after break-through

Sand/bentonite seal		**65/35**	**65/35**	**50/50**	**50/50**
Gas injection rate	[ml/min]	0.02	0.2	0.02	0.2
Gas break-through pressure	[MPa]	0.7	0.9	1.1	2.0
Gas outflow rate	[ml/min]	$4.3 \cdot 10^{-2}$	$9.6 \cdot 10^{-2}$	$1.4 \cdot 10^{-4}$	$6.6 \cdot 10^{-3}$
Time for gas break-through	[d]	35	25	340	80
Time for collecting 100 ml gas	[d]	1.6	0.7	198	10.5

The time for the gas break-through in the seal with 65/35 sand/bentonite ratio varies between 25 and 35 days, whereas the gas break-through in the seal with 50/50 sand/bentonite ratio occurs after 80 days at the injection rate of 0.2 ml/min and after about 1 year at the rate of 0.02 ml/min. To collect a normal gas volume of 100 ml at a steady state flow, the time needed is about 1 to 2 days for the seal with 65/35 sand/bentonite ratio and 10 to 200 days for the seal with 50/50 sand/bentonite ratio.

Total stress and swelling pressure

Fig. 3.19 and Fig. 3.20 illustrate the development of radial and vertical total stress in the seal with 65/35 sand/bentonite ratio during the whole test at a water injection pressure of 1 MPa and a gas injection rate of 0.02 ml/min, while the modelled results for the seal with 65/35 sand/bentonite ratio under the same conditions are shown in Fig. 3.21 and Fig. 3.22. In case of the tests without applying external loads, the total stress σ is taken to be the sum of the swelling pressure P_s induced by expansion of clay minerals and the pore water or gas pressure P_l or P_g. Comparing the resulting total stresses with the water saturation (Fig. 3.9/3.10 and Fig. 3.11/3.12) and the pore water pressure (Fig. 3.17 and Fig. 3.18), it can be seen that the total stresses increase with water saturation and pore water pressure. Fig. 3.19 and Fig. 3.20 and Fig. 3.21 and Fig. 3.22 show also that the radial total stress varies in dependence of location in the seal because of the water pressure gradient and the maximum is reached at the bottom. The vertical total stress is the same in the whole seal. After reaching full saturation, the water injection pressure is adjusted to be constant for measurement of the water permeability. In this phase, the total stress reaches the maximum level: $\sigma_{r\text{-}max} = \sigma_{v-max}$ = 1.6 MPa for the seal with 65/35 sand/bentonite ratio and for the seal with 50/50 sand/bentonite ratio $\sigma_{r\text{-}max} = \sigma_{v-max}$ = 2.4 MPa. At a water injection pressure of 0.5 MPa, the maximum total stress is lower: $\sigma_{r\text{-}max} = \sigma_{v-max}$ = 1.0 MPa for the seal with 65/35 sand/bentonite ratio and $\sigma_{r\text{-}max} = \sigma_{v-max}$ = 1.4 MPa for the seal with 50/50 sand/bentonite ratio.

In the third test phase, the water injection pressure is dropped down to zero to determine the pure swelling pressure, as depicted in Fig. 3.19 and Fig. 3.20 and Fig. 3.21 and Fig. 3.22. It can be seen that the resulting swelling pressure in radial direction depends on the location due to the variation of porosity, as shown in Fig. 3.23 and Fig. 3.24. The water saturation results in local swelling in a region near the water inlet, causing compaction in the remaining domain. The radial swelling pressure in the seal with 65/35 sand/bentonite ratio varies in a small range of 0.8 to 0.85 MPa, whereas the radial swelling pressure in the seal with 50/50 sand/bentonite ratio lies between 1.25 and 1.55 MPa. The vertical swelling pressure is independent on the location: $P_{s\text{-}v}$ = 1.0 MPa for the seal with 65/35 sand/bentonite ratio and $P_{s\text{-}v}$ = 1.5 MPa for the seal with 50/50 sand/bentonite ratio.

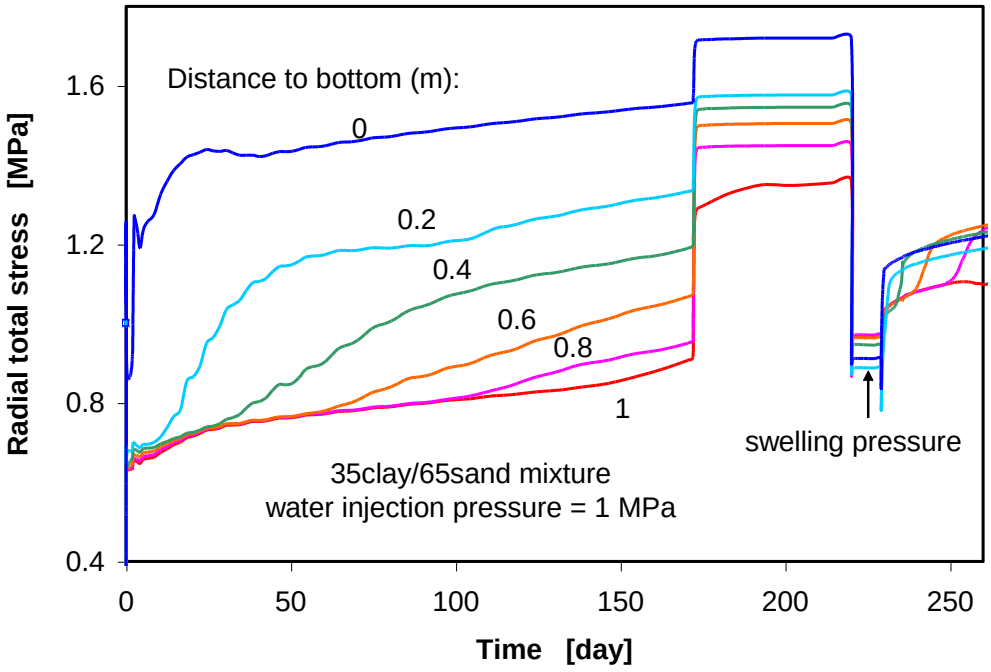

Fig. 3.19 Development of radial total stress in the seal with 65/35 sand/bentonite ratio at a water injection pressure of 1 MPa and a gas injection rate of 0.02 ml/min

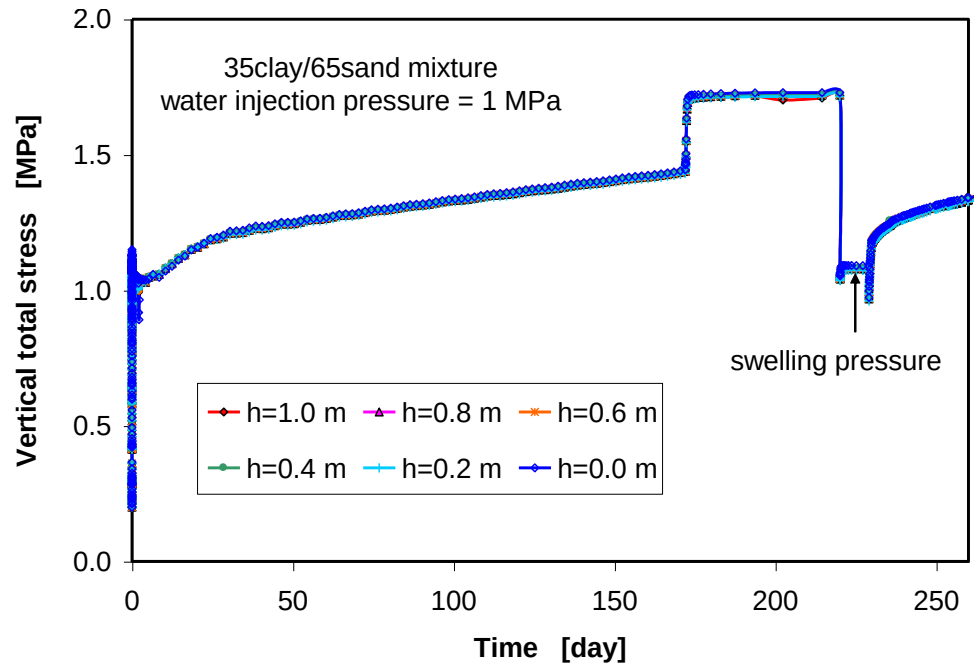

Fig. 3.20 Development of vertical total stress in the seal with 65/35 sand/bentonite ratio at water injection pressure of 1 MPa and gas injection rate of 0.02 ml/min

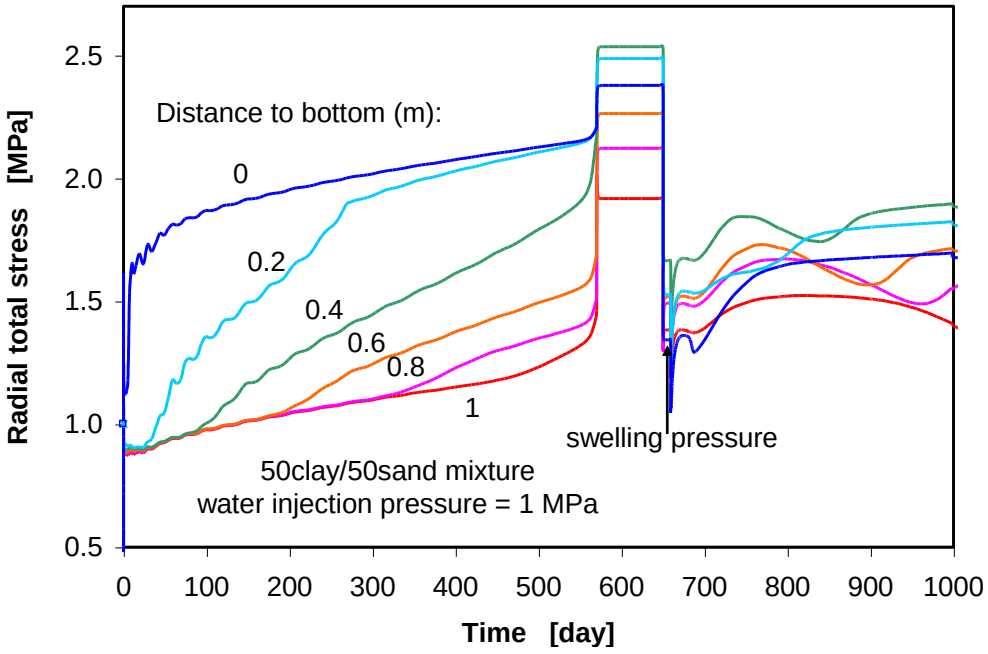

Fig. 3.21 Development of radial total stress in the seal with 50/50 sand/bentonite ratio at water injection pressure of 1 MPa and gas injection rate of 0.02 ml/min

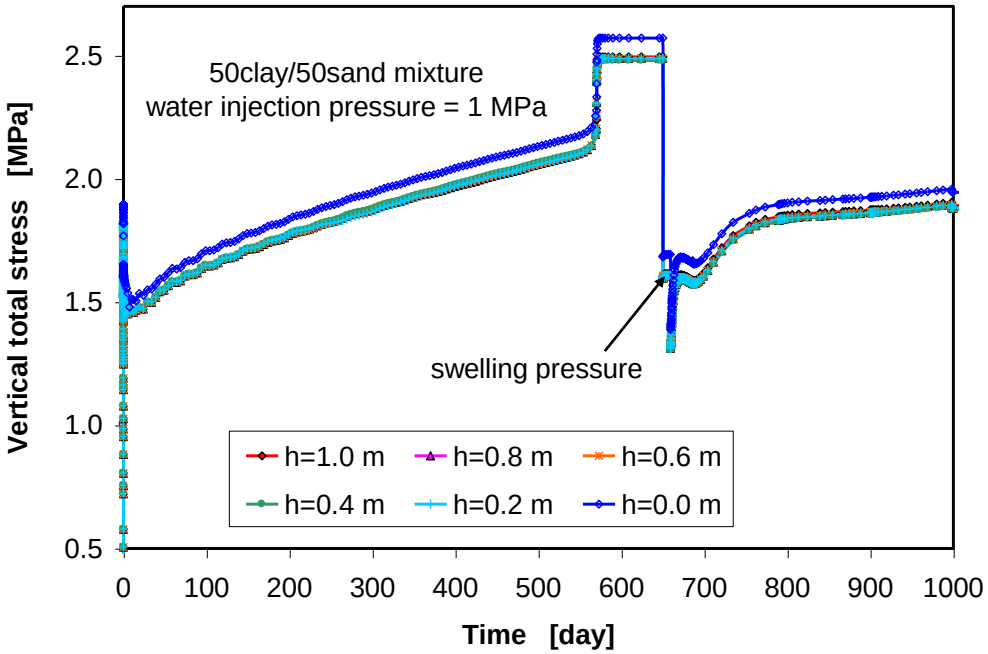

Fig. 3.22 Development of vertical total stress in the seal with 50/50 sand/bentonite ratio at a water injection pressure of 1 MPa and a gas injection rate of 0.02 ml/min

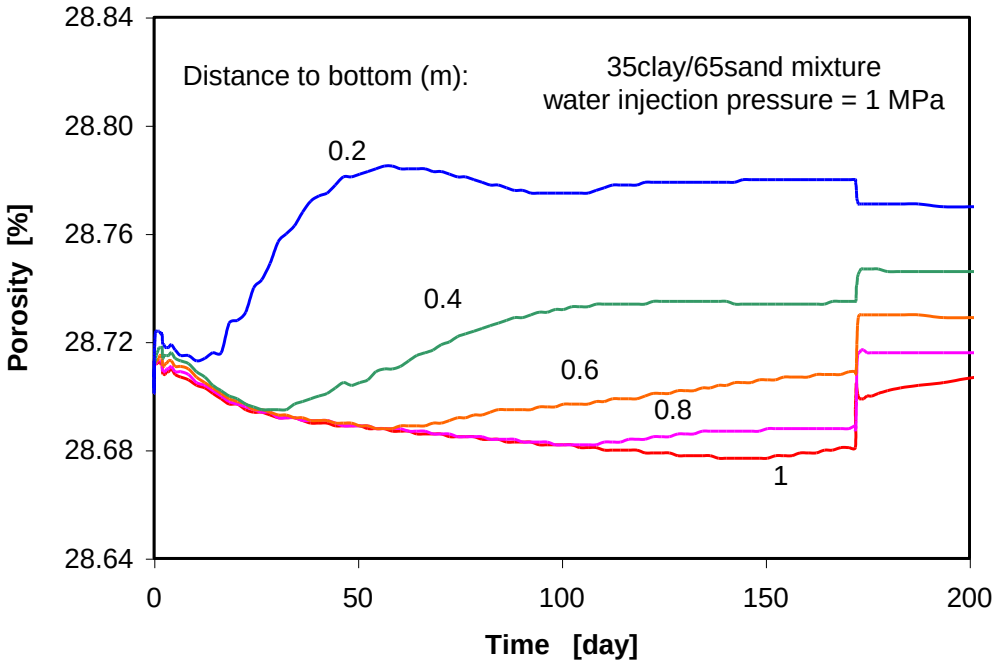

Fig. 3.23 Porosity change in the seal with 65/35 sand/bentonite ratio during water saturation at an injection pressure of 1 MPa

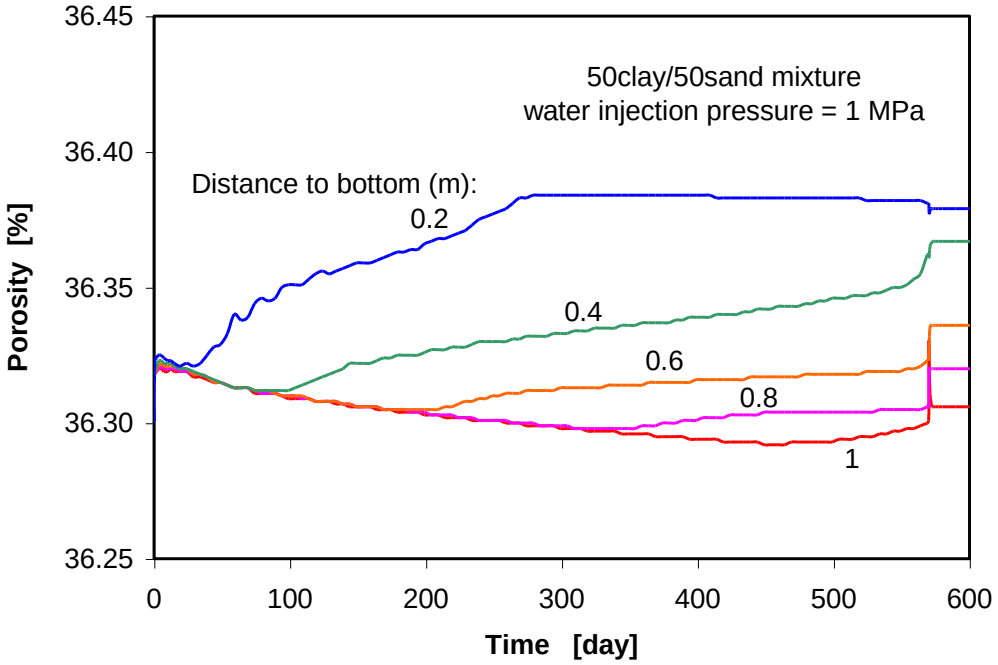

Fig. 3.24 Porosity change in the seal with 50/50 sand/bentonite ratio during water saturation at an injection pressure of 1 MPa

The total stress does not change significantly during the gas injection. The swelling pressure may reduce due to de-saturation in this phase. Therefore, the pore gas pressure may dominate the total stress.

3.5.1.3 Conclusions and recommendations for the mock-up tests

From the modelled results, the testing procedure and conditions were recommended for the mock-up tests and summarised in Tab. 3.6 with predictions of some important measuring parameters and testing durations. To avoid possible fracturing of the host rock during water injection to the seals in the in-situ experiment and also to minimise possible perturbations of the seal, the injection pressure was planned to be limited to below 1 MPa. An additional reason for the low injection pressures was that the groundwater pressure acting on seals in the clay formations during the saturation phase was assumed to be very low. To investigate the effect of the water injection pressure on the saturation time, water injection pressures of 0.5 and 1 MPa were planned to be applied in the mock-up tests. The modelled swelling pressures of 0.5 to 1.5 MPa are overestimated for both sand/bentonite mixtures in comparison with the preliminary test results of 0.2 to 0.5 MPa. Therefore, the total stress of 2.4 MPa calculated for Test 4 with a sand/bentonite ratio of 50/50 could be lower in reality. In Test 2 on the seal with 50/50 sand/bentonite ratio, the high gas injection rate of 0.2 ml/min could cause a high gas entry/break-through pressure of 2 MPa. Under consideration of the maximum permitted pressure of 1.6 MPa for the steel tube, it was thus necessary that the water injection pressure, the build-up of gas pressure and the total stress on the tube wall were monitored and controlled to maintain them below the allowed limits of the testing system during the whole test procedure.

The prediction suggested that the tests with the sand/bentonite ratio of 65/35 could be finished within 1 year, whereas the conduction of the tests with 50/50 sand/bentonite ratio could need about 3 years. To reduce the testing duration with the 50/50 sand/bentonite ratio, it was concluded to reduce the seal length to 0.5 m. In this case, all the tests were assumed to be finished within 2 years.

Tab. 3.6 Prediction of the mock-up tests

Mock-up test	**Test 1**	**Test 2**	**Test 3**	**Test 4**
Tube type	Type 1	Type1	Type 2	Type 2
Sand/bentonite ratio	65/35	50/50	65/35	50/50
Phase 1: Water saturation of the unsaturated seals				
Water injection pressure [MPa]	0.5	0.5	1.0	1.0
Saturation time [day]	240	700	170	570
Phase 2: Water through the saturated seals				
Water injection pressure [MPa]	0.5	0.5	1.0	1.0
Maximum total stress [MPa]	1.0	1.4	1.6	2.4
Water outflow rate [ml/min]	$1.5 \cdot 10^{-4}$	$4.5 \cdot 10^{-5}$	$2.9 \cdot 10^{-4}$	$9.0 \cdot 10^{-5}$
Time for 10 ml water [day]	50	160	25	80
Phase 3: Determination of swelling pressure				
Water injection pressure [MPa]	0.0	0.0	0.0	0.0
Swelling pressure [MPa]	0.7 – 0.9	0.5 – 1.2	0.8 – 1.0	1.2 – 1.5
Time [day]	15	15	15	15
Phase 4: Gas injection through the saturated seal				
Gas injection rate [ml/min]	0.2	0.2	0.02	0.02
Break-through pressure [MPa]	0.9	2.0	0.7	1.1
Gas outflow rate [ml/min]	$9.6 \cdot 10^{-2}$	$6.6 \cdot 10^{-3}$	$4.3 \cdot 10^{-2}$	$1.4 \cdot 10^{-4}$
Time until gas break [day]	25	80	35	340
Total testing time [day]	330	955	245	1005

3.5.2 In-situ experiments

The scoping calculations for the in-situ experiments were necessary to gain a first estimation of initial and boundary conditions, the water and gas injection pressures as well as for an assessment of the duration of the experiments. Due to excavation and ventilation of the SB-niche, the hydro-mechanical state of the surrounding rock is disturbed. Additionally, hydro-mechanical interactions between the boreholes drilled down from the floor of the SB-niche may play an important role. In situ, coupled hydro-mechanical processes will not only occur in the seals but also in the surrounding rock during injection of water and gas to the seals. The theoretical considerations and constitutive models used were already presented in Section 3.1.

3.5.2.1 Numerical model

Regarding the envisaged layout of the boreholes in the test niche at the MTRL (Fig. 1.1), a 2D plane strain model in a plane normal to the axis of the SB-niche was adopted by axisymmetric geometry. The modelling region extends by 40 m x 40 m. The lower and upper boundary are located at distances of -20 m and +20 m from the niche floor, respectively. In the model the test niche is 2.5 m wide and 5 m high. A test borehole of 300 mm in diameter is drilled from the niche floor down to 3 m depth. The borehole axis is located 1 m distant to the niche wall. The borehole is filled sequentially from the bottom with sand representing the injection chamber of 0.3 m height, one of the selected sand/bentonite mixtures as seal of 1 m height, one sintered filter of 10 mm thickness, one packer of 1 m height and concrete of 0.7 m to seal the upper part of the borehole. Fig. 3.25 shows the finite element mesh, the boundary conditions and the different materials installed in the borehole in detail.

In the model, the materials were assumed homogeneous and isotropic. Both sand/bentonite mixtures with bentonite contents of 35 % and 50 % were considered in the calculations. The average properties and parameters of the materials given in Tables 3.1, 3.2, and 3.3 were adopted. Because of a lack of data for the injection chamber, packer and concrete, the properties and mechanical parameters of the clay rock were assumed for them. A high permeability of 10^{-12} m^2 was applied to the injection chamber, while the packer was assumed impermeable. Such simplifications are considered acceptable for the purpose of the scoping calculations focusing on hydro-mechanical processes in the seal and surrounding rock.

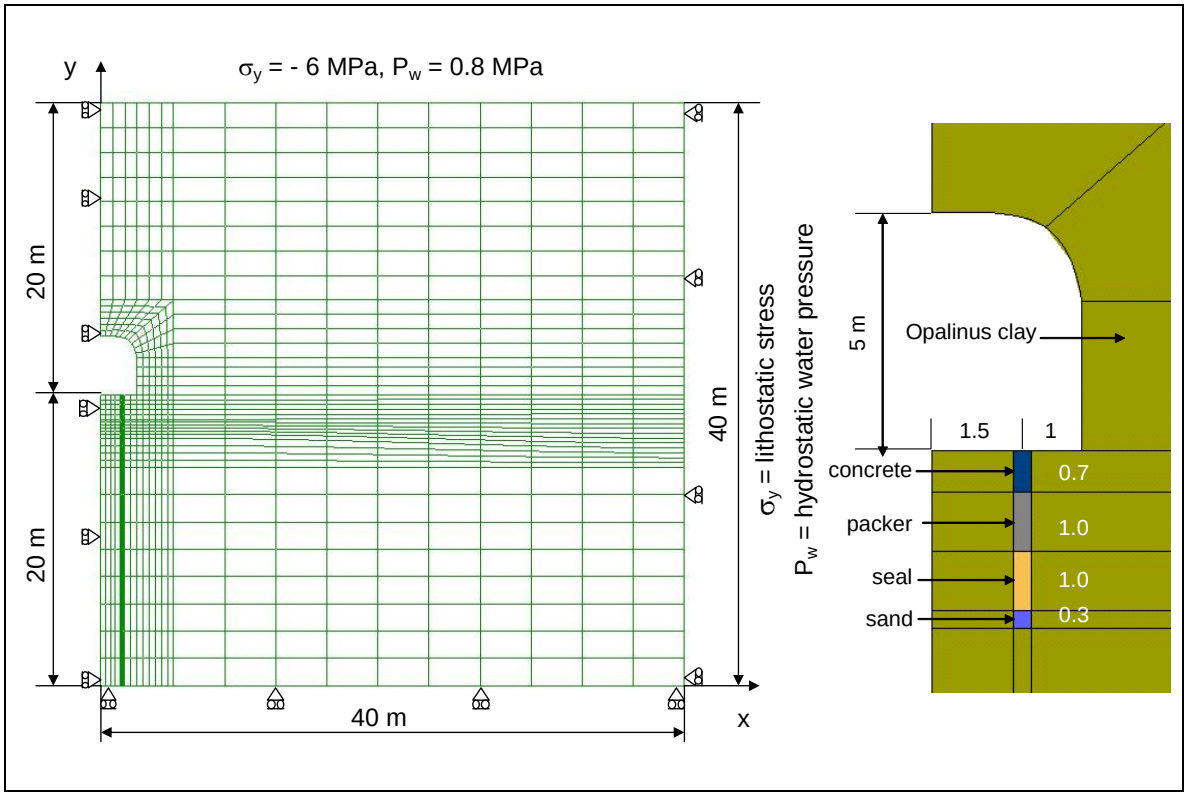

Fig. 3.25 Numerical model and materials considered in the scoping calculations

In the calculations, the prevailing in-situ conditions at the MTRL were taken into account. The temperature in the rock and in the niche is 17 °C for the initial state. A vertical total stress of 6 MPa applied on the top boundary and the gravity effect result in an initial vertical total stress equal to 6.48 MPa at the level of the niche floor (y = 0). Assumption of the ratio K_o = 0.77 of effective horizontal stress ($\sigma'_x = \sigma_x - P_w$) to vertical stress ($\sigma'_y = \sigma_y - P_w$) leads to an initial total horizontal stress of 5.2 MPa at the floor level. A water pressure of 0.8 MPa supplied to the top boundary and its hydrostatic distribution in the modelling region result in an initial pore water pressure of 1.0 MPa at the floor level. The atmospheric pressure of 0.1 MPa was taken as the initial gas pressure. Flow of water and gas through the other boundaries is not allowed.

According to the envisaged test procedure the following steps were simulated by applying suitable conditions:

Step 1: Excavation and ventilation of the test niche for 180 days to estimate hydro-mechanical state in the surrounding rock, by applying (1) null supporting stress on the niche wall to simulate the niche excavation, and (2) gas flowing along the niche wall with relative humidity of 85 % (gas density

ρ_g = 1.194 kg/m^3, vapour mass fraction ω_g^w =1.005 %) and the turbulence coefficient of 10^{-4} m/s to simulate the niche ventilation.

Step 2: Drilling and ventilation of the test borehole for 8 days to examine changes of the hydro-mechanical state in the surrounding rock, by applying (1) null supporting stress on the borehole wall to simulate the drilling, and (2) gas flowing along the borehole with relative humidity of 85 % to simulate the ventilation.

Step 3: Installation of the sand, seal, packer and concrete into the test borehole for 2 days by applying an initial stress of σ_{1o} = σ_{2o} = σ_{3o} = 0.1 MPa to them to represent the compaction effect on the materials.

Step 4: Water injection into the initially unsaturated seal to determine the evolution of saturation and the time needed for full saturation by applying a constant water pressure of 0.5 or 1 MPa to the lower porous chamber.

Step 5: Gas injection into the saturated seal to determine its gas entry/break-through pressure and gas outflow by applying a constant gas injection rate of 0.2 ml/min to the lower porous chamber.

3.5.2.2 Modelling results

3.5.2.2.1 Perturbations in the clay rock induced by excavation and ventilation

Mechanical aspect

After the niche excavation, the horizontal stress relaxes in a zone around the niche whereas the vertical stress concentrates in a zone near the niche wall. Fig. 3.26 shows the distributions of the horizontal and vertical stresses 180 days after excavation. The redistribution of the stresses causes convergence of the niche. The radial displacement of the wall reaches 7.5 mm, while the roof drops down by 6.7 mm and the floor rises up by 7.1 mm, as shown in Fig. 3.27. The envisaged location of the borehole seems to be less disturbed before drilling.

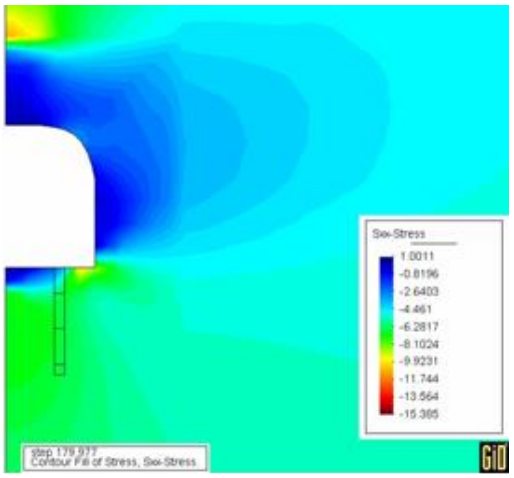

a) horizontal total stress

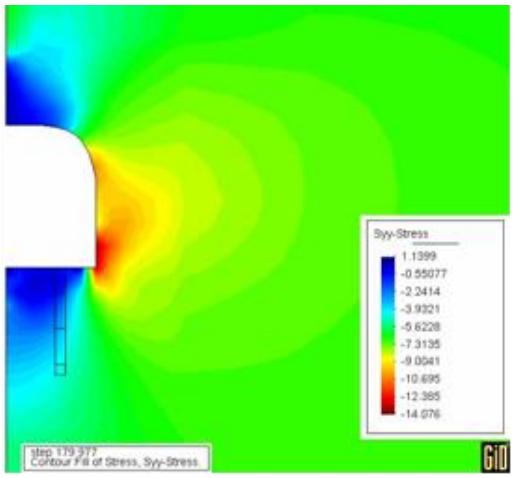

b) vertical total stress

Fig. 3.26 Distributions of total stresses 180 days after excavation of the SB-niche

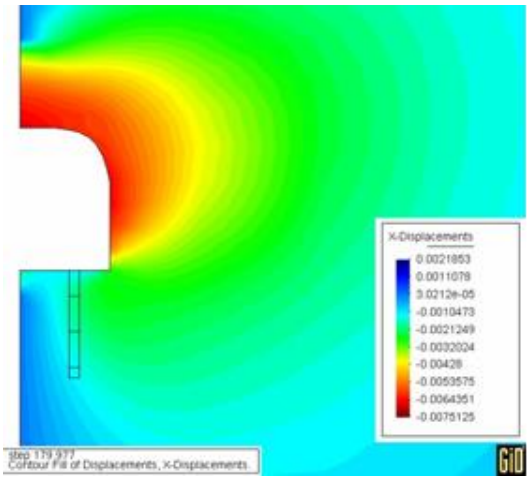

a) horizontal displacement

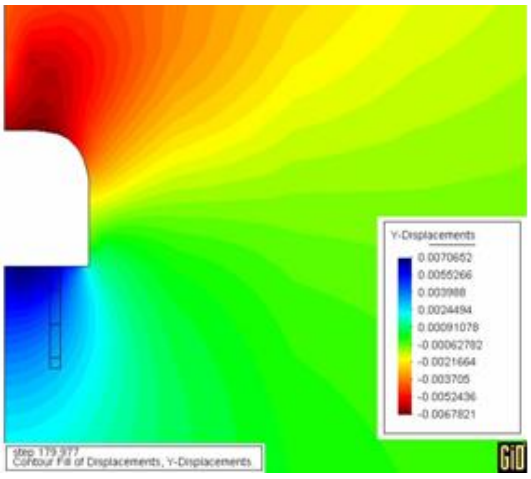

b) vertical displacement

Fig. 3.27 Displacement distributions 180 days after excavation of the SB niche

Six months later after the niche excavation, a borehole is drilled from the niche floor down to 3 m depth. The borehole excavation results in an additional perturbation of the mechanical state in the surrounding rock. Fig. 3.28 shows the stress distributions 8 days after drilling, whereas the displacement of the rock is illustrated in Fig. 3.29. The borehole drilling generates a relaxation of the radial stress around the borehole and contrastively a concentration of the vertical stress at the corner of the borehole bottom. The resulting convergence of the borehole reaches about 10 mm. It should be noticed

that the modelled convergence of the borehole may be overestimated because the borehole is modelled as an infinite cut along the niche axis (Fig. 3.25) and hence the support effect of the surrounding rock is eliminated in the calculations. This is not a very realistic case.

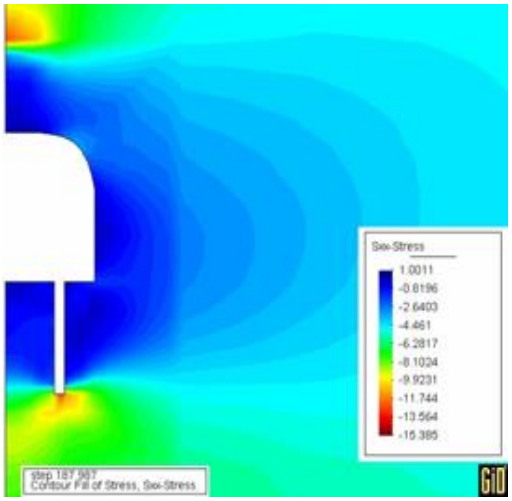

a) horizontal total stress

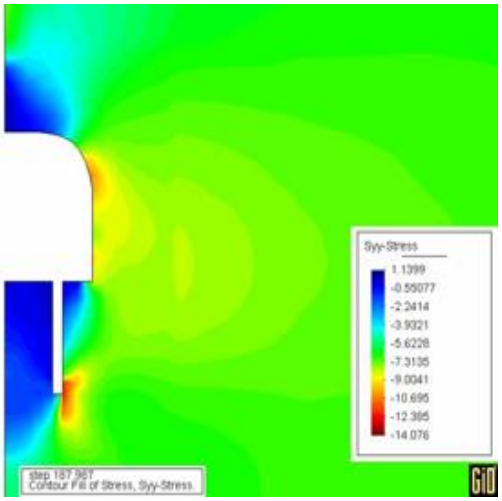

b) vertical total stress

Fig. 3.28 Distributions of total stresses 8 days after drilling of SB borehole

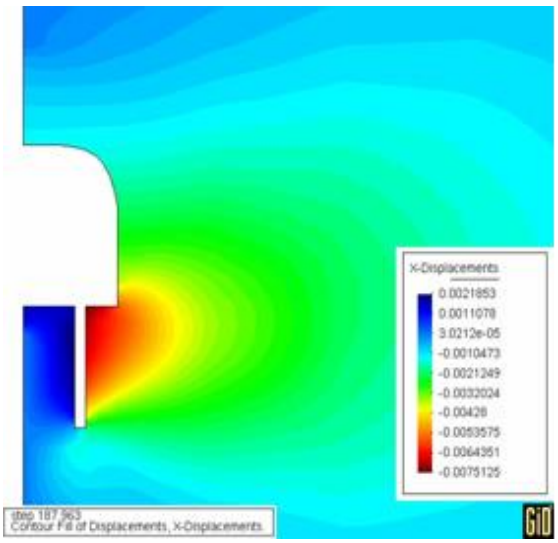

a) horizontal displacement

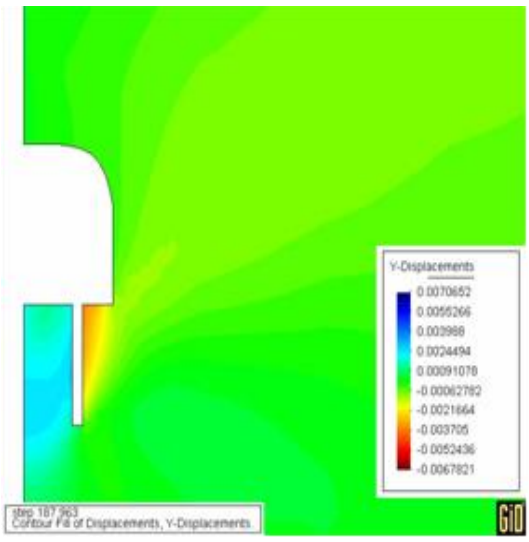

b) vertical displacement

Fig. 3.29 Displacement Distributions 8 days after drilling of the SB-borehole

Hydraulic aspect

The hydraulic response of the rock mass to excavation and ventilation of the niche and borehole is shown in Fig. 3.30. Just after the niche excavation, the porosities in the zones over the roof and under the floor of the niche expand somewhat due to the stress relaxation (Fig. 3.26, Fig. 3.27). This induces a sudden reduction of the pore water pressure even to a negative value (suction) of -1 MPa. In contrast to this, the highly concentrated stress near the lower corner compresses the material and hence generates a high pore water pressure up to 6 MPa, which is close to the minor principal component of the stress. During the ventilation with air of relative humidity of 85 %, the pore water pressure reduces steadily. Six months later, the zone with negative pore water pressure extends to about 1 m from the niche wall into the rock mass. The borehole drilling induces an additional dilatancy of the surrounding rock and hence a higher reduction of the pore water pressure.

Due to excavation and ventilation of the niche and borehole, the surrounding rock is de-saturated. Fig. 3.31 shows the distribution of water saturation in the surrounding rock at the end of the borehole drilling and ventilation. The de-saturated zone with water saturation less than 95 % is limited in 0.5 m to the niche wall. The de-saturation which is mainly caused by the dilatancy of the clay rock is not significant.

3.5.2.2.2 Water saturation and flow

After the installation of the seal into the borehole, the water injection phase is simulated by applying a water pressure of 0.5 or 1 MPa to the lower porous injection chamber. Fig. 3.32 and Fig. 3.33 illustrate the evolution of water saturation at some selected points in both the 65/35 and 50/50 seals at an injection pressure of 1 MPa. The seals are saturated from the bottom to the top. The time needed for full saturation at 1 MPa injection pressure is about 10 months for the 65/35 sand/bentonite mixture and 28 months for the 50/50 mixture, which is longer than the saturation times of 6 and 19 months predicted for the mock-up tests (Section 3.5.1.2). When a lower water injection pressure of 0.5 MPa is applied, the saturation phase in the in-situ experiment will last longer. The calculation resulted in 13 and 35 months for the 65/35 and the 50/50 seals, respectively. Because the permeabilities of the seals are higher than that of the surrounding clay rock (EDZ was not simulated here), the water flow occurs mainly through the seal as shown in Fig. 3.34, in which the pattern of the water flow through the 65/35 sand/bentonite seal and the surrounding rock is illustrated.

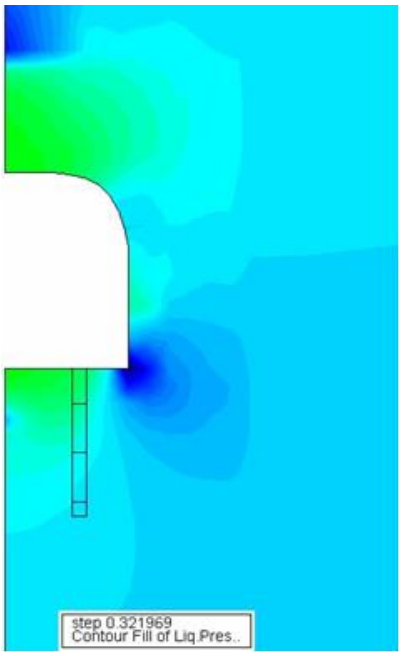

a) just after niche excavation

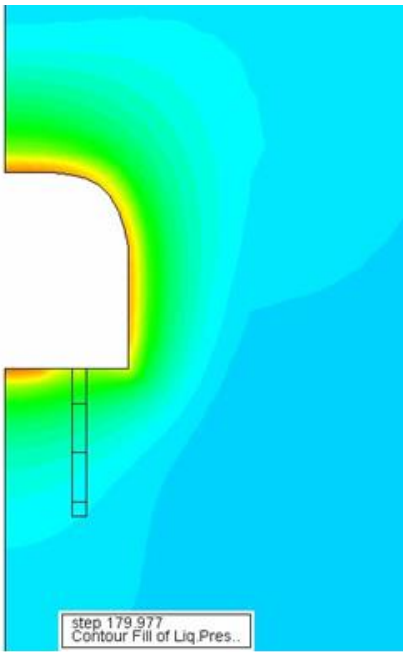

b) 180 days after niche excavation

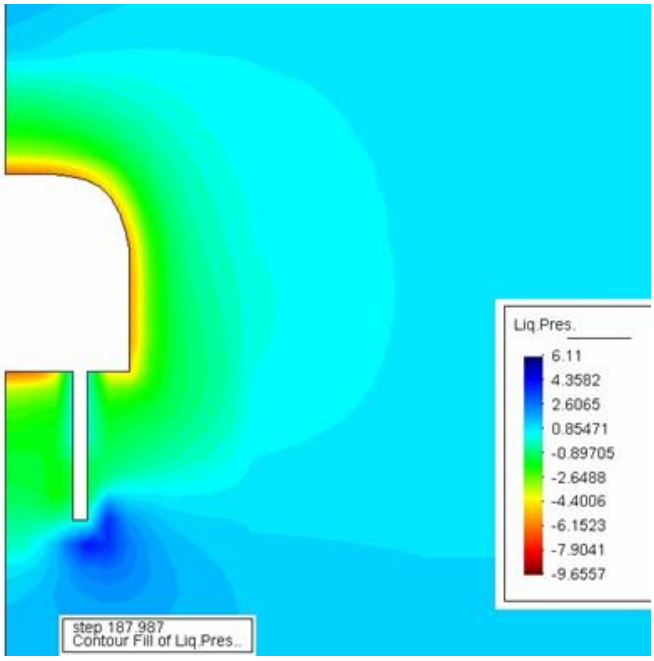

c) 8 days after borehole drilling

Fig. 3.30 Redistribution of pore water pressure in the surrounding rock induced by excavation and ventilation of SB niche and borehole

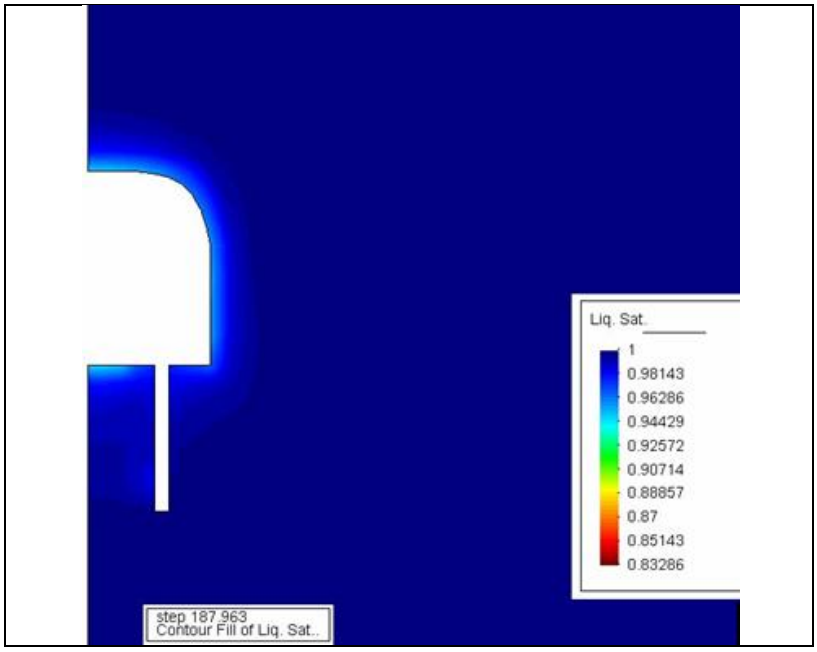

Fig. 3.31 Distribution of water saturation in the surrounding rock

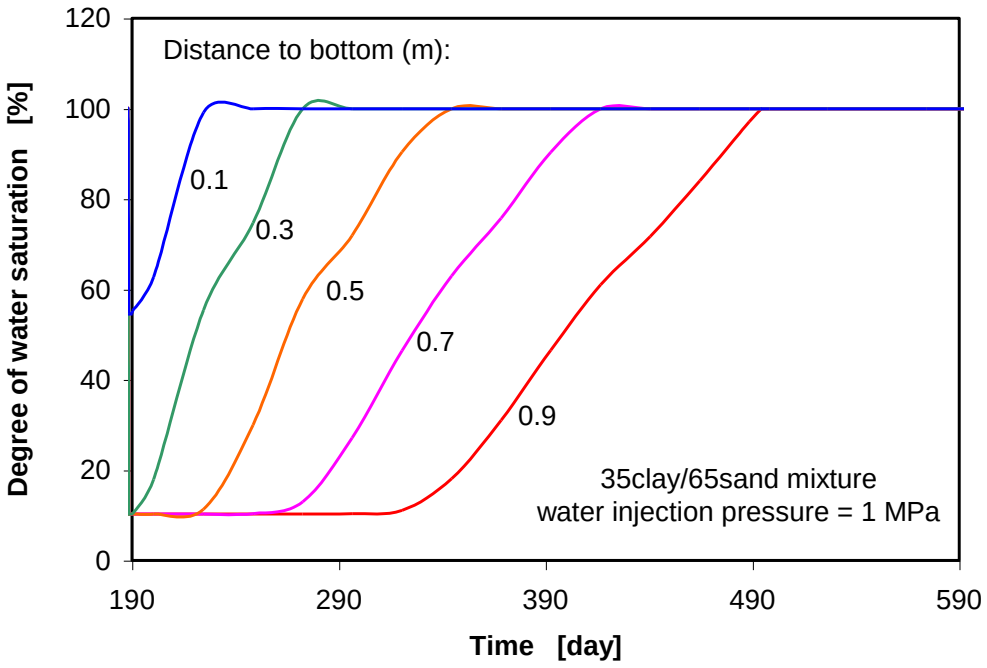

Fig. 3.32 Evolution of water saturation in the 65/35 sand/bentonite seal at an injection pressure of 1 MPa

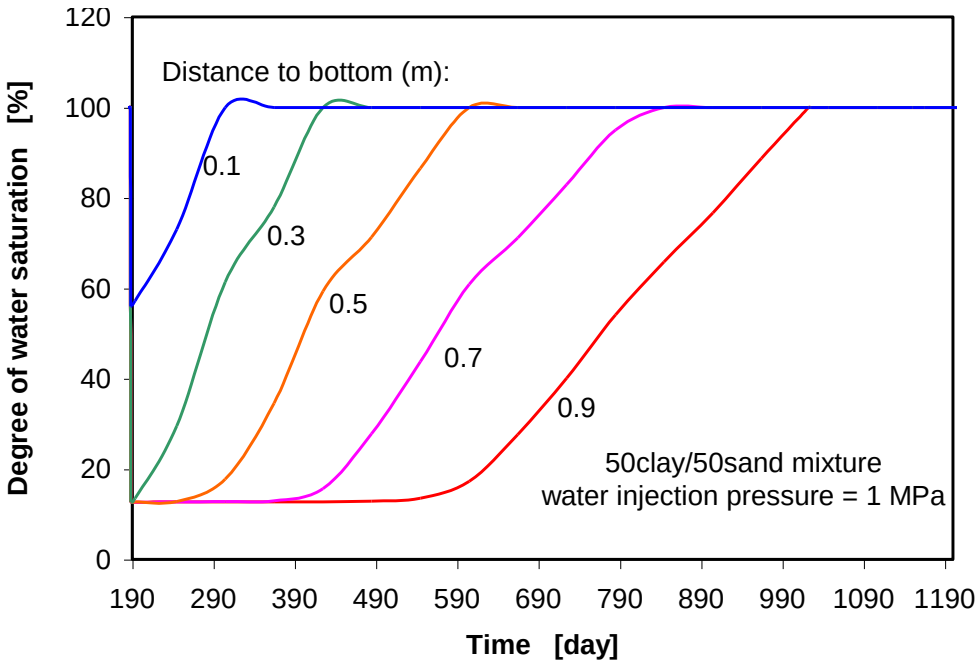

Fig. 3.33 Evolution of water saturation in 50/50 sand/bentonite seal at an injection pressure of 1 MPa

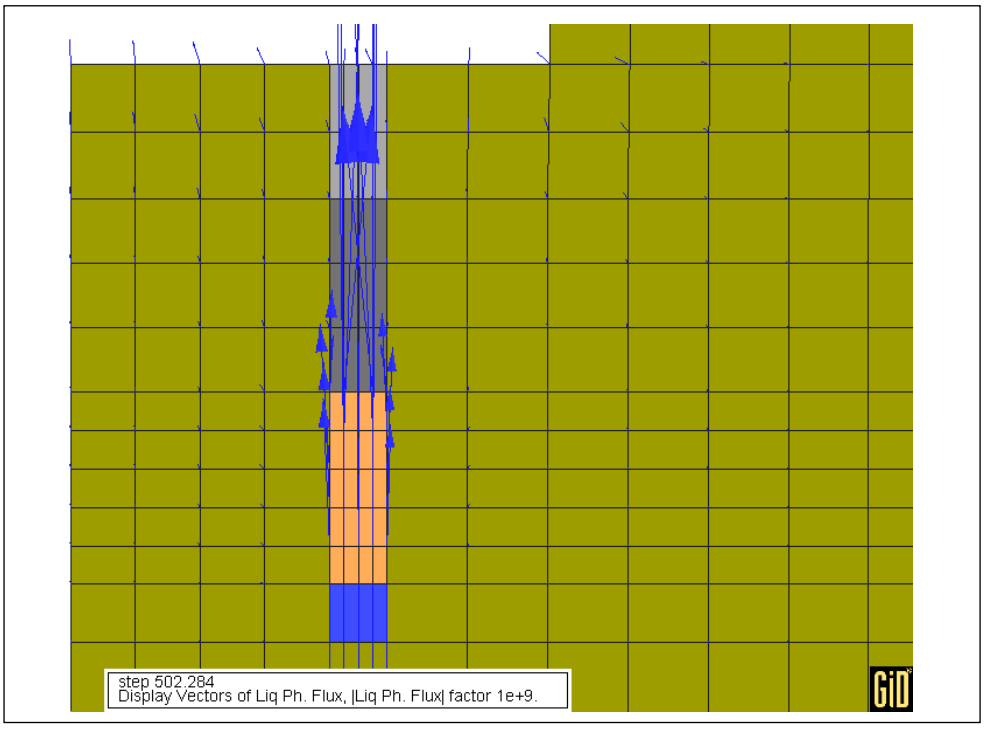

Fig. 3.34 Water flow through the rock-seal system (65/35 sand/bentonite ratio)

After reaching steady state flow, the water outflow rate and the time needed for collecting a water volume of 10 ml are predicted for both sand/bentonite seals for the different injection pressures. The results are summarised in Tab. 3.7.

Tab. 3.7 Modelling results for the water injection phase in the in-situ experiment

Sand/bentonite seal	**65/35**	**65/35**	**50/50**	**50/50**
Water injection pressure [MPa]	0.5	1.0	0.5	1.0
Water outflow after saturation [ml/min]	$4.5 \cdot 10^{-5}$	$9.4 \cdot 10^{-5}$	$1.3 \cdot 10^{-5}$	$6.6 \cdot 10^{-3}$
Time for full saturation [d]	400	300	830	1050
Time for collecting 10 ml water [d]	150	75	530	230
Total time for water injection phase [d]	550	375	1260	1280

3.5.2.2.3 Gas entry/break-through pressure and flow

Gas injection into the saturated seals was simulated by applying a constant gas inflow rate of 0.2 ml/min to the lower porous chamber. Fig. 3.35 and Fig. 3.36 show the evolution of the gas pressure at the entry face and the gas outflow rate at the outlet face of the 65/35 sand/bentonite and 50/50 sand/bentonite seals. With continuous gas injection, the gas pressure at the entry face builds up until a gas break-through occurs. After the peak point, the gas pressure reduces somewhat and the gas outflow increases further up to a maximum and remains relatively constant. However, for the 50/50 seal the gas break-through occurs later after the peak gas pressure. Generally, the pattern of the computed gas pressure is similar as the laboratory observation on the sand/bentonite mixtures presented in Section 2.2.2. But the significant peak behaviour of the gas outflow observed in the tests is not well represented in the calculations. The calculated gas entry/break-through pressure is about 0.7 MPa for the 65/35 sand/bentonite seal and 1.6 MPa for the 50/50 seal at a gas inflow rate of 0.2 ml/min. The time until the gas break-through is about 5 days for the 65/35 sand/bentonite seal and 30 days for the 50/50 seal. Fig. 3.37 indicates that the gas migration occurs mainly through the saturated seals, but not or only very limited through the surrounding rock.

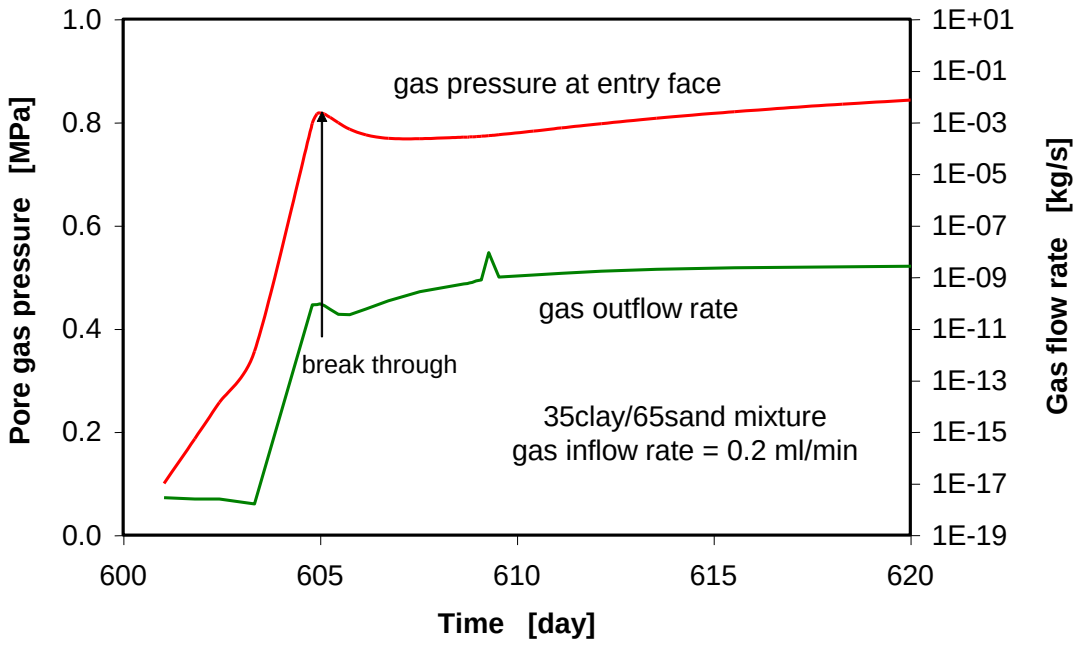

Fig. 3.35 Evolution of gas pressure at the entry face and gas outflow rate of the 65/35 sand/bentonite seal

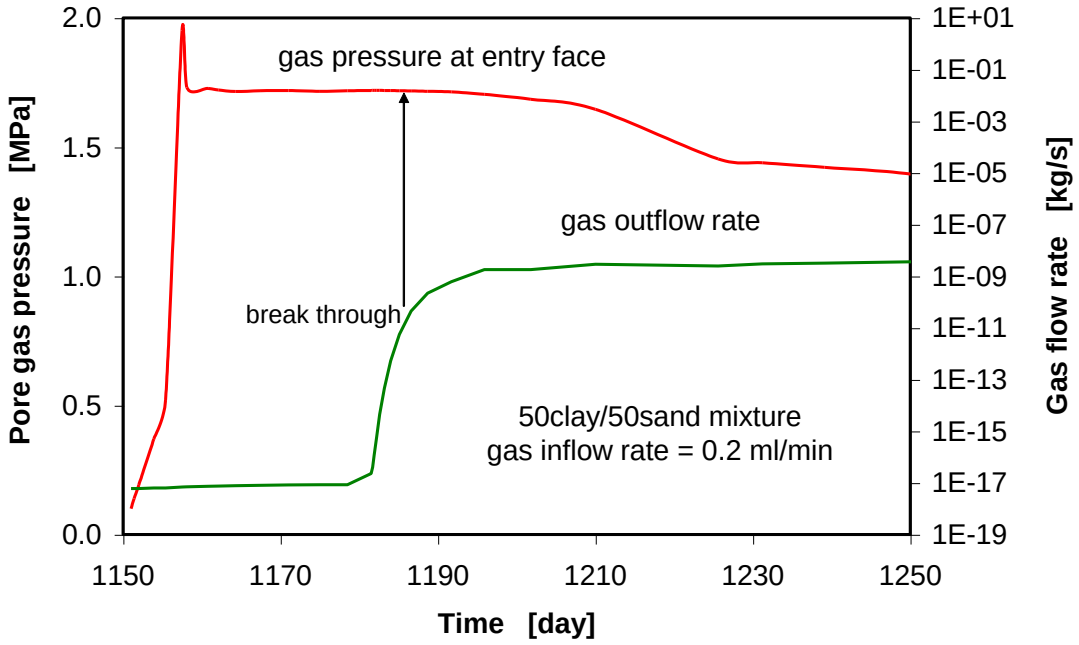

Fig. 3.36 Evolution of gas pressure at the entry face and gas outflow rate of the 50/50 sand/bentonite seal

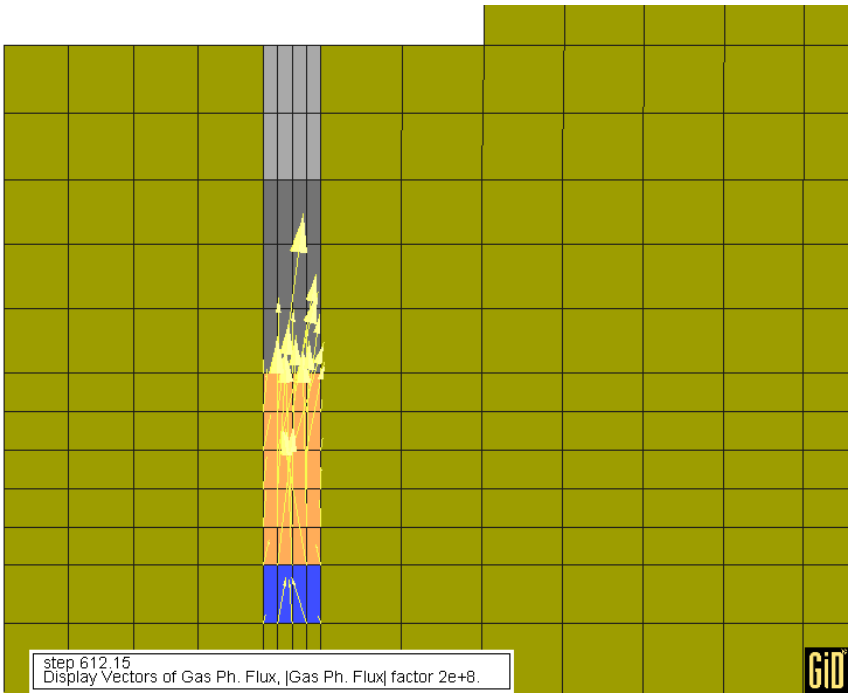

Fig. 3.37 Gas migration through the rock-seal system (65/35 sand/bentonite ratio)

3.5.2.2.4 Total stress and porosity

Fig. 3.38 shows the evolution of total stresses and porosity near the bottom boundary of the 65/35 sand/bentonite seal during the water injection at 1 MPa pressure, whereas the modelling results for the 50/50 seal are illustrated in Fig. 3.39. From the figures it can generally be seen that (a) the horizontal and vertical stresses increase due to a coupling effect of the applied water injection pressure, the resulting swelling pressures of the seals and also the clay rock and (b) the porosity increases first with water saturation, then decreases with compaction caused by swelling of other parts of the seal and the surrounding rock, and finally remains relatively constant. It should be noted that the periodical changes of the stresses may be caused by application of unsuitable values of error tolerances to achieve a calculation convergence for the very complete modelling steps.

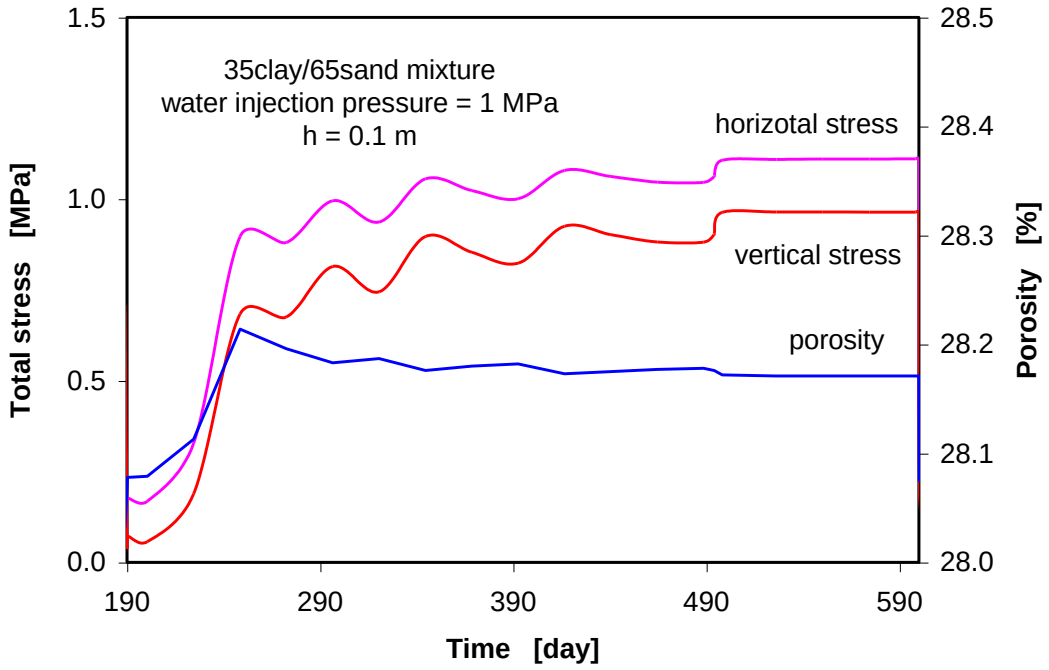

Fig. 3.38 Evolution of total stresses and porosity near the bottom and top of the 65/35 sand/bentonite seal

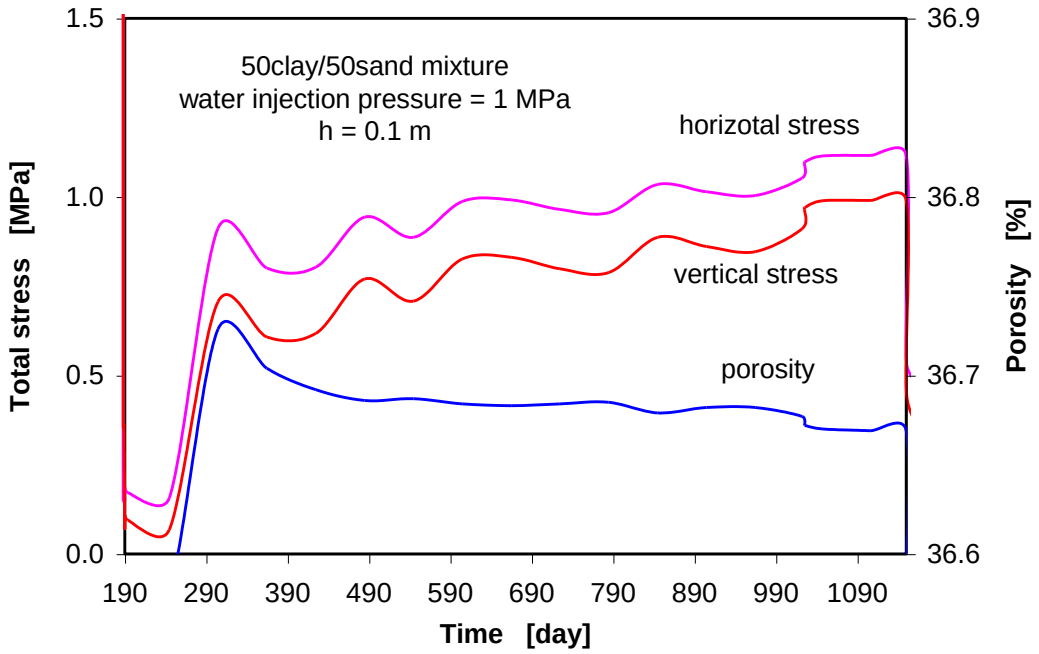

Fig. 3.39 Evolution of total stresses and porosity near the bottom and top of the 50/50 sand/bentonite seal

3.5.2.3 Conclusions and recommendations for the in-situ experiment

From the scoping calculations the following conclusions and recommendations for the in-situ experiment can be drawn:

- The hydro-mechanical state of the clay rock is disturbed by the excavation and ventilation of the test niche. Because any material damage process could not be modelled with the used version of CODE_BRIGHT, the development of the excavation disturbed zone (EDZ) around the niche and its impact on the hydraulic conductivity could not be identified from the modelling results. On the basis of in-situ observations in the MTRL /BOS 02/, the extension of the EDZ consisting of an air-filled fracture network around the SB-niche is probably limited to about 1 m and a plastically deformed outer zone to about 2 m. This leads to a maximum ratio of the EDZ extension to the drift radius of about 1. The permeability of the EDZ in the MTRL was measured between 10^{-17} m^2 and 10^{-14} m^2. The scoping calculations indicated that the de-saturated zone with negative pore water pressure extends to about 1 m from the niche wall into the rock mass. To install the sand/bentonite seals in an undisturbed or less disturbed zone, the boreholes were to be drilled down beyond the EDZ. Therefore, a borehole depth of 3 m with the seal region lying 1.5 – 2.5 m below the floor was selected.

- The altered hydro-mechanical state after niche excavation is further disturbed by sequentially drilling of the boreholes. Because of the small borehole diameter of 0.31 m, the EDZ around the boreholes could be expected also to be small ranging up to a maximum of 0.3 m. The calculations suggested additionally that the desaturation in the surrounding rock due to the dilatancy of the pores during the borehole drilling should not be significant. From the above conclusions, the distance between the test boreholes should be larger than 0.6 m. Hence, the selected borehole distance of more than 3 m between the test boreholes in the test niche (Fig. 5.2) should be sufficient.

- According to the scoping calculations, the water saturation of the considered sand/bentonite seals was expected to take 1 to 3.5 years for a water injection pressure of 0.5 to 1 MPa. After full saturation, the total stress reaches a maximum of about 1.2 MPa near the bottom. The gas injection with a constant inflow rate of 0.2 ml/min generates a gas entry/break-through pressure of about 0.7 MPa for the 65/35 sand/bentonite seal and 1.6 MPa for the 50/50 sand/bentonite seal. In the calculations, the gas injection lasts for several weeks to one month. To avoid a high

gas pressure of 1.6 MPa, a lower gas inflow rate of 0.02 ml/min, for instance, was recommended for the 50/50 sand/bentonite seal, but the test will then last longer. The total testing time for the 50/50 sand/bentonite ratio, applying the above mentioned testing conditions, is beyond the time of about 2.5 years which was originally foreseen for the in-situ experiment within the project ESDRED /DEB 09/ /SEI 09/. Therefore, in case of the 50/50 sand/bentonite ratio, it was decided to reduce the seal length to 0.5 m. It was assumed that with this adaption the in-situ experiments with both sand/bentonite mixtures could be finished within the planned testing time of approximately 2.5 years.

4 Mock-up tests

4.1 Design

Before going in situ, both the installation techniques and the required saturation time for the material mixtures should be investigated and optimized through mock-up tests on a 1:1 scale in the geoscientific laboratory of the GRS in Braunschweig. The principle layout of the mock-up test set-up is shown in Fig. 4.1.

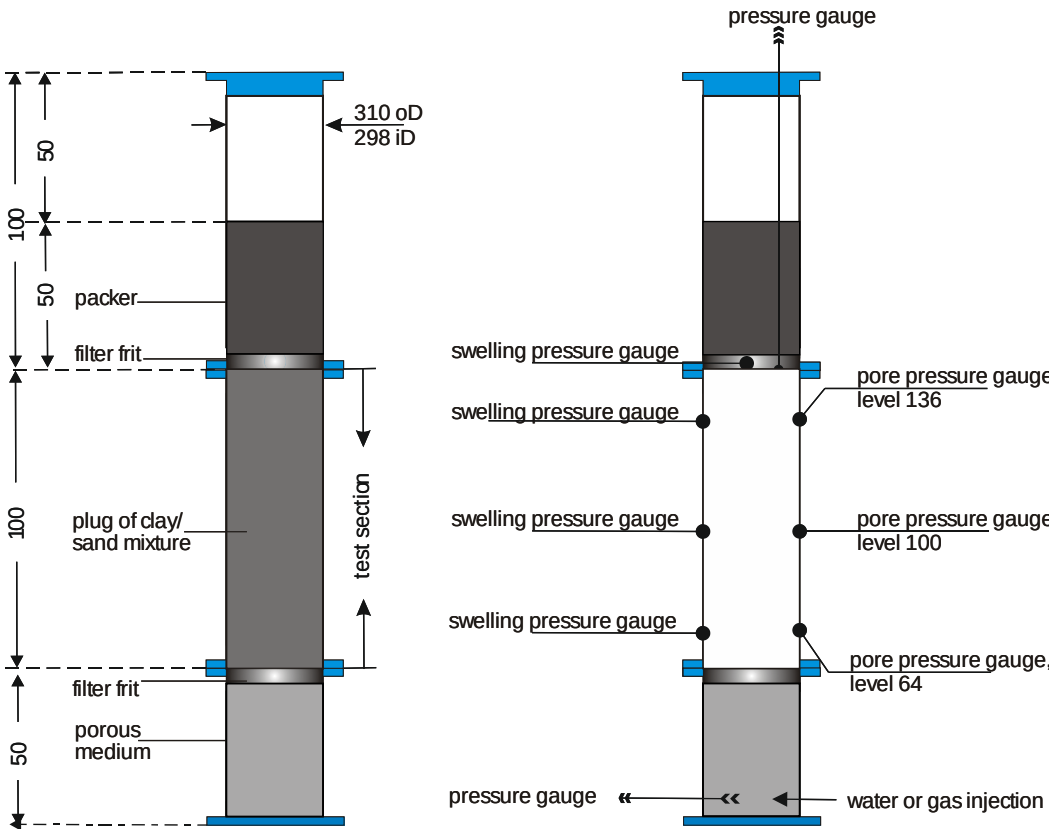

Fig. 4.1 Principle layout of the SB-mock-up test-set-up with locations of measuring sensors

As already outlined in Section 3.2.1, the mock-up tests were designed as a full-scale replica of the envisaged in-situ experiments (Fig. 1.1, Fig. 5.2). The tube length in the laboratory was 2.5 m and the seal material was installed in thin layers of about 5 to 10 cm in a similar way as envisaged in situ. Different techniques (hand stamping, vibrator technique) were tested (see Section 2.1.) and the achievable density was determined.

The detailed objectives of the mock-up tests were to:

- Develop and test seal material installation techniques
- Determine the time needed to reach full seal saturation
- Test the measuring procedures for the determination of the gas and water permeability as well as gas entry pressure at dry and saturated conditions under somewhat different, but better defined conditions, compared to the in-situ situation.

4.2 Test procedure

The following actions were foreseen at the test set-ups:

1. Instrumentation of the test tubes,
2. Determination of the initial installation density of the granular sand/bentonite mixture,
3. Determination of the initial gas permeability,
4. Water injection to simulate the formation water flow to the seals,
5. Determination of seal permeability to water at full saturation,
6. Gas injection to simulate the gas generation in the boreholes,
7. Determination of seal permeability to gas at full saturation,
8. Post-test investigations for determination of the final water content in the seal.

During the different test stages, the following hydro-mechanical parameters of the borehole sealing system were directly measured or determined, respectively:

- Gas and water flow rate and accumulated mass of water,
- Gas and water injection pressure,
- Swelling pressure of the seals,
- Seal permeability to water at full saturation, and finally
- Gas entry pressure of the saturated seal and effective gas permeability after gas break-through.

4.3 Execution of the mock-up tests

The mock-up tests were started in October 2004. The investigations of mock-up Test 1 were performed with the most promising 65/35 sand/bentonite mixture. The installation density of the seal amounted to 1904 kg/m^3, the initial gas permeability was determined to $6.5 \cdot 10^{-14}$ m^2. Both values corresponded very well with those determined in the laboratory tests on small samples. Afterwards, the seal was saturated with synthetic Opalinus clay solution. At the very beginning, the flow rates had been set too high so that the solution flowed along the inner surface of the tube. In order to ensure representative test conditions, the system was closed and kept under atmospheric pressure to allow self-healing of the seal. After some days, a continuous saturation process with reduced flow rate was initiated. After almost complete saturation of the seal in June 2005, the water permeability was determined to $1.9 \cdot 10^{-17}$ m^2, which was in good agreement with the results of the preceding laboratory measurements on small samples (compareTab 2.9).

Based on the experiences from this test, the mock-up Test 2 was prepared more carefully. A total amount of 148728 g of the 65/35 sand/bentonite mixture was installed with an installation density of 2.07 g/cm^3, which is slightly better than the target value of 1.93 g/cm^3. The start porosity amounted to 27 % and the water content was about 5.8 % with a corresponding degree of saturation of about 42 %. The test was started by determining the initial gas permeability to $6.4 \cdot 10^{-14}$ m^2 which corresponds also very well with the gas permeability determined in the preceding investigations on small samples (see Tab. 2.9). Seal saturation in the mock-up Test 2 was started in April 2005 with an injection pressure of 1.1 MPa.

As can be seen in Fig. 4.2, after about 18 months of testing, the total pressure in the seal equalized in the lower and middle part of the seal (red and light green lines) at a value of about 1.1 MPa which corresponds to the applied water injection pressure. Surprisingly, one does not see a similar evolution of the pressure at top of the seal (dark blue line).

The first water break-through, indicating a situation close to full seal saturation, was observed in September 2007, after more than 29 months of testing representing a period of time being 5 times greater than predicted (compare Tab. 3.5). In July 2008, 39 months after start-up of testing, the water inflow and outflow rates had equalized at

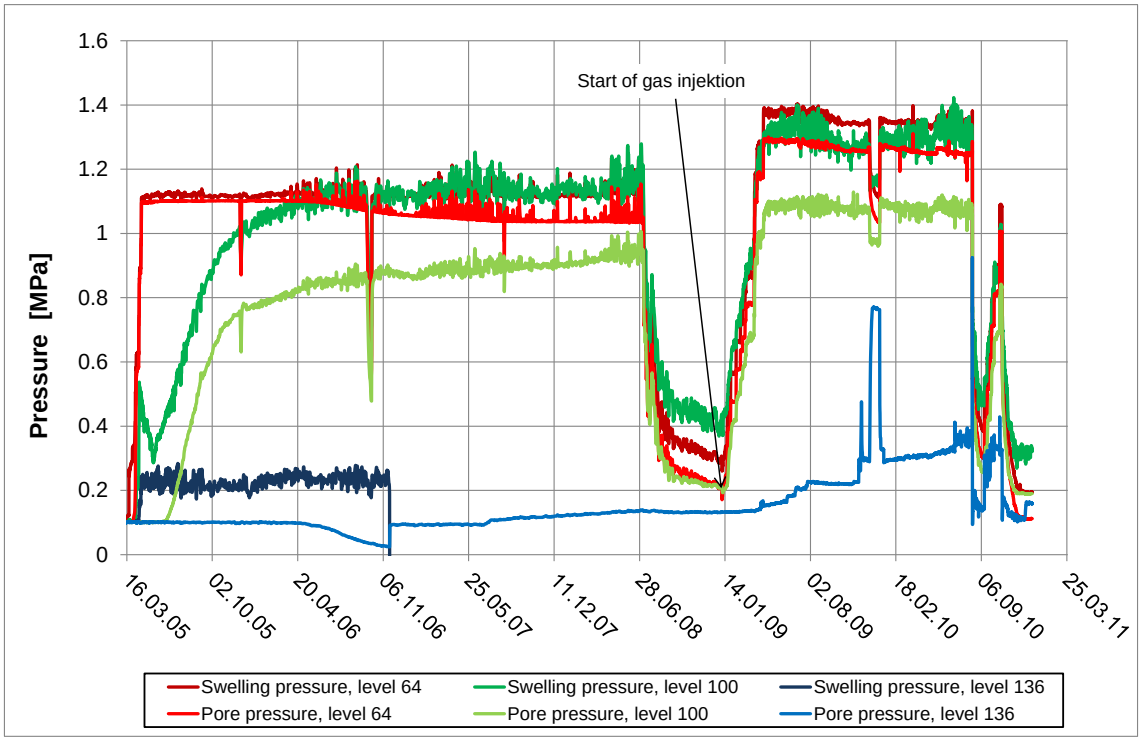

Fig. 4.2 Mock-up test: Evolution of pore and total pressure within the seal

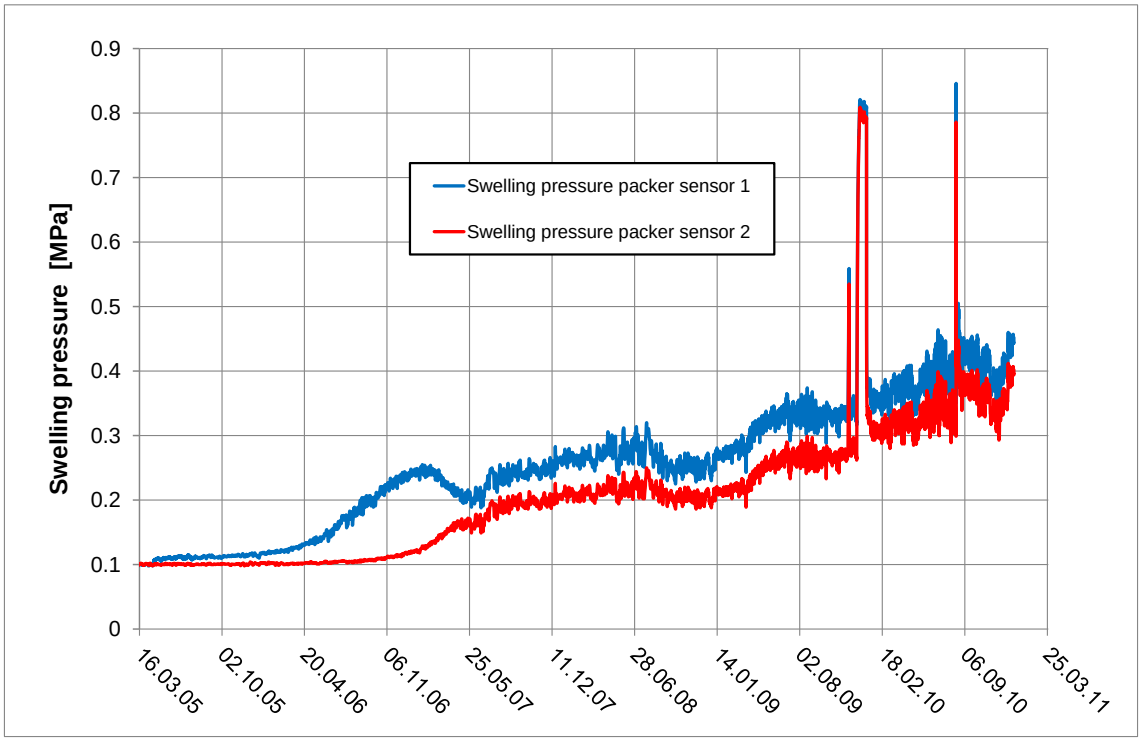

Fig. 4.3 Mock-up test: Evolution of the swelling pressure below the packer

about 10 ml/day yielding a water permeability value of about $1.47 \cdot 10^{-18}$ m^2, which was in very good agreement with the data obtained from the small samples used in the preceding laboratory tests. The water injection which resulted in a total amount of 28540 g (Fig. 4.4) was then stopped by reducing the injection pressure to zero on July 6, 2008.

In the following, the swelling pressure was allowed to equalize and stabilize in the whole seal before the pending gas injection tests would be started. In January 2009, after a testing period of about 44 months, the total pressure stabilized at a final value of about 0.35 MPa in the seal (Fig. 4.2) and of 0.25 MPa at the packer bottom (Fig. 4.3). These values agree with the swelling pressures determined on the small laboratory samples (compare Tab. 2.9) and thus confirm the expected seal properties.

The remaining gas injection test was started on January 7, 2009 (Fig. 4.2 and Fig. 4.5). From the very beginning (Fig. 4.5) one can clearly see the gas entry and the corresponding water outflow from the seal starting at a low pressure of only 0.25 MPa. This behaviour agrees also very well with the requirements given in Tab. 2.9.

By the end of November 2009 the inlet and outlet valves were closed for technical reasons for a certain period of time. An increase of the total pressure inside the seal could be observed in this period of time (Fig. 4.2). After opening the valves the pressure dropped down to the values monitored before. Over Christmas the valves were closed again and a similar pressure increase was observed. The higher values are due to the longer period of time. And again, after valve opening, the pressure dropped down to the values monitored before. This behaviour confirms the hydraulic connection over the seal length which was also confirmed by the first gas break-through which occurred some days before on 27 November 2009, 324 days after the start of the gas injection in January 2009.

A measurable continuous gas flow was only observed some months later in early March 2010 (see Fig. 4.6). The variability of the data is due to the continuing mobilization of water in the seal material which influences the gas flow. On the whole, an increase of the gas flow rate was observed with parallel decreasing water discharge rates. From August 9, 2010 onwards, 577 days after start-up of the gas injection, no further water discharge was observed and the gas flow rate stabilized at 83 cm^3/min.

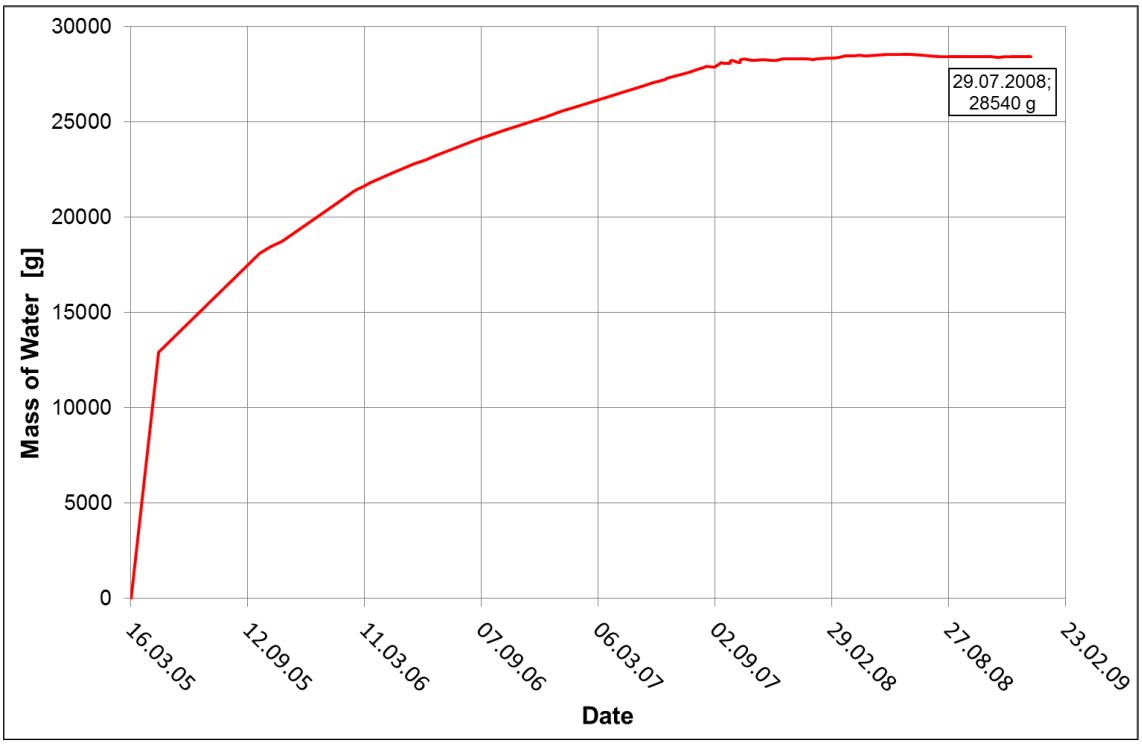

Fig. 4.4 Mock-up test: Cumulative mass of injected water

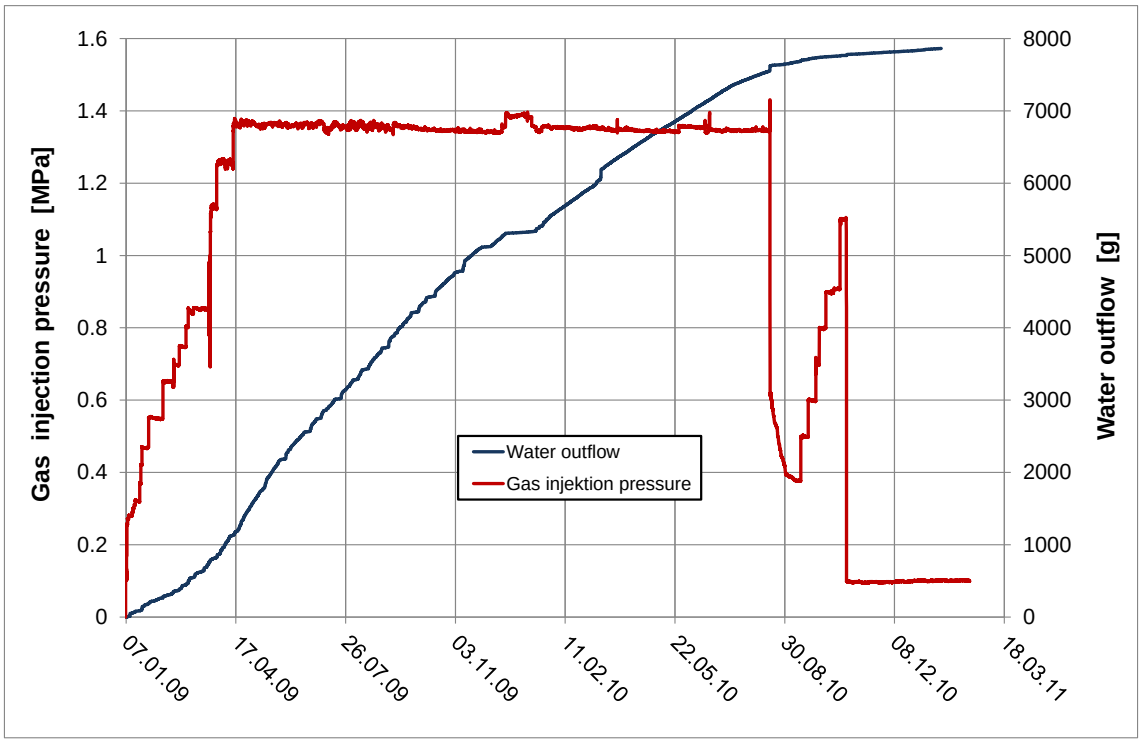

Fig. 4.5 Mock-up test: Evolution of water discharge from the beginning of the gas injection (for the gas entry pressure determination)

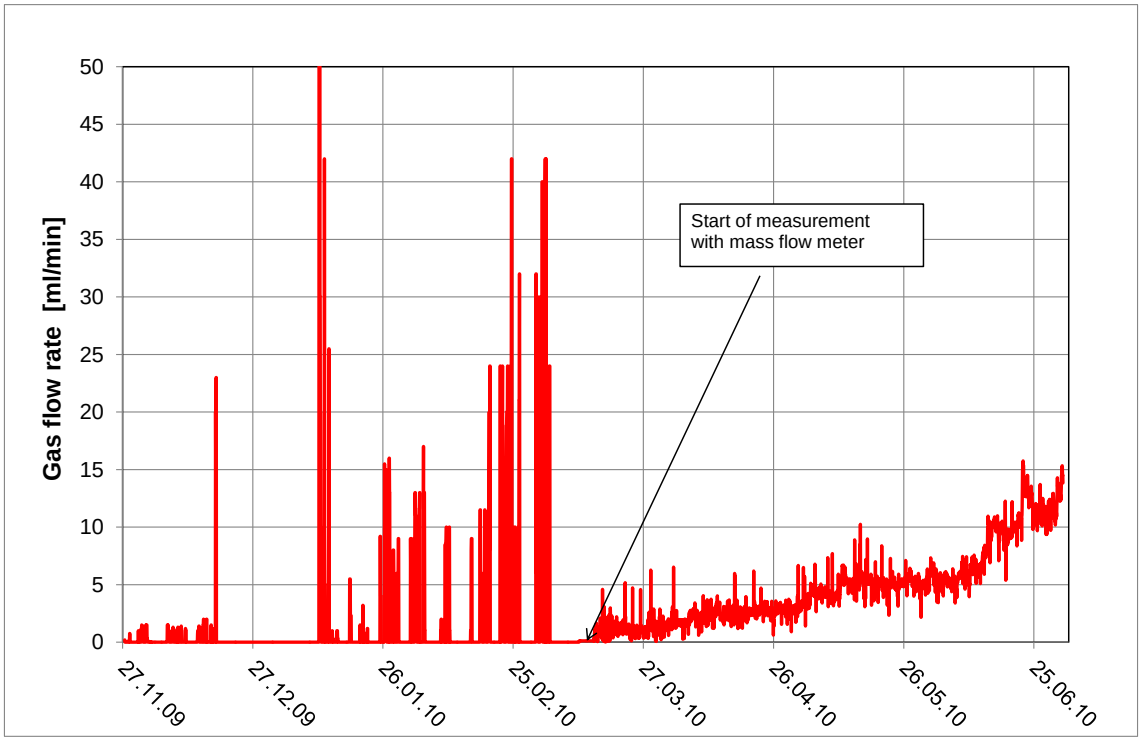

Fig. 4.6 Mock-up test: Evolution of the gas flow rate after gas break-through

The seal permeability to gas at this point of the experiment was evaluated to $3.7 \cdot 10^{-17}$ m^2. This value is also in excellent agreement with the data obtained on the small laboratory samples earlier (see Tab. 2.9).

In order to check whether the water discharge from the seal was dependent on the gas injection pressure or not, the gas pressure was increased in a final step to 1.4 MPa. This resulted in a distinct increase of the gas flow rate and an increase of the gas permeability to $2 \cdot 10^{-15}$ m^2, but a further discharge of water from the seal was not observed.

At this point of time, 7.92 l of the 28.4 l of water injected in total into the seal were finally discharged due to the gas injection (see Fig. 4.5).

In the following, the gas pressure was reduced to zero until pressure equilibrium was reached in the seal and then the gas pressure was increased again stepwise to check whether the gas pressure reduction had led to a reduction of the material permeability. The accompanying water discharge was monitored simultaneously. And in fact, it was found that the pressure reduction had led to a distinct decrease of the permeability. The increase of the gas pressure, on the contrary, led to an increase of the gas

permeability (see data in Tab. 4.1). Because of the relatively small amounts of water discharged in this phase the increase of permeability can be attributed relatively clearly to a widening of the prevailing flow paths. Because the discharged amounts of water in this phase are small in comparison to those discharged in the earlier phases a remarkable difference in saturation is not to be assumed.

The evolution of the pore and the total pressure in the seal is shown in Fig. 4.2. After termination of the gas injection test, the gas pressure was finally reduced to zero and the pressure in the seal was allowed to equalize over a time period of about five months. The swelling pressure remaining thereafter at top of the seal below the upper filter frit (Fig. 4.3) ranges from 0.4 – 0.45 MPa and confirms the requirements given in Tab. 2.9 as well.

Tab. 4.1 Mock-up Test 2: Effective gas permeability and amounts of discharged water for different gas injection pressures

Gas injection pressure [MPa]	**Effective gas permeability** [m^2]	**Discharged amount of water per pressure step** [ml]
0.493	$7.78 \cdot 10^{-17}$	24
0.594	$8.16 \cdot 10^{-17}$	20.8
0.695	$1.21 \cdot 10^{-16}$	7.3
0.795	$1.44 \cdot 10^{-16}$	9
0.899	$1.57 \cdot 10^{-16}$	11.1
1.102	$6.17 \cdot 10^{-16}$	8.5

4.4 Post-test investigations

Following the gas injection testing, post-test sampling of the seal material was started in April 2011. Sampling was performed horizontally through the lead-through holes of the swelling sensors mounted at the mock-up test tube at different levels (see below) and vertically from the bottom and the top of the SB seal. The water content determinations were made in accordance with DIN 18121-1 by drying at 105 °C until weight constancy. The sampling locations are depicted in Fig. 4.7.

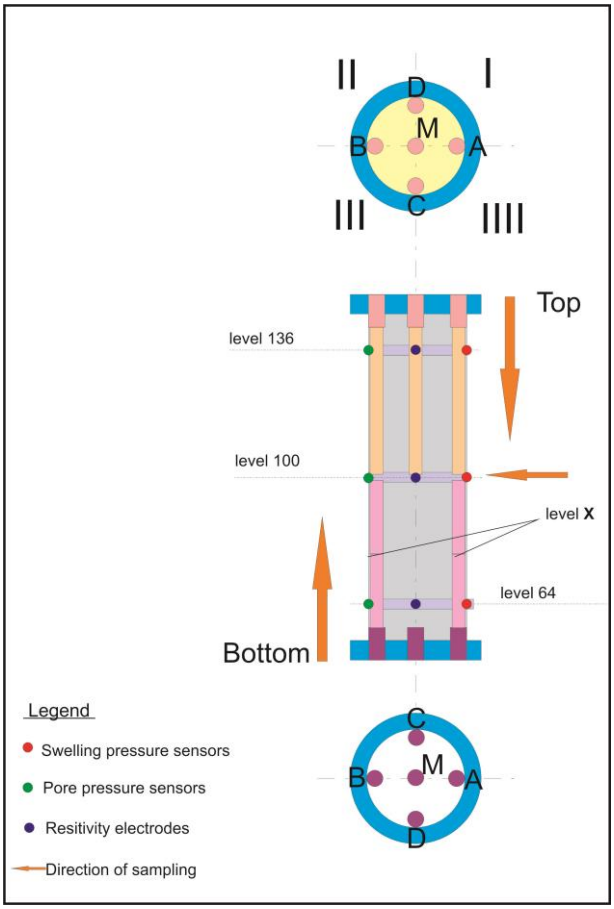

Fig. 4.7 Sampling locations in the mock-up test section

4.4.1 Horizontal sampling

Horizontal sampling was performed at the three measuring levels 64 cm (lower), 100 cm (middle), and 136 cm (upper) through existing openings at which swelling pressure sensors were mounted.

Fig. 4.8a shows a view into one of the openings and the sealing material behind. Fig. 4.8b shows the front face of one of the swelling pressure sensors still being in a good shape after the long test period.

For the sampling, a core cutting tube with an outer diameter slightly smaller than the diameter of the opening was taken (Fig. 4.8c). The tube with an inner diameter of 1.5 cm was pushed by a hammer to the opposite side of the mock-up test tube and afterwards retrieved. Fig. 4.8d shows a cut-open tube with one of the samples taken over the whole sampling length.

a) Lead-through of a swelling pressure sensor

b) Dismantled swelling pressure sensor

c) Horizontal sampling

d) Uncovered sample taken horizontally from the mock-up test section

Fig. 4.8 Details of horizontal sampling

Pushing of the core cutting tube led to a certain compaction of the sand/bentonite mixture which was gastight sealed into a plastic bag right after sampling.

The sample was cut into three pieces (front, middle, rear) to enable the determination of the water content over the test tube diameter.

Fig. 4.9 shows the water content distribution for the individual sampling locations and positions along the tube diameter.

A decrease of the water content from the bottom to the top is to be noted with a smaller difference between the data of the middle and the top level. Furthermore, the water contents are somewhat higher at the tube wall than at the middle. The higher water content at the lower level can certainly be related to the small distance to the water inlet at the lower end of the mock-up test tube. A preferred water migration along the tube wall can be concluded from the data, but this effect is not very clear as can be seen in Fig. 4.9.

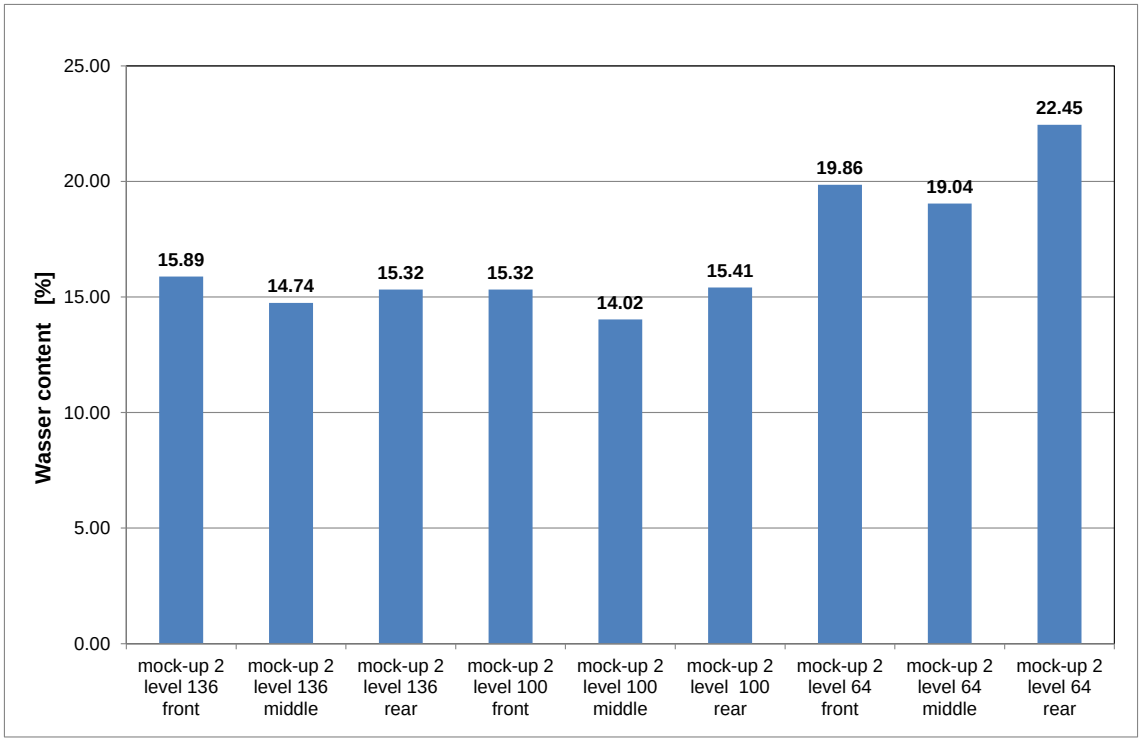

Fig. 4.9 Distribution of the water content of samples taken at three different horizontal sampling levels

After dismantling of these components, it was recognized that the seal material emerged by about 5 cm out of the upper end of the tube (see Fig. 4.10a). Considering an original installation length of 103 cm an extrusion of the seal material of about 2 cm took place after dismantling of the packer. Fig. 4.10b shows the separation of this part into four segments. All segments showed water contents of about 17.6 % except for segment I which showed a water content of about 18.8 % (Fig. 4.11).

a) seal material emerging out of the mock-up test section

b) segmentation of the emerging seal material

Fig. 4.10 Emerging seal material observed at the upper end of the mock-up test section after dismantling of the packer

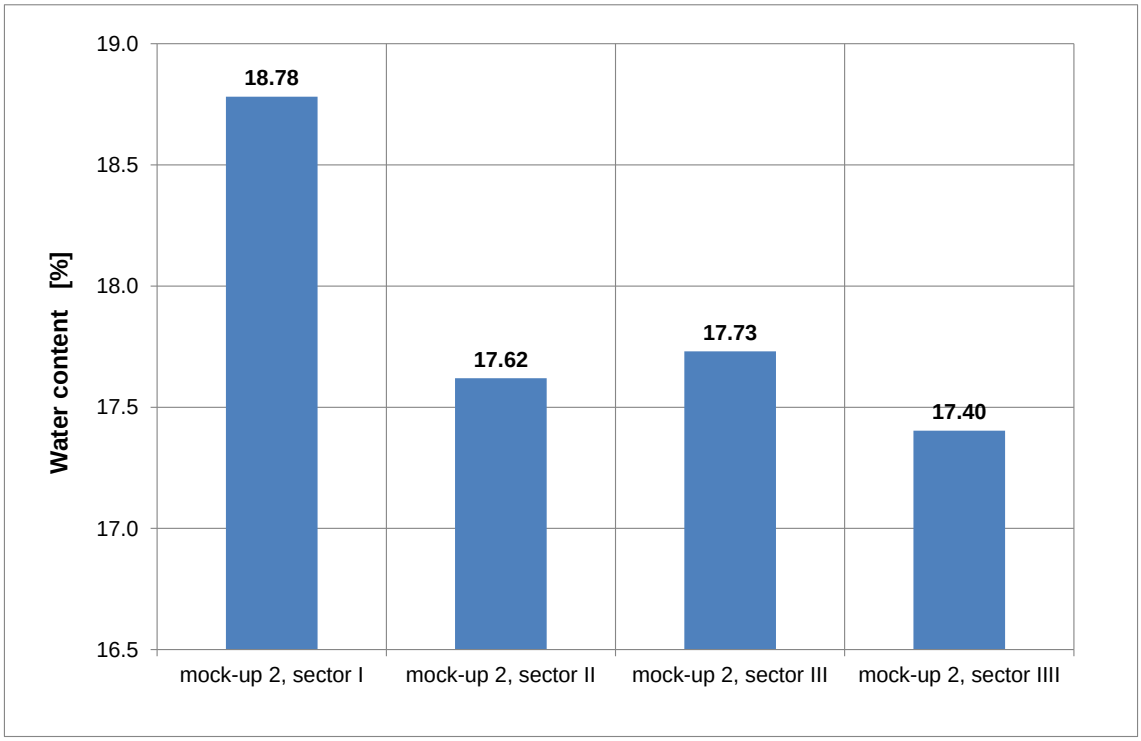

Fig. 4.11 Water content of the four segments emerging out of the mock-up test section

4.4.2 Vertical sampling

Before sampling in vertical direction, the packer and the injection chamber were to be dismantled from the test section of the mock-up test tube.

In the following, after the emerging material was taken away, in a first step about 10 cm long samples were taken from the seal material with a core cutting tube of 5 cm inner diameter (Fig. 4.12a).

The distribution of the sampling locations over the seal cross section can be seen in Fig. 4.12b. The same was applied at the lower part of the mock-up test section. For a better determination of the distribution of the water content all samples were cut at their mid-height into two halves.

The water contents of the samples from the lower end range with about 20.3 % somewhat higher than the average water content of the samples from the upper end (see Fig. 4.13 and 4.14). This result is comparable to that obtained from the horizontally taken samples (compare Fig. 4.9).

a) sampling with a core cutting tube

b) sample locations at the upper end of the sand/bentonite seal

Fig. 4.12 Sampling at upper and lower end of the mock-up test section

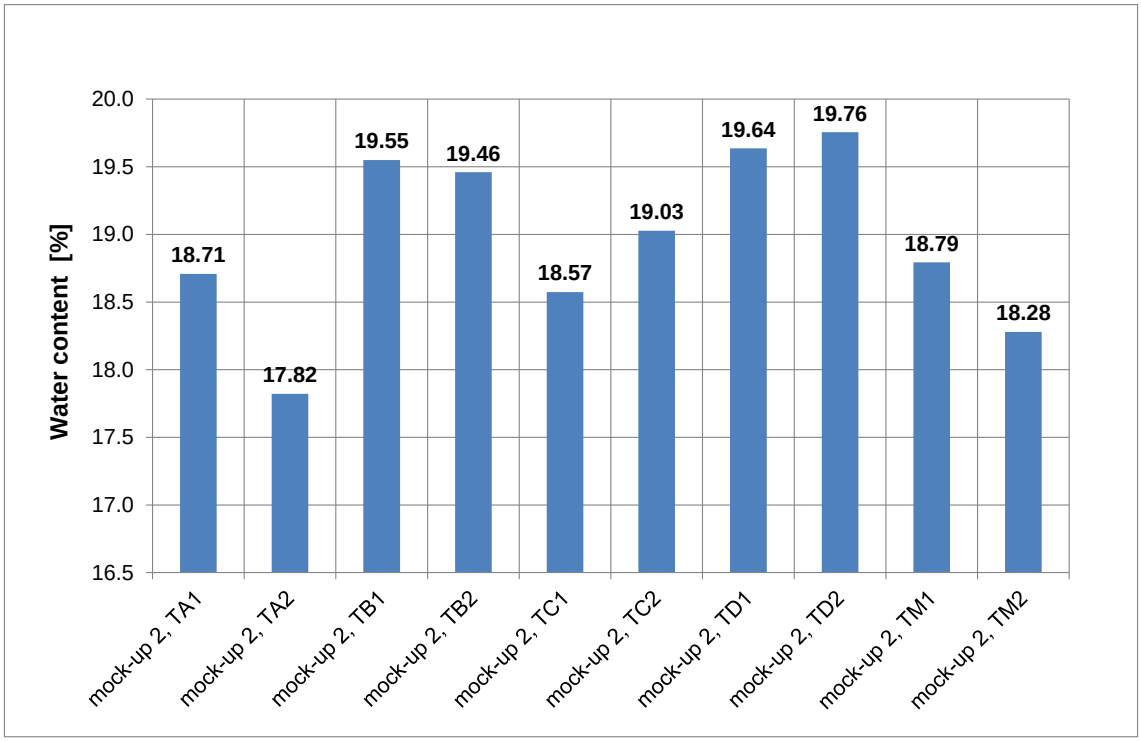

Fig. 4.13 Water content at the upper end of the mock-up test section

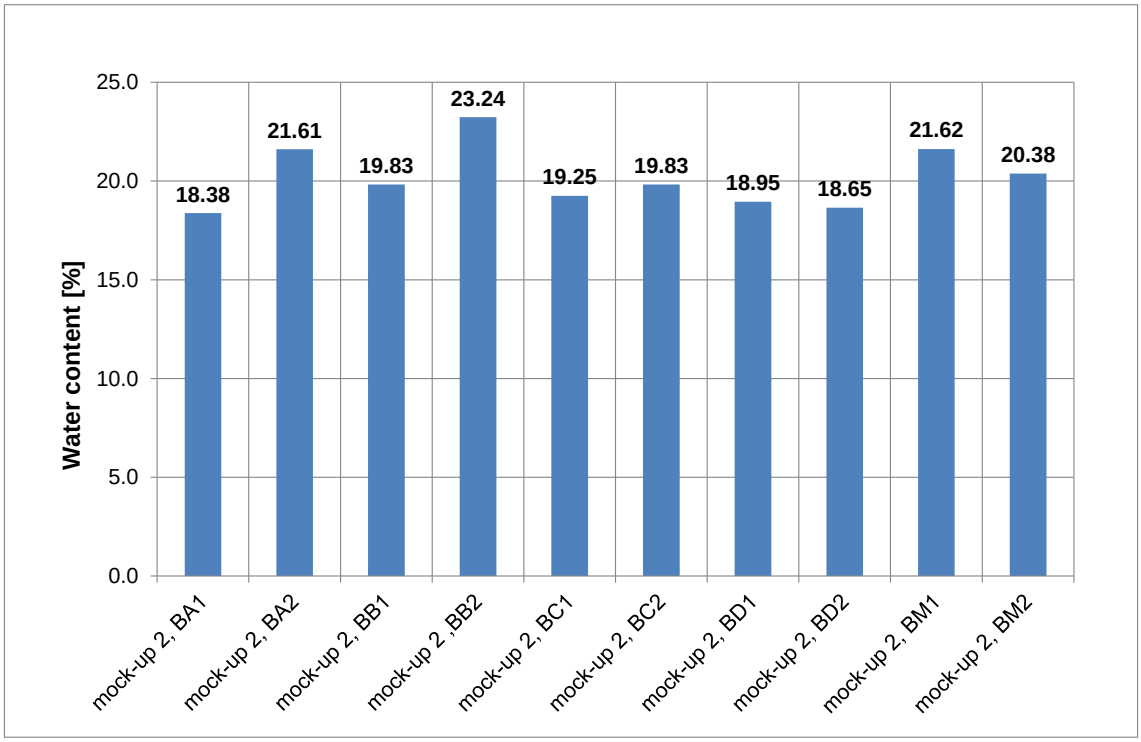

Fig. 4.14 Water content at the lower end of the mock-up test section

Further samples were taken by pushing a longer core cutting tube into the remaining inner parts of the seal material (Fig. 4.15a). Because of very high adhesion a fork lift was used for the retrieval of the core cutting tube from the seal material (Fig. 4.15b).

a) sampling by pushing a longer core cutting tube

b) retrieval of the core cutting tube with a fork lift

c) compacted seal material sample

Fig. 4.15 Sampling over the whole test section with a long core cutting tube

A certain compaction of the seal material occurred during the tube pushing as was the case with the horizontally taken samples. A further compaction could not be avoided during the pushing out of the seal material from the core cutting tube (Fig. 4.15c). For this reason, a precise determination of the sample location within the test section was not possible and thus, a further separation of the material was not appropriate.

Sampling at the lower side of the mock-up test tube was done at two locations close to the tube wall. Here, the core cutting tube could not be pushed to the middle, but had to be retrieved at only half the way (see level X in Fig. 4.7). Successful sampling up to the middle was only possible after tube retrieval.

From the upper end of the mock-up test tube it was possible to push the core cutting tube up to the middle and consequently further samples were taken from a third core taken at the middle of the seal cross section. This sampling behaviour confirms the higher water content in the lower part of the seal. Fig. 4.16 shows the results of the water content determinations.

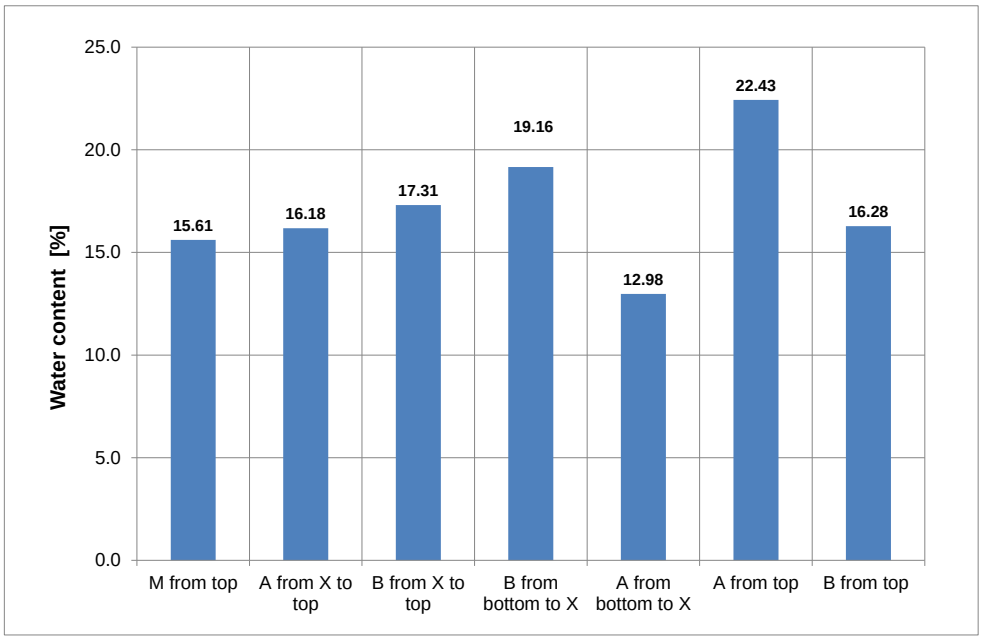

Fig. 4.16 Water content of the samples taken vertically from the inner part of the seal

Except for one sample taken at position A at the top with a water content of about 22 % and a further sample from position A at the lower end with a water content of 13 % the water content of the samples from the lower part range between 16.2 and 19.2 % and those from the upper part range between 15.6 and 16.3 %. This result confirms again

the previously described trend of a higher water content in the lower part of the seal. The relatively low water content of 13 % in the upper part might be due to a moisture loss in consequence of a water condensation in the plastic bags due to comparably long sample storage before the water content determination. The average water content over all samples is about 18.4 % which corresponds to a total amount of injected water of 27366 g. This value is in fairly good agreement with the measured amount of injected water of 28540 g (see Section 4.3). Being a little bit smaller, reflects the water loss due to the final gas injection test.

4.5 Conclusions drawn from the mock-up test

On the whole, the observations of the mock-up test confirm the seal properties of the selected 65/35 sand/bentonite mixture excellently and underline the fulfilment of the seal requirements given in Tab. 2.9. This is also demonstrated by respective data compiled in Tab. 4.2 below which shows the underlying requirements – the design values – again in comparison to the results obtained in the preceding laboratory investigations and in the mock-up Test 2.

The porosity calculated under consideration of the natural water content (sand: 4.3 %, bentonite: 8.7 % /MIE 07/ at seal installation (3986 g + 4166 g) and the 28400 g of water injected afterwards during the seal saturation phase results in a value of 51 %.

In contrast, the porosity determined on basis of the grain densities (see Tab. 2.3 and Tab. 2.4) and the dry installation density results in a value of only 27 %. Considering the total amount of water injected during seal saturation of 28400 g and the initial water content of 8150 g, the determined porosity of 27 % results in a theoretical saturation degree of 188 %. This oversaturation is concluded to be explainable by parts of water adsorbed at higher density to the interstitial layers of the clay particles, a possible effect reported earlier by Hartge et al. /HAR 91/.

A most surprising matter experienced during the mock-up test, however, was the fact that seal saturation required much more time (more than 5 times of the calculated time of 170 days or 5.6 months, respectively) than expected from the scoping calculations which – of course – had been performed on the basis of uncertain parameters. Process understanding is obviously not adequately developed at this point of time and hence, an improvement of respective models implemented in the various computer codes to date seems to be required.

Tab. 4.2 Overview of laboratory investigations and determined parameters

Test parameter	Unit	Index	Initial state	Status at full saturation	Status after gas break-through	Comm.
Design values (see Tab. 2.9)						
Installation density	[g/cm^3]	ρ	1.93	-	-	Tab. 2.4
Fluid permeability	[m^2]	K_{fluid}	> $1.0 \cdot 10^{-15}$ (K_{gas})	10^{-18} – 10^{-17} (K_{water})	> $1.0 \cdot 10^{-18}$ (K_{gas})	-
Pressure	[MPa]	P	-	< 2.0 ($P_{swelling}$)	< 2.0 ($P_{gas\text{-}entry}$)	-
Data from laboratory tests						
Installation density	[g/cm^3]	ρ	1.87 – 1.93	-	-	-
Fluid permeability	[m^2]	K_{fluid}	$1.2 \cdot 10^{-13}$ (K_{gas})	$5.2 \cdot 10^{-18}$ (K_{water})	$1.4 \cdot 10^{-17}$ (K_{gas})	-
Pressure	[MPa]	P	-	0.2 – 0.4 ($P_{swelling}$)	0.4 – 1.1 ($P_{gas\text{-}entry}$)	-
Data from mock-up Test 2						
Density	[g/cm^3]	ρ	2.07 / 1.95 / 2.67 (ρ_{bulk} / ρ_{dry} / ρ_{grain})	-	-	-
Porosity	[-]	ϕ_0	0.27	-	-	-
Saturation	[-]	S	0.42(*)	1.88(*)	1.47(*)	-
Mass of water	[g]	M_w	8150 ($M_{w\text{-}initial}$)	36550 ($\Delta M_{w\text{-}in}$=28400)	28630 ($\Delta M_{w\text{-}out}$=79200)	-
Water content	[-]	w	0.058	0.26	0.20	related to V_s = 140.58 kg
Fluid permeability	[m^2]	K_{fluid}	$6.4 \cdot 10^{-14}$ (K_{gas})	$1.5 \cdot 10^{-18}$ (K_{water})	$2.0 \cdot 10^{-15}$ ($K_{gas\text{-}break\text{-}through}$ = $3.7 \cdot 10^{-17}$)	-
Fluid injection pressure	[MPa]	P_{fluid}	0.1 – 0.6 (P_{gas})	1.1 (P_{water})	1.4 ($P_{gas\text{-}entry}$=0.25)	-
Swelling pressure	[MPa]	P_{sw}	-	~ 0.4	0.25 – 0.35	-

(*) related to the calculated porosity of 27 % ($0.27 \cdot 72000$ cm^3 = 19440 cm^3)

5 In-situ experiments

As already explained in Section 2, the mixtures with 65/35 and 50/50 sand/bentonite ratio were selected to be used and investigated in the in-situ experiments at the MTRL. In addition, one borehole was proposed by NAGRA to be sealed with a pure MX-80 bentonite granulate representing the buffer material in the Swiss HLW disposal concept. This experimental set-up was regarded an excellent possibility to compare the sealing properties of the different sealing materials under representative in-situ conditions.

5.1 Test design

The entrance part of a drift connecting Gallery 04 to the security gallery of the Mt. Terri motorway tunnel was excavated and prepared for the SB experiments (see Fig. 5.1).

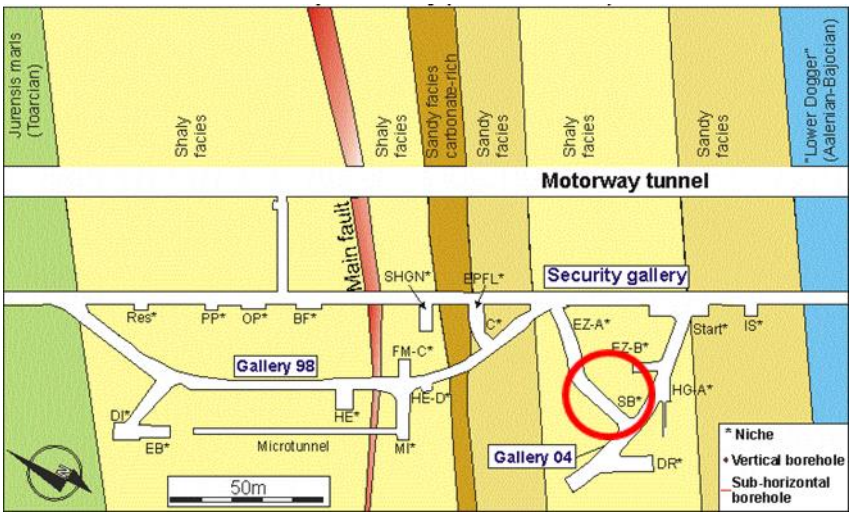

Fig. 5.1 Location of the SB experiment in the Mt. Terri Rock Laboratory

The test area has a length of about 8 m, a width of 5 m, and a height of 4 m. Four test boreholes of 0.31 m diameter were drilled in the test room's floor to a depth of about 3 m (Fig. 5.2).

The two boreholes in the direction of the Gallery 98 were equipped with seals of 1 m length consisting of 65/35 sand/bentonite mixtures as originally planned and considered in the scoping calculations. The length of the seals in the two remaining boreholes in the foreground of the test area close to Gallery 04 were reduced to 0.5 m

because of the long saturation times predicted in the scoping calculations for the 50/50 sand/bentonite mixture to keep the saturation time within the originally assessed testing duration of about 2.5 years.

Instruments for measuring different hydro-mechanical parameters were installed as well. In the lower part of the boreholes (Fig. 1.1 and Fig. 5.2), the injection volume was filled with gravel as porous medium. At the top of the porous medium, a filter frit was placed for ensuring a homogeneous distribution of the injected water over the entire borehole cross section. Above the filter frit, the seal was installed in several layers.

Above the seal, a further filter frit was installed for water and gas collection. This filter frit was connected via a measuring tube to the control panel at the test room's floor in order to enable the measurement of water outflow from the seal after saturation. The entire borehole was sealed against the ambient atmosphere by a gastight packer. At the bottom of the packer, two swelling pressure sensors were installed. The uppermost part of the test borehole was grouted for keeping the packer in place at higher swelling pressures developed by the SB seal during water uptake.

For saturation or desaturation of the seal water or gas could be injected through an injection tube running from the valve panel in the test room via an inclined borehole into the lower fluid injection volume.

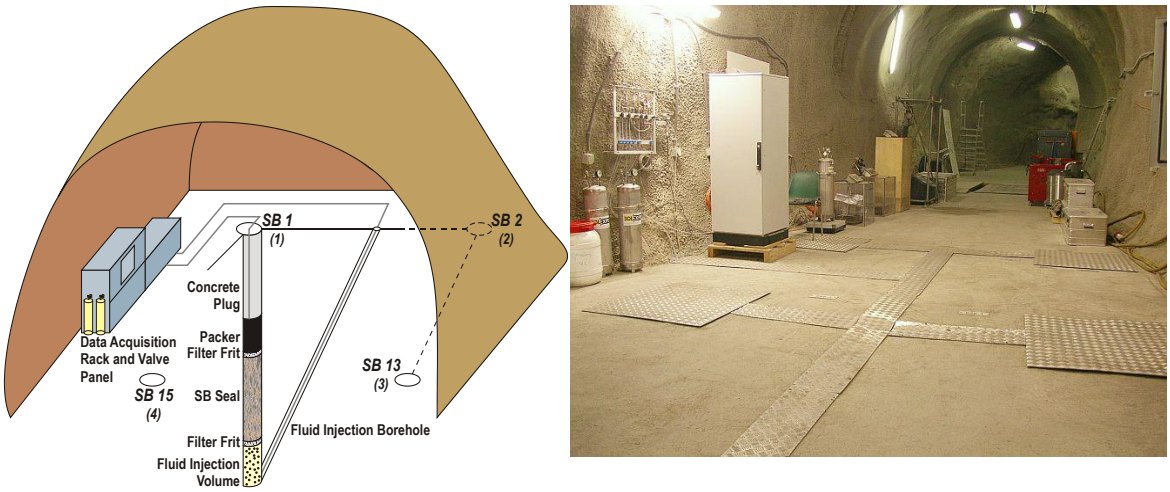

a) arrangement of test boreholes b) view into test gallery

Fig. 5.2 SB test set-up

5.2 Test procedure

The following actions and tests were foreseen at the individual test boreholes:

1. Drilling and instrumentation of the test boreholes,
2. Determination of the initial installation density of the granular sand/bentonite mixture,
3. Determination of the initial gas permeability,
4. Water injection to simulate the formation water flow to the seals,
5. Determination of seal permeability to water at full saturation,
6. Gas injection to simulate the gas generation in the boreholes and determination of the gas entry pressure,
7. Determination of seal permeability to gas after gas break-through,
8. Post-test investigations for determination of the final water content in the seal.

During the different test stages, similar as for the mock-up test, the following hydro-mechanical parameters of the borehole sealing system were directly measured or determined, respectively:

- Gas or water flow rate,
- Accumulated volume of injected water,
- Gas or water injection pressure,
- Swelling pressure of the seals,
- Seal permeability to water of the saturated seal, and
- Gas entry pressure of the saturated seal.

5.3 Execution of the in-situ experiments

The in-situ experiments were installed at the MTRL between October 2005 and late October 2006. Fig. 5.3 shows a collection of photos taken during the installation of test SB2.

a) Empty borehole SB2

b) Gravel of fluid injection volume together with water injection tubes emerging from the inclined injection borehole

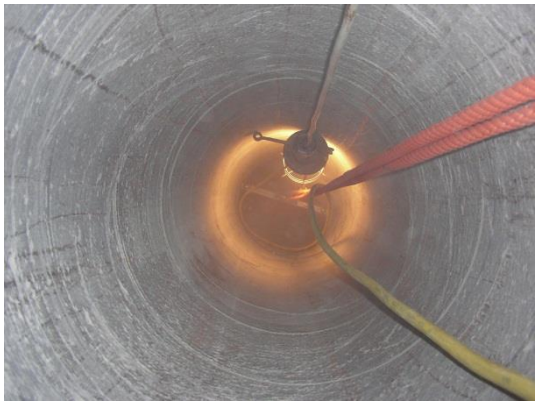

c) Installation and compaction of seal material

d) Filter frit at top of seal

e) Packer in borehole SB2

f) Grouted borehole cellar

Fig. 5.3 Photos taken during installation of in-situ experiments

The installation densities achieved in the test boreholes at the MTRL are shown in Tab. 5.1.

Tab. 5.1 Installation densities achieved in the test boreholes at MTRL

Experiment	**Installation density [g/cm^3]**	
	achieved in situ	**achieved in the laboratory (Tab. 2.3 and Tab. 2.4)**
SB1	1.72	1.87 – 1.93
SB2	1.91	1.87 – 1.93
SB13	1.64	n. d.
SB15	1.69	1.73 – 1.82
Mock-up Test 2 (for comparison)		2.07

n. d.: not determined

The value of 1.91 g/cm^3 achieved in the test borehole SB2 is best and is very close to those values determined earlier in the laboratory (for comparison: the value achieved in the mock-up Test 2 was 2.07 g/cm^3, see Section 4.3). The values achieved in the in-situ boreholes are generally somewhat lower which reflects the comparably unfavourable installation conditions in situ. The values of gas permeability in the dry stage measured before stat-up of water injection are shown in Tab. 5.2.

These values are quite close to those determined on small samples investigated in the laboratory and were considered to fulfil the requirement given in Tab. 2.9. The values achieved in situ were somewhat lower than those achieved in the laboratory.

Tab. 5.2 Gas permeability of the seal material as installed in the test boreholes at MTRL

Experiment	Gas permeability [m^2]	
	achieved in situ	**achieved in the laboratory (see Tab. 2.9)**
SB1	not determined because of blocked measuring tube; reason not detectable	$1.2 \cdot 10^{-13}$
SB2	$3.29 \cdot 10^{-14}$	$1.2 \cdot 10^{-13}$
SB13	$2.26 \cdot 10^{-13}$	n. d.
SB15	$3.41 \cdot 10^{-15}$	$7.5 \cdot 10^{-14}$

n. d.: not determined

5.3.1 Tests SB1 and SB15

Tests SB1 and SB15, located on the southern side of the test room, where started on November 1, 2006 with an initially moderate water injection pressure ranging up to 0.14 MPa. Compared to the mock-up test both tests showed a relatively early increase of the swelling pressure reaching intermediate levels between 0.14 and 0.17 MPa in the early state of the test (see Fig. 5.4 and Fig. 5.5). Simultaneously with increasing the injection pressure to values close to 0.4 MPa in August and September 2008, respectively, the pressure measured at top of the seals increased to the similar values as the injection pressure. This behaviour indicated a bypassing of the injected water along the borehole wall or through the excavation damaged zone close to the borehole wall. And in fact, a water outflow at the top of the seal was observed in this early stage of the test. At this moment it was decided to close the upper outlet valves to avoid an undesired loss of water, to keep the water within the seal/borehole-system, and to attain seal saturation in the long term of the test. In the following 19 months until May 2008, both swelling pressure sensors of test SB1 failed thereby making any further assessment of the progress of seal saturation impossible. A similar test development was observed at test SB15. It is concluded that an unknown poor rock quality around the tests on the southern side of the test room yielded this undesired test performance.

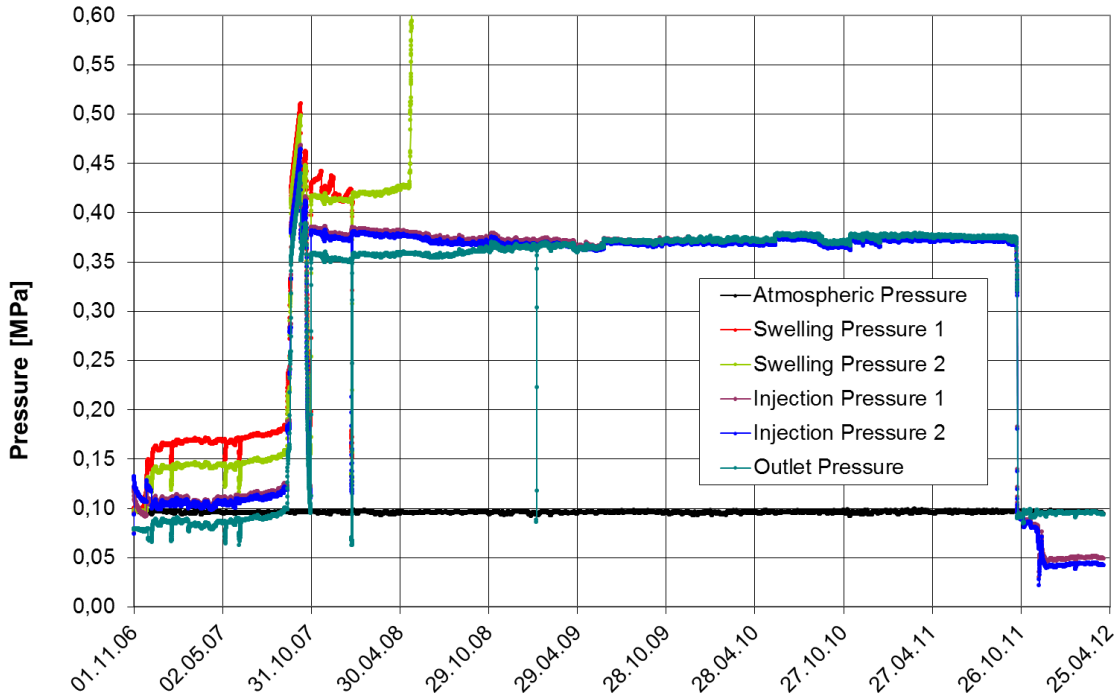

Fig. 5.4 Pressure evolution in test SB1 sealed with a 65/35 sand/bentonite mixture

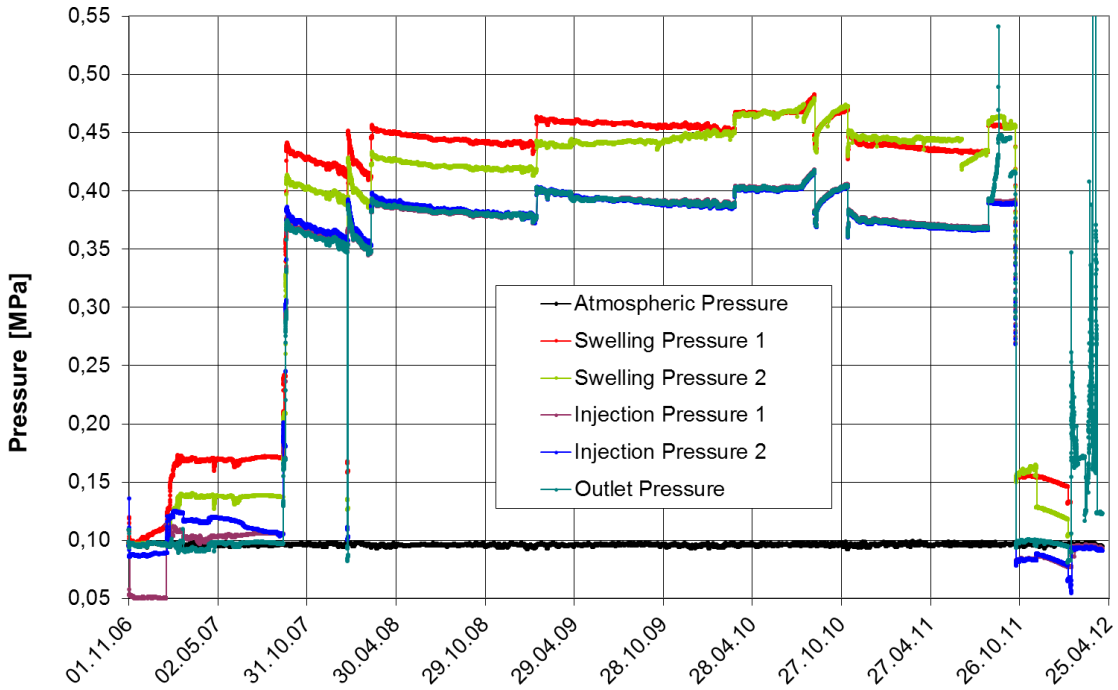

Fig. 5.5 Pressure evolution in test SB15 sealed with a 65/35 sand/bentonite mixture

A further reason could be seen in the relatively low installation density achieved at these two test sites. An inadequate evolution of the seal material's swelling behaviour could have contributed to this poor test performance. The comparably high water content of about 26 % measured on samples taken from the seal at the end of testing in late 2011/early 2012 seems to confirm this assumption.

The final gas injection test at the end of the almost 5 years testing period at test SB15 showed a similar bypassing of the gas along the seal/borehole wall interface and a corresponding gas outflow at the upper end of the seal. A determination of the seal permeability to gas was unfortunately not possible. Gas injection at test SB1 failed because of a plugged measuring tube.

5.3.2 Test SB13

The test SB13 with pure bentonite ran excellently from the beginning and showed no disturbances in the first phase of testing (see Fig. 5.6). In August 2009, 21 months after start-up of water injection, the swelling pressure reached maximum measurable values of 3 MPa (full scale of sensors) confirming the impressive swelling properties of bentonite.

One year later in August 2010 one of the sensors began to show a decreasing swelling pressure. This behaviour may be attributed to a local re-arrangement of the bentonite seal material or to pressure induced fracturing of the surrounding rock. Anyway, in December 2010 the pressure sensor readings started again to increase.

The gas injection in December 2011 revealed the expected low permeability to gas of the pure bentonite. No gas outflow could be seen at the upper end of the seal up to the maximum applied gas pressure of 0.7 MPa. A rapid gas pressure decay, however, was observed after gas shut-in in the gas injection volume (pink and blue curves in Fig. 5.6) which indicated a preferential gas flow into the surrounding rock.

To estimate the effective permeability of the surrounding rock to gas at the prevailing saturation state the gas pressure decay measured after gas shut-in was simulated with the computer code WELTEST /SCH 97/. The simulation was done by using different parameter combinations in the calculations, assuming that a certain fraction of the total porosity is accessible to gas and that no interaction between the gaseous and the liquid phase occurs. The best data fit was reached under consideration of an accessible rock porosity of 1.5 % to gas (in fact, the result is not very sensitive to porosity changes in

the same order of magnitude) and an effective rock permeability of $k = 2 \cdot 10^{-19}$ m^2, a value which is assumed to be considerably higher than that of the re-saturated bentonite seal and which confirms the assumption made above.

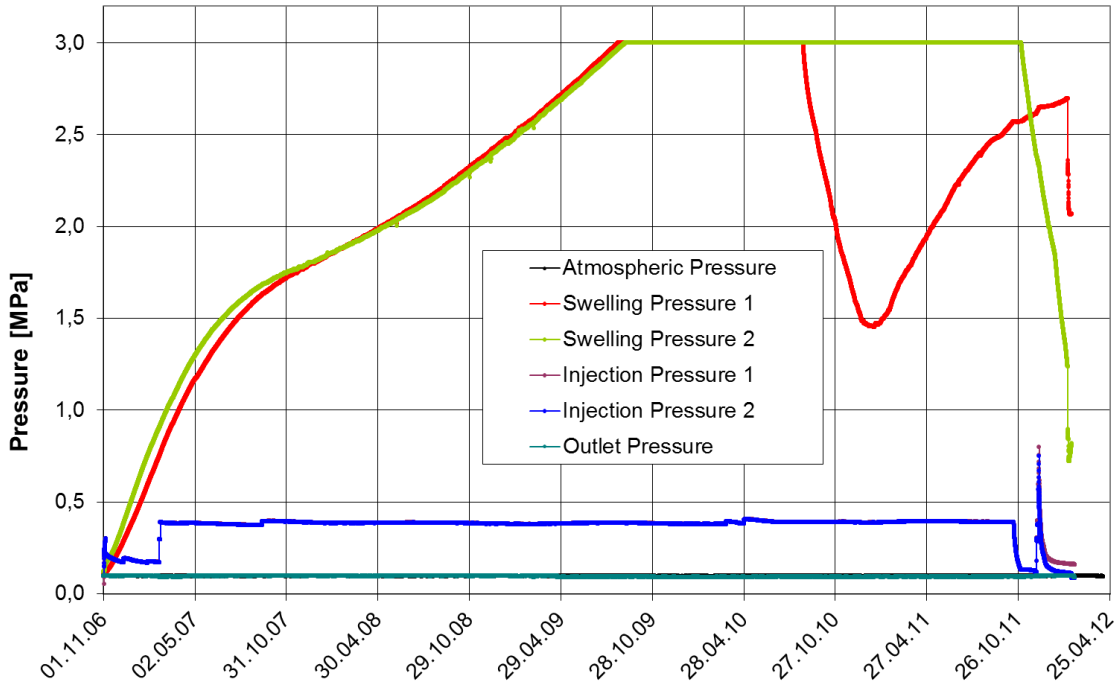

Fig. 5.6 Pressure evolution in test SB13 sealed with a 65/35 sand/bentonite mixture

5.3.3 Lead test SB2

The first – and according to the achieved installation data – best installed test set-up of test SB2 with a 65/35 sand/bentonite seal was already started in October 2005 (Fig. 5.7). Different from the mock-up test, the pressure was initially kept at a comparably low level for two reasons: (1) to avoid an undesired greater loss of water into the surrounding rock the porosity and permeability of which being high in comparison to the situation in the mock-up test where a steel tube replaced the surrounding rock and (2) because it was assumed that the surrounding rock would contribute to the seal saturation because of its natural water content and the high suction in the initially dry seal, both possibly leading to a comparably quick saturation of the seal.

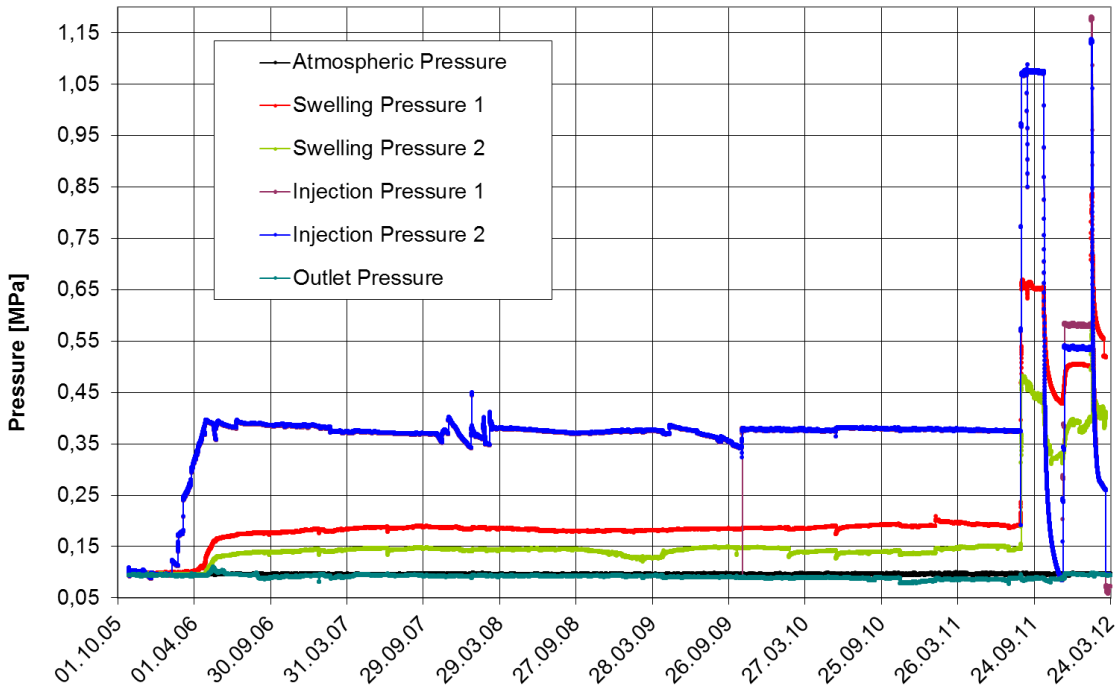

Fig. 5.7 Pressure evolution in test SB2 sealed with a 65/35 sand/bentonite mixture

After 3.5 months, from February to April 2006, the injection pressure was increased stepwise to a value of about 0.38 MPa, similar to tests SB1 and SB15. And indeed, different from the mock-up test, the swelling pressure sensors showed a quick response and reached almost final values between 0.15 and 0.19 MPa within a relatively short period of time of less than one year after start-up of water injection.

The measured maximum swelling pressure values between 0.15 and 0.19 MPa were almost in the same order of magnitude as those determined on small laboratory test samples (compare Tab. 2.9 in Section 2.2.4) and thus, similar sealing properties as those observed on small samples in the laboratory could be expected at that moment in this in-situ experiment.

At this stage by the end of 2006 it was already known from the mock-up test (compare Section 4.3) that the saturation time for the in-situ experiment would most probably exceed the calculated period of time significantly. It was, however, expected that this in-situ experiment with a 65/35 sand/bentonite mixture could be finished within a similar period of time as observed in the mock-up test.

However, in June 2011, 68 months (almost twice of the mock-up saturation time) after start-up of test SB2 no water outflow was observed in this in-situ experiment and after

this long waiting time, it was decided to do explicit numerical modelling work taking into account the interaction between sealing material and host rock to come to a reliable explanation of the current status and, as far as possible, making a prognosis how to finalize the experiment successfully within a reasonable period of time.

5.3.3.1 Model calibration and interpretative calculations

The idea was to perform first a sensitivity analysis on basis of a variation of porosity and permeability data which could explain the mock-up saturation time adequately. The most promising data are marked in yellow in Fig. 5.8. For the further calculations this parameter combination of K = $1.2 \cdot 10^{-18}$ m^2 and ϕ = 0.4 was selected.

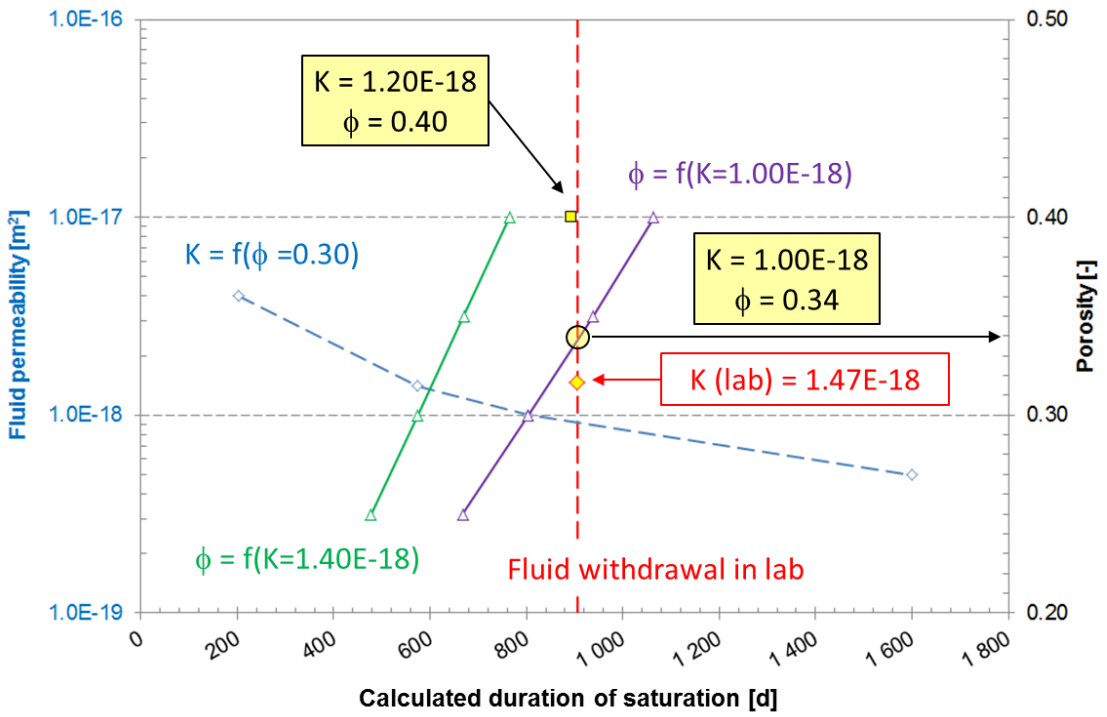

Fig. 5.8 Results of the sensitivity analysis with determined parameter combinations

The calibrated model was then used to re-calculate the saturation process in both the mock-up test and the SB2 test. Fig. 5.9 shows the evolution of the saturation process in the mock-up test and Fig. 5.10 shows that of the SB2 test, neglecting any hydraulic impact of the surrounding rock. The calculation indicated good agreement of the measured (Section 4.3) and the re-calculated saturation time of about 29 months for

the mock-up and a saturation time of about four years for the in-situ experiment with a 65/35 sand/bentonite seal which in fact was not observed at the SB2 test at this moment.

Because of this finding it was then decided to take the interaction between sealing material and host rock in the modelling into account in order to come to a more reliable explanation of the current status and, as far as possible, making a prognosis how to finalize the experiment in 2011 successfully.

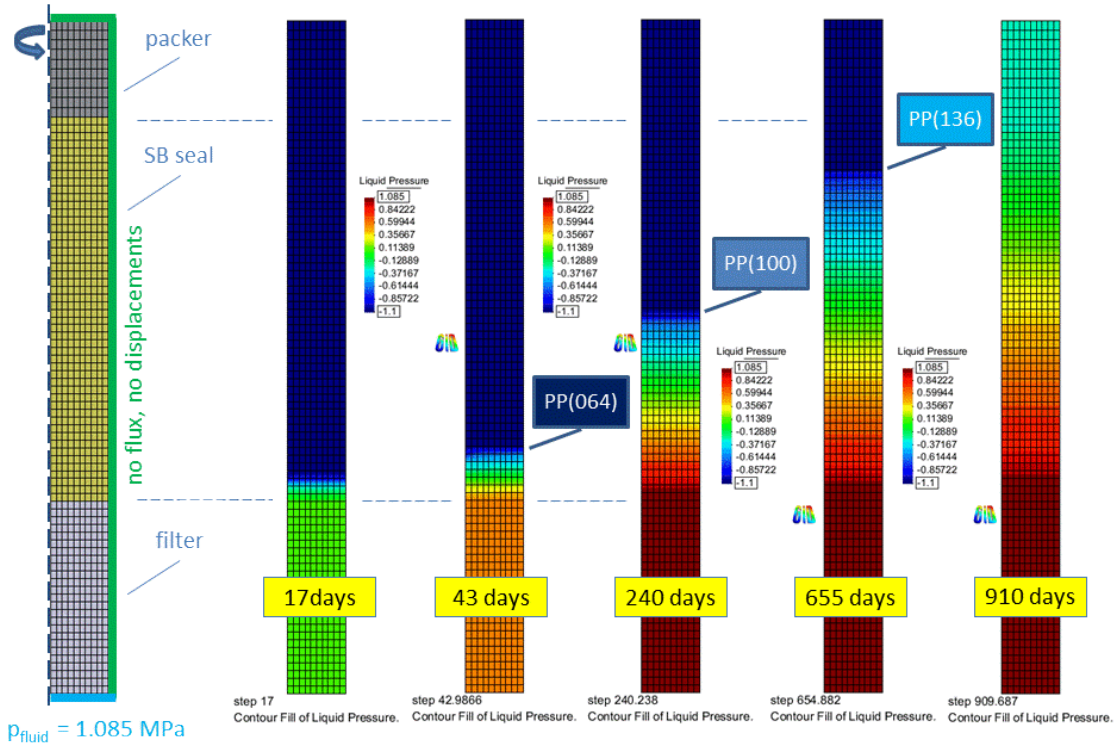

Fig. 5.9 Evolution of the fluid pressure over time in the mock-up test ($p_{injection}$ = 1.085 MPa)

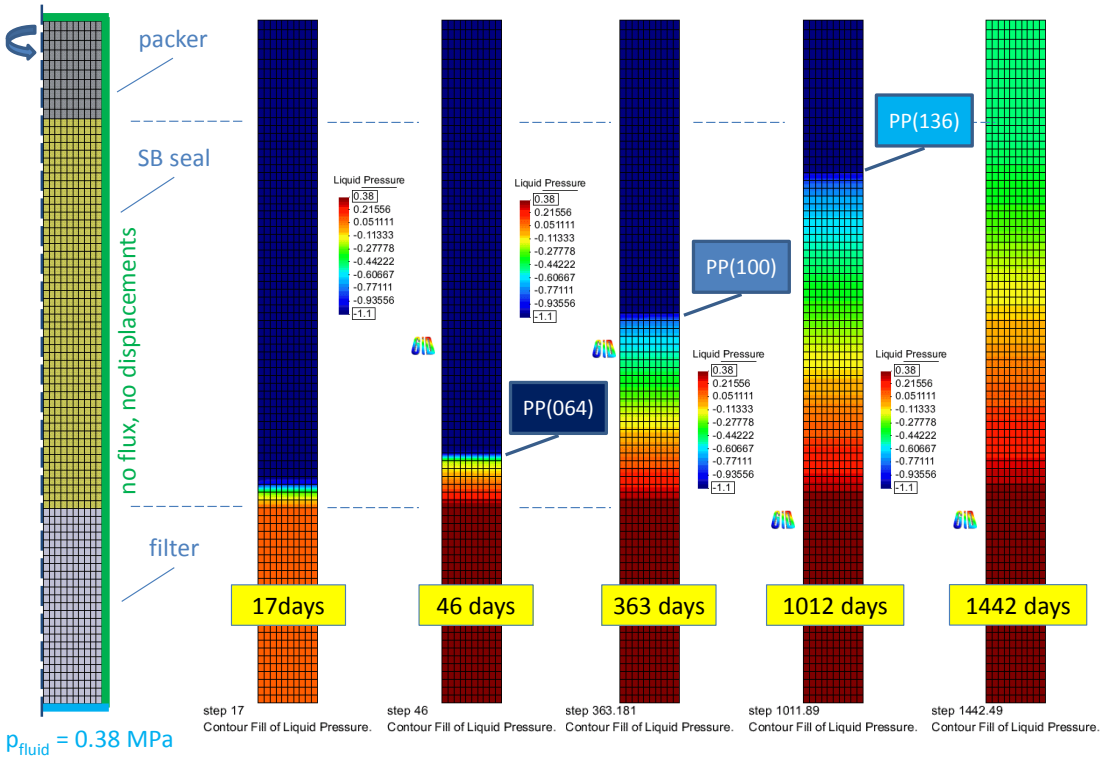

Fig. 5.10 Evolution of the fluid pressure over time in the in-situ experiment ($p_{injection}$ = 0.38 MPa)

A rotation symmetrical model with 100 m in height and 50 m in length – similar as that used in the scoping calculations (Section 3.5.2.1) – was used for the improved interpretative modelling (Fig. 5.11). In the centre of the model the SB niche is located. The SB2 experimental layout was abstracted and modelled as a cylindrical borehole of 0.31 m diameter without explicit modelling of the instrumentation to keep the calculation effort low. In contrast to the scoping calculations the anisotropic stress state and the hydraulic anisotropy was considered as follows: At the MTRL the maximum principal stress at laboratory level is in the order of 6.5 MPa, sub-vertically oriented, and its magnitude corresponds to the overburden of 250 m to 300 m. One of the two sub-horizontal principal stresses is roughly aligned with the orientation of the security tunnel and the other one perpendicular to this drift. The described stress state is to be considered a best estimate because stress measurements in clay rich rocks are problematic because of the low strength, the high anisotropy and the swelling properties of the Opalinus Clay. An extensive discussion of the stress state can be found in Martin et al. /MAR 03/. According to Vietor et al. /VIE 06/ the minor principal stress, which is perpendicular to the orientation of the security tunnel, is assumed to be 2.2 MPa, whereas the intermediate principal stress is parallel oriented and its value is

about 4.3 MPa. Intact Opalinus Clay exhibits a very low hydraulic conductivity, with a mean of $k_f = 2.0 \cdot 10^{-13}$ m/s within the rock matrix and a much lower value in the direction perpendicular to the bedding planes of $k_f = 6.0 \cdot 10^{-14}$ m/s. The very fine pore network is assumed to be fully saturated with an average porosity of 13.7 % and the pore pressure is assumed to be 2 MPa at laboratory scale /Boc 08/.

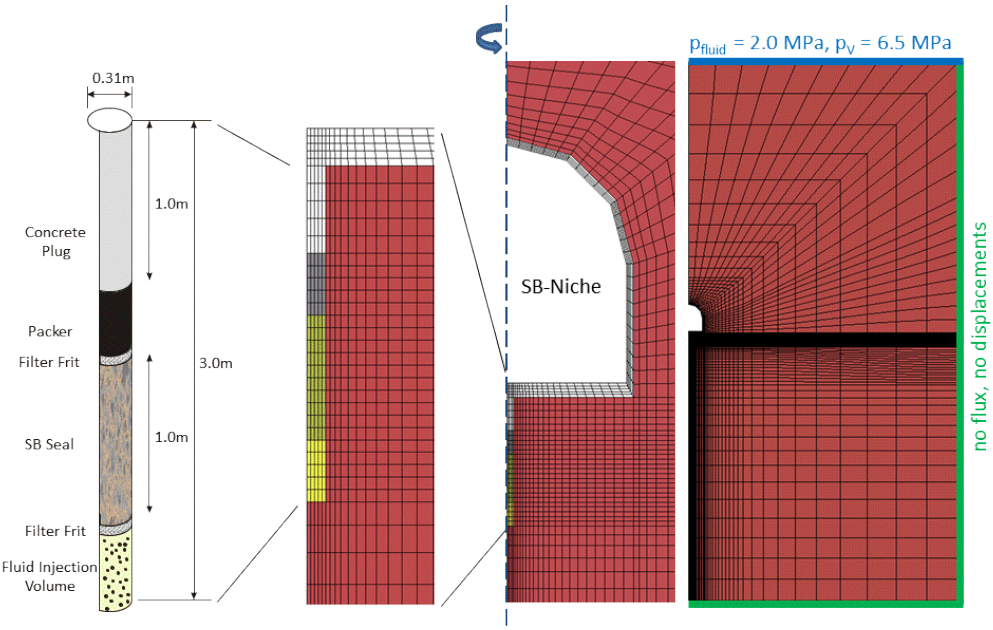

Fig. 5.11 Rotation symmetrical model

As far as possible, the simulation process goes along with the realistic time schedule, which means that after simulation of the excavation process of the SB-test room, about 5 months (from mid of November 2004 to end of April 2005) of ventilation and associated de-saturation of the whole system was simulated. Due to the capabilities of the adopted simplified approach without taking into account any damaging process the development of an excavation damaged zone (EDZ) at the gallery contour was not simulated; the time-dependent desaturation process of the surrounding rock mass induced by ventilation was, however, modelled by setting the hydraulic boundary condition to a negative pore pressure of about -5 MPa. Consequently, the contour zone was de-saturated up to values of about Sr = 95 % and the pore pressure field inside the rock mass varies with time. On 29 April 2005, the borehole was excavated and prepared for installation.

Fig. 5.12 shows the pore pressure propagation as a result of hydro-mechanical coupled simulation at different time steps due to the installation sequence of the SB2

experiment. The used spectrum of colours for the water pressure is identical in the different figures (a) to (d) and is also limited by p_{fluid} = 0.1 MPa (marked in blue) and p_{fluid} = 1.9 MPa (marked in red). Values of pore pressure that are outside this range are not shown.

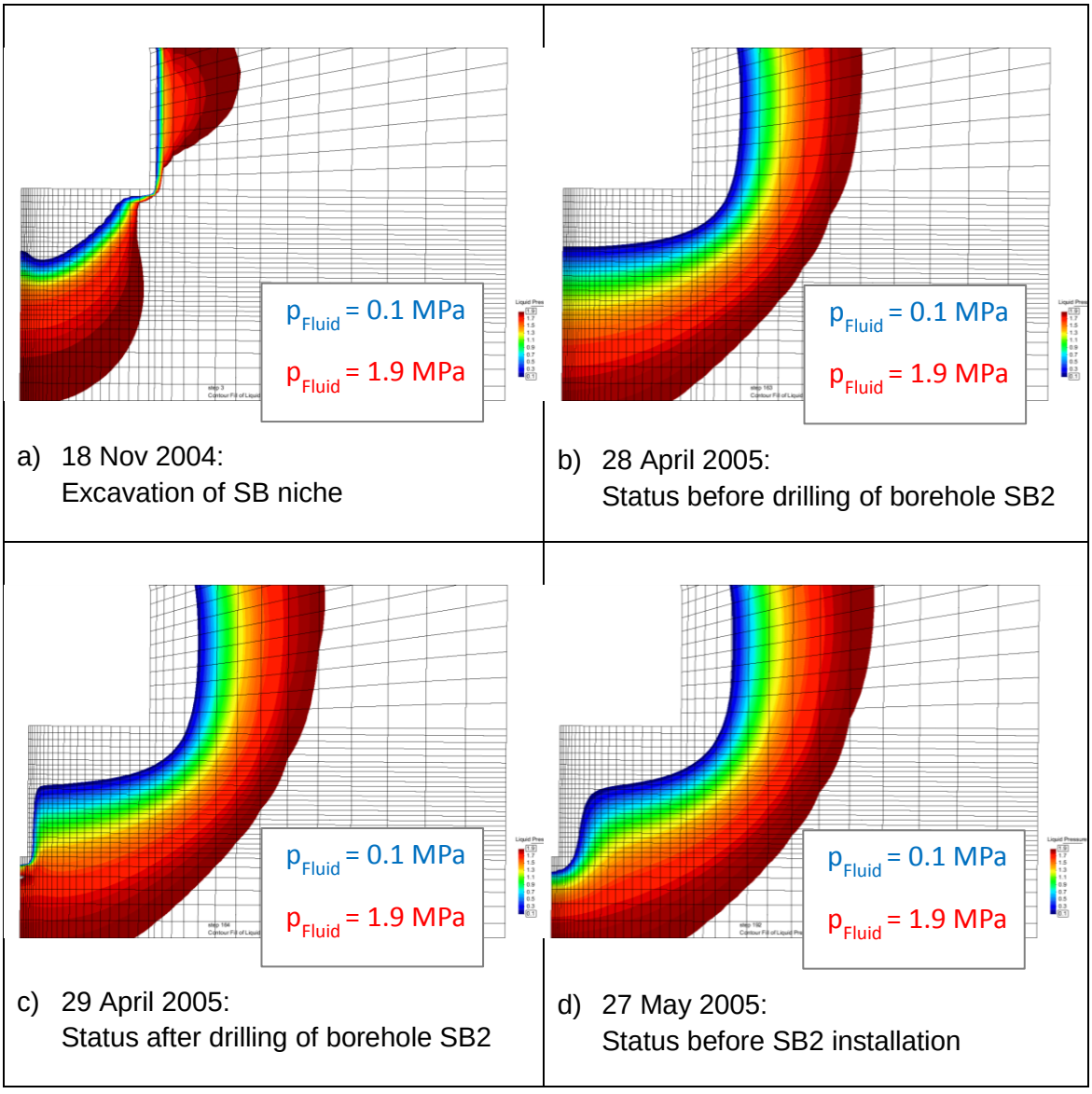

Fig. 5.12 Pore pressure propagation as a result of hydro-mechanical coupled simulation at different time steps due to the installation sequence of the SB2 experiment

Fig. 5.13 gives an impression on the impact of de-saturation in a horizontal cross section in the rock mass around the SB2 borehole at the buffer material mid-height at selected time steps. The results show that the level of pore water pressure of 0.7 MPa that was calculated before SB2 excavation is reached after 1 month of de-saturation at a distance of approx. 1.5 m to the borehole contour.

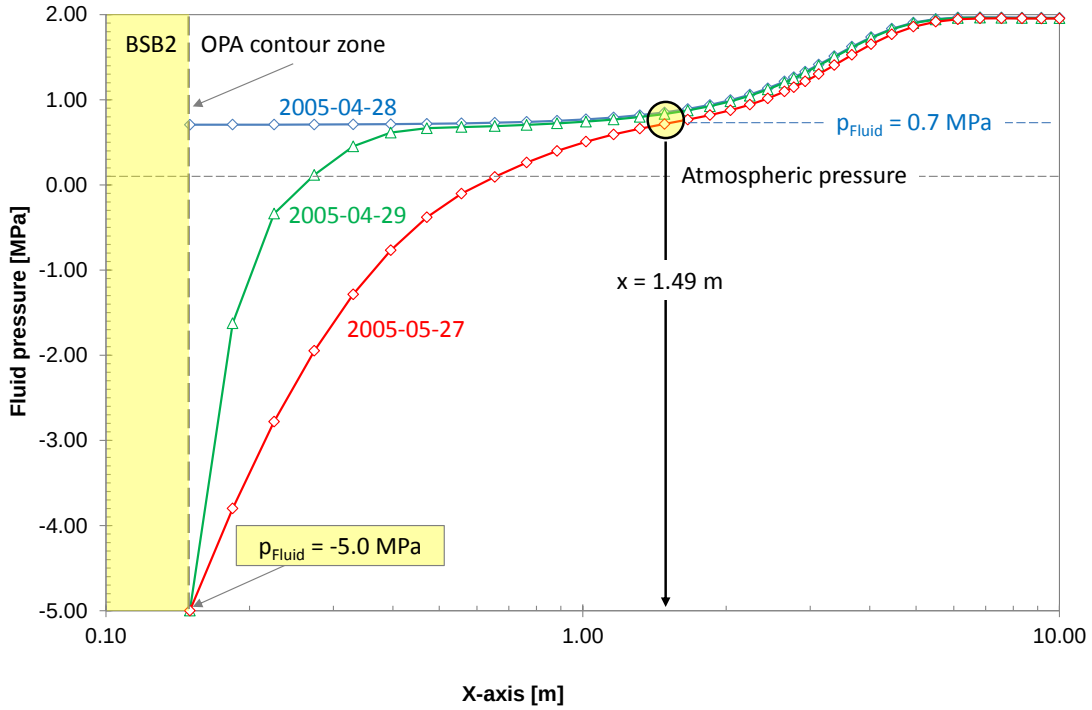

Fig. 5.13 Pore pressure propagation as a result of hydro-mechanical coupled simulation at different time steps due to the installation sequence of the SB2 experiment in a horizontal cross section

Several pore water pressure sensors were installed in the vicinity of the experimental area between the BSB1 and BSB2 boreholes. Fig. 5.14 shows the position of the corresponding boreholes BSB6 – BSB10. The sensors are located at levels of 1 m to 2 m below the niche floor. The sensors SB-PWP9 and SB-PWP8 are located at a horizontal distance to the BSB2 axis of 0.36 m, whereas the sensor SB-PWP7 and SB-PWP6 are located at distances of 0.75 m and 1.5 m.

According to Fig. 5.14 the measurement results of SB-PWP7 show pore pressure values similar to the atmospheric pressure. This shows that a circular area around the BSB2 borehole with a minimum radius of about 0.75 m is highly influenced by the pre-installation process. Nevertheless it could not be excluded that the fluid injection pressure itself has a certain influence on the near field rock mass.In a second step, the existing model was then extended to be able to take into account the interaction between the sealing material and host rock in order to come to a more reliable explanation of the current status. Taking advantage of earlier investigations made within the project, the FE mesh used for the interpretative calculations of the mock-up test was extended by a rectangular body representing the influenced part of the near

field rock mass with a radial extension of about 1.5 m. The modified mesh and the new boundary conditions are shown in Fig. 5.15 in detail.

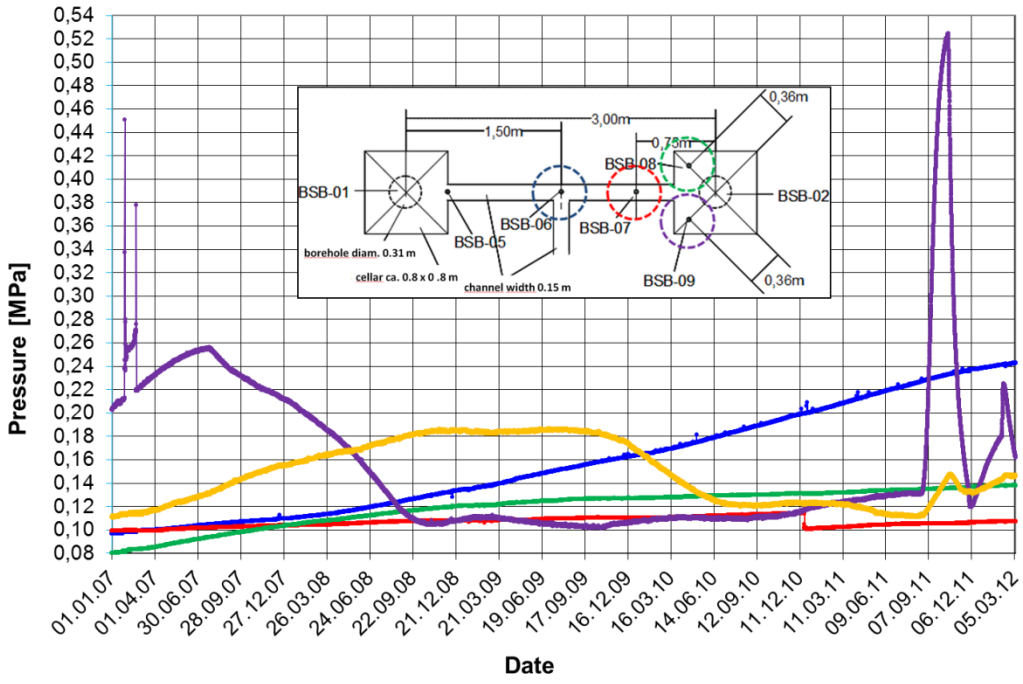

Fig. 5.14 Pore pressure measurement results in the near field of the BSB1 and BSB2 boreholes

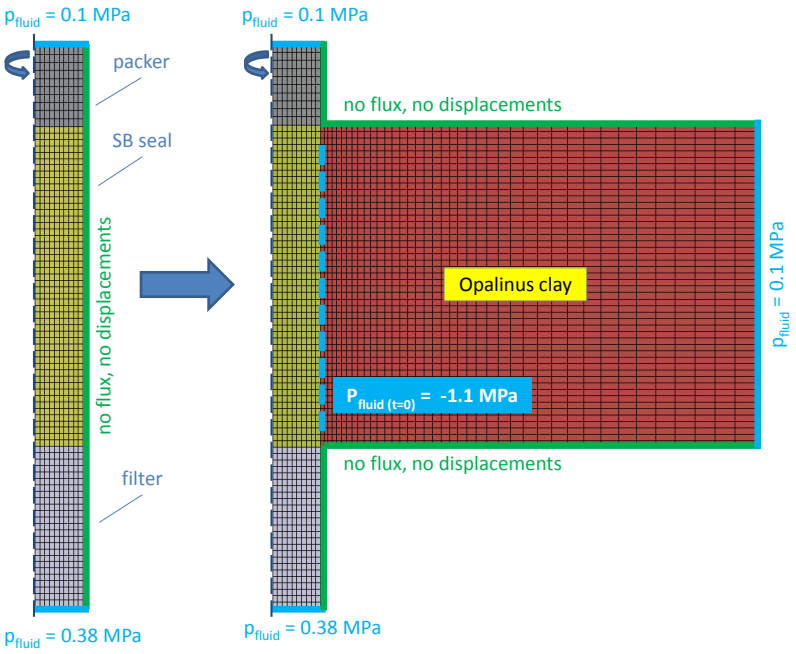

Fig. 5.15 Modified FE mesh with boundary conditions

Fig. 5.16a shows simulation results for the pore water distribution 5 years after experiment installation. Analogue to Fig. 5.12 the used spectrum of colours for the water pressure is limited at a minimum value of p_{fluid} = 0.2 MPa (marked in blue), whereas the maximum value (here: p_{fluid} = 0.38 MPa) is marked in brown. Values in the range of the atmospheric pressure are not shown. The results show furthermore the importance of the consideration of the rock contour zone and its hydro-mechanical influence on the experimental trend. The simulation results show a full saturation of the buffer after nearly 1.5 years (not shown in the figure).

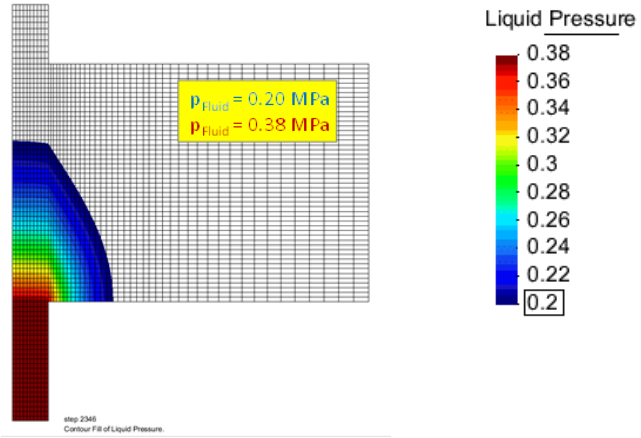

a) after 5 years at an injection pressure of 0.38 MPa

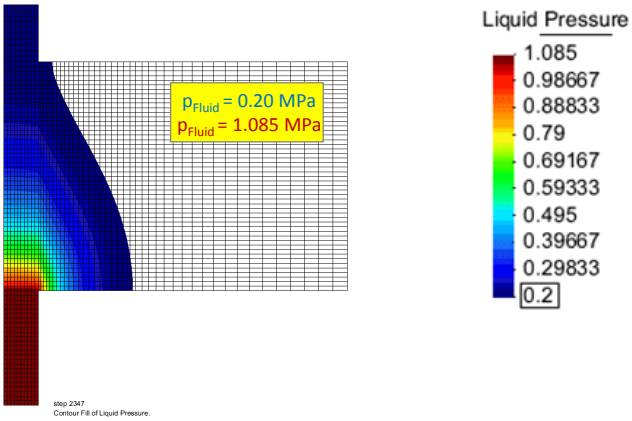

b) 1 day after injection pressure increase to 1.085 MPa

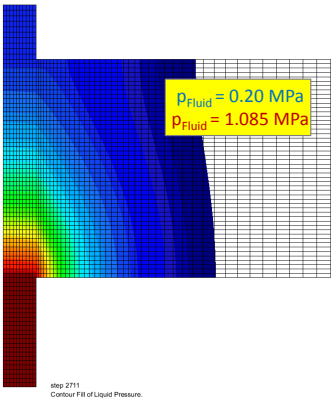

c) 1 year after injection pressure increase to 1.085 MPa

Fig. 5.16 Distribution of porewater pressure around test SB2

But the water injection pressure of 0.38 MPa applied in the in-situ experiment does not lead to a measurable pressure increase (< 0.18 MPa) at top of the SB2 sand/bentonite

seal. In fact, the pressure distribution leads to equilibrium with the hydraulic boundary conditions of the near field rock mass. Vice versa, the pore water pressure flux towards the SB2 borehole leads to a faster re-saturation than interpretatively calculated for the laboratory experiment.

In order to analyse how to finalise the experiment in 2011 successfully the water injection pressure was then increased to the same level of about 1.085 MPa which was applied in the mock-up test. Fig. 5.16 shows the evolution of the pore water pressure in the system for (b) 1 day after pressure increase and (c) 365 days later. The simulation results show clearly that a distinct increase of the pore pressure to 0.37 MPa inside the seal and the adjacent rock will occur. This pressure level exceeds the pore water pressure of 0.2 MPa prevailing in the system before and will thus lead to a measurable water outflow at top of the seal within a very short period of time of only 24 hours thereby enabling the pending final determination of the seal permeability.

5.3.3.2 Successful termination of test SB2

In accordance with the outcomes of the interpretative modelling it was consequently decided to increase the fluid injection pressure in August 2011 as was done in the modelling. In order to enable the measurement of water flowing through the seal a small measuring container (Fig. 5.17) was placed on a balance outside the borehole at the control valve panel and connected via a water filled tube to the upper filter frit.

During the pressure increase phase, the water injection pressure was first increased to 1 MPa (absolute) resulting in a slight and soon stagnating water outflow. To enforce a water outflow the pressure was again slightly increased to 1.1 MPa (Fig. 5.18). In fact, from this point onwards – similar as in the mock-up test – a periodic water outflow could be seen together with an increase of the swelling pressure sensors signals. Fig. 5.18 shows the evolution of the injection pressure and the measured cumulative mass of water. The steps in the balance reading curve are explainable by some gas volumes still remaining in the seal. These gas volumes are displaced by the injected water and interrupt a continuous water flow from the seal to the upper filter frit and the outlet tube.

Fig. 5.17 Measuring container placed on a high precision balance located outside the borehole

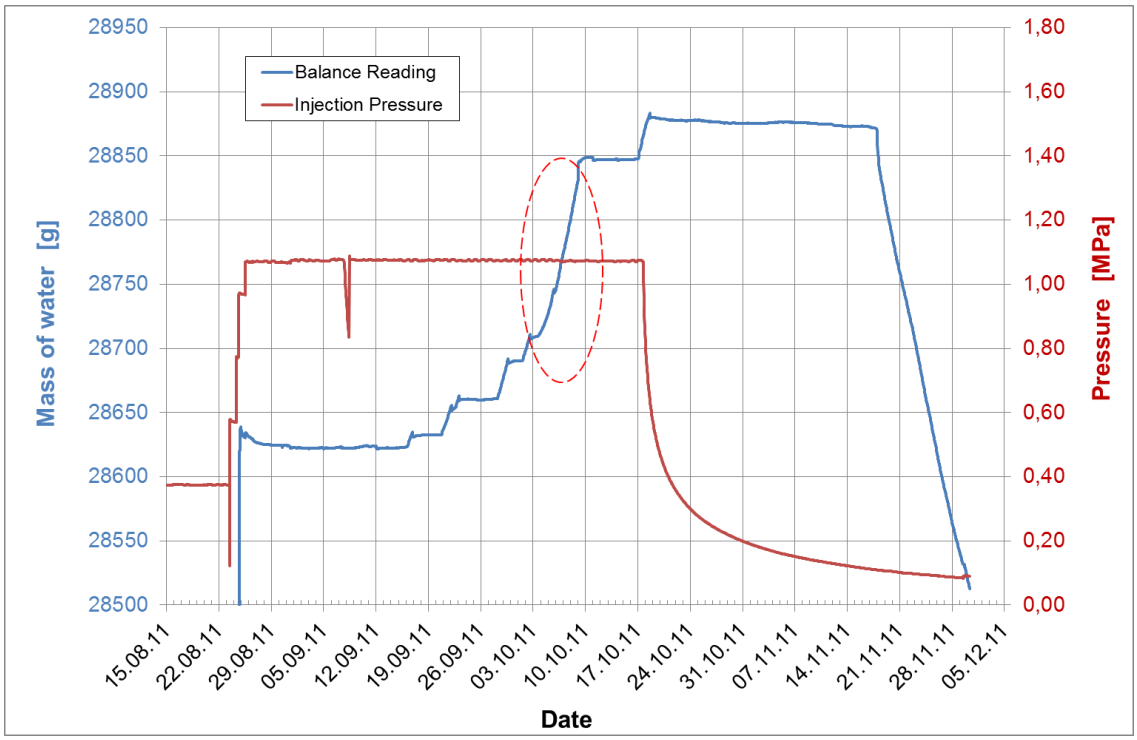

Fig. 5.18 Injection pressure (red) and mass of water (blue) collected in the measuring container at the control panel

Determination of the seal material's water permeability

The water outflow rates in the different outflow phases were quite similar. In the more detailed Fig. 5.19 the area marked in Fig. 5.18 by an ellipsis shows steady state water outflow from the seal and could thus be used to determine the seal permeability to water in the saturated seal state. It amounts to $4.2 \cdot 10^{-18}$ m^2, a value which is in excellent agreement with the value determined on the small laboratory samples (see Tab. 2.9) and hence confirms the expected seal properties.

On November 17, 2011, a while after reduction of the water injection pressure (see Fig. 5.18), some water began to flow back into the seal or the surrounding rock mass, respectively. This behaviour is also in accordance with the results of the numerical simulation which are based on equilibrium between the fluid injection pressure and the pore pressure in the rock.

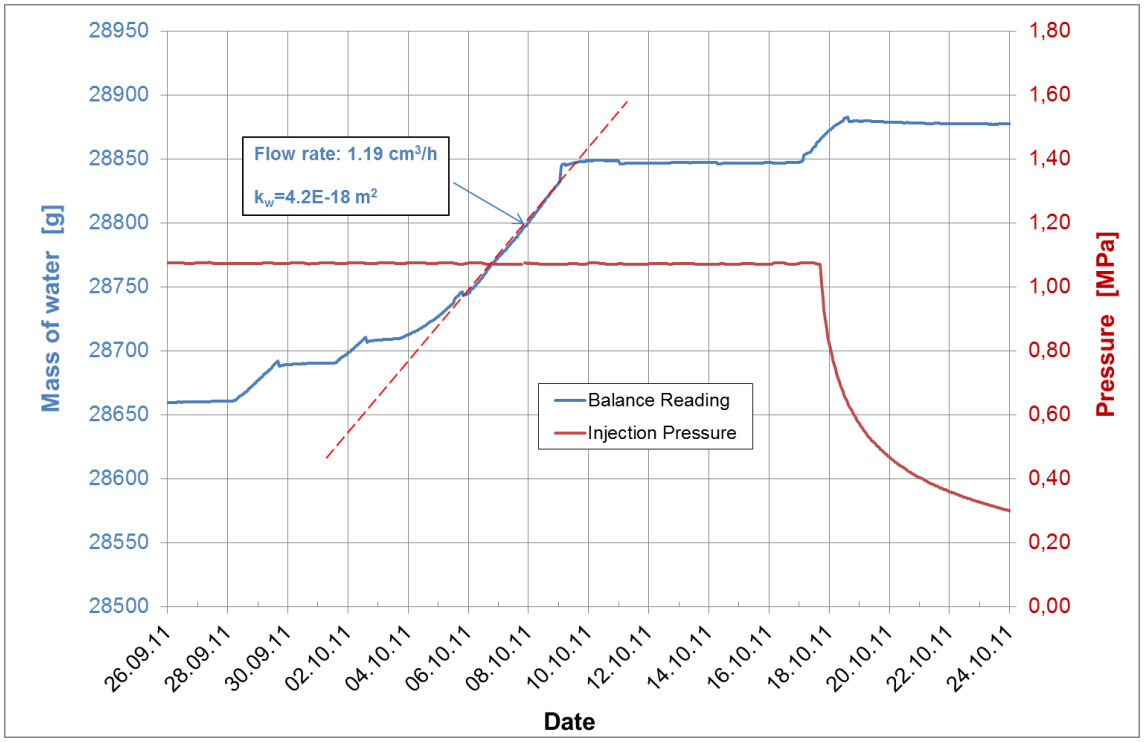

Fig. 5.19 Determination of seal permeability to water on basis of measured steady state water outflow from the SB2 seal

Following the determination of the water permeability the pending gas injection test was prepared by the preceding pressure equalization phase already mentioned above. The system was closed at the injection side, allowing the pressure to reduce and equalize via the seal and the surrounding rock (see Fig. 5.18 and Fig. 5.20). The relatively slow pressure reduction measured in contrast to that observed in the tests SB1 and SB15 is obviously due to a tight contact of the seal to the rock in this test set-up. The pressure reduction lasted until it faded almost completely.

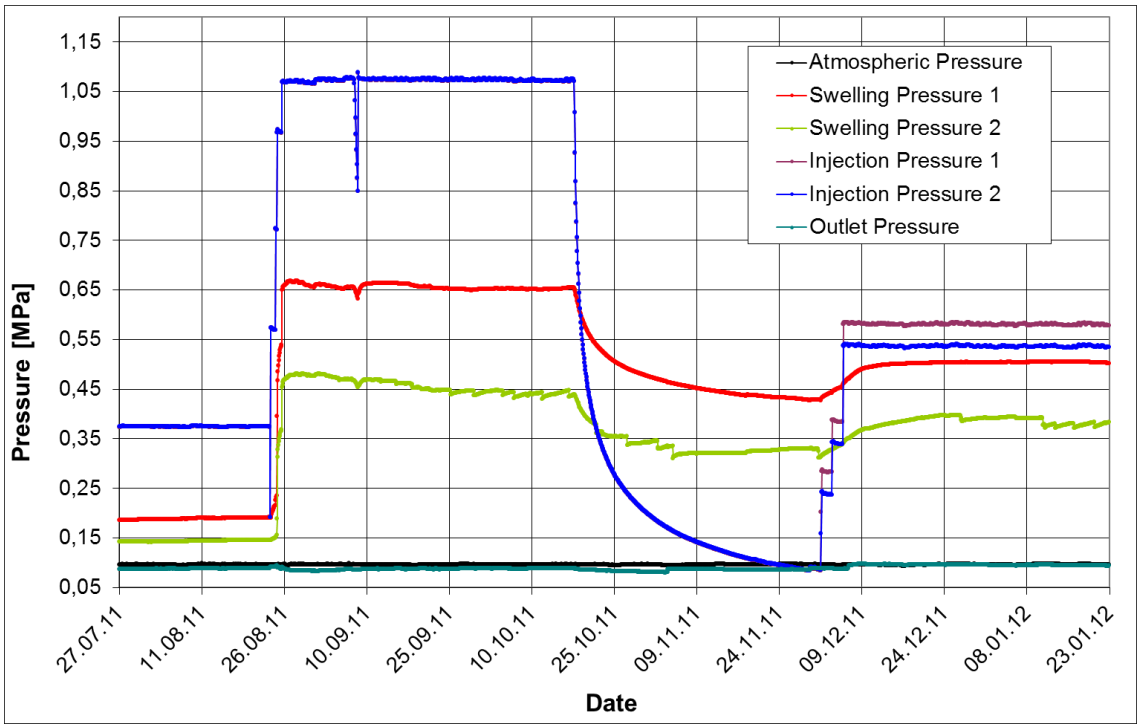

Fig. 5.20 Pressure signals of test SB2 during the water injection phase, the pressure equalization phase, and the final gas injection phase

Determination of the seal material's gas entry pressure

The gas injection was then started on 1 December 2011 (see pressure curves in Fig. 5.20 and Fig. 5.21). Two effects could be observed during the gas injection phase. First, the swelling pressure sensors readings were increasing with the injection pressure finally approaching values of 0.33 MPa and 0.43 MPa, respectively. This behaviour reflects the mechanical compaction of the saturated seal caused by the increasing gas pressure. Second, a the amount of water flowing back into the seal decreased. This reduction of the water backflow is most probably due to the closing of existing flow paths within the seal material because of its aforementioned compaction.

24 hours after increasing the pressure in a second step to 0.4 MPa on December 3, 2011, the water backflow started to fade for the first time. A further pressure increase on December 5, 2011 led finally to a complete stagnation of the water backflow. This behaviour reflects the starting gas entry into the seal material which hinders a further backflow of water from the outside measuring container.

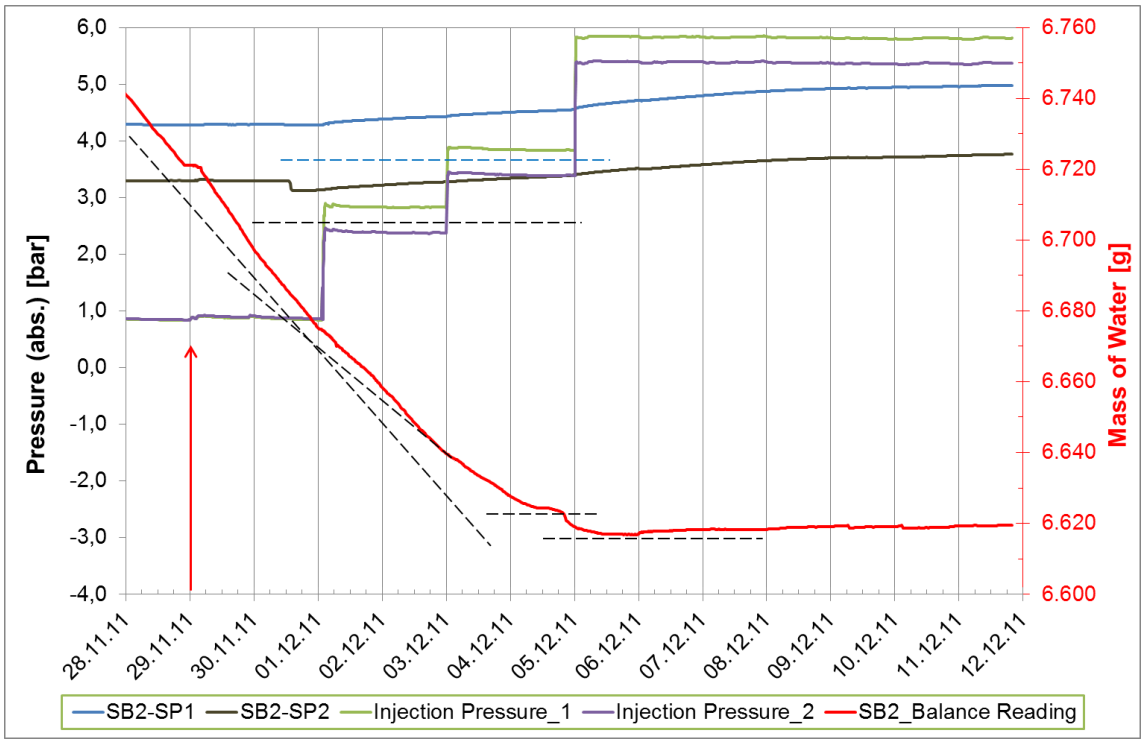

Fig. 5.21 Gas injection pressure (green and pink), swelling pressure readings (blue and black), and mass of water (red) monitored in the measuring container outside the borehole SB2

The swelling pressure amounting to about 0.45 MPa at this moment represents the gas entry pressure which is exceeded by the applied gas pressure ranging between 0.55 to 0.6 MPa. The gas entry pressure value determined in this way is in good agreement with the values determined on the small laboratory samples (compare Tab. 2.9) and confirms the expected and desired seal properties excellently.

Test SB2 was then shut-in during the turn of the years 2011/2012. Gas injection was continued from February 6, 2012 onwards with increasing the injection pressure to 1.2 MPa, the value that was also applied in the mock-up test. The awaited gas break-through was observed two days later on February 8, 2012 with continuously increasing gas flow rates as shown in Fig. 5.22.

Due to the fact that the SB-project was to be terminated in agreement with the funding institution PTKA before June 30, 2012, the GRS-technicians stopped gas injection on February 10, 2012. The permeability to gas of the partly de-saturated seal as determined on basis of the measured gas flow rates between February 8 and 10 ranges between $9.3 \cdot 10^{-17}$ m^2 and $4.1 \cdot 10^{-16}$ m^2. This range of values agrees very fine with the value determined for the mock-up test (see Section 4.3) and also with the values determined on the small laboratory samples (see Tab. 2.9) and thus fulfils the requirements given in Tab. 2.9 and confirms the expected seal properties excellently.

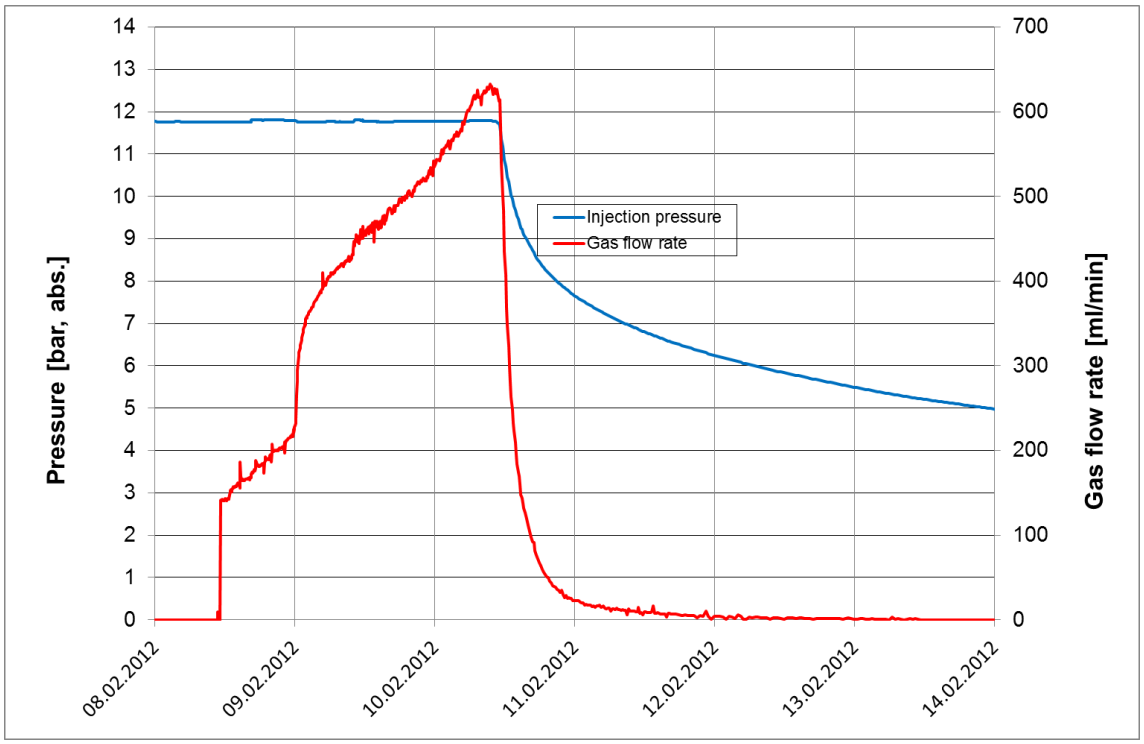

Fig. 5.22 Gas injection pressure and gas flow rate measured at test SB2 after gas break-through

With this, the overall objective of this project "to test and demonstrate that the sealing properties of sand/bentonite mixtures determined in the laboratory can technically be realized and maintained in situ under repository relevant conditions" can be considered as being – finally – achieved successfully.

5.4 Post-test investigations

Operation of all four tests was finished in October 2011, after the successful termination of the leading test SB2 (see Sections 5.3.3.1 and 5.3.3.2). In the following, post-test investigations on representative samples drilled from the seal and the surrounding rock were to be conducted for reasons of quality assurance to characterize the achieved in-situ state of seal saturation in the individual test set-ups.

Post-test sampling was done in three campaigns as listed below:

- 28 November – 8 December 2011: test SB1
- 6 February – 16 February 2012: tests SB13 and SB15
- 12 March – 21 March 2012: test SB2

It was decided to start sampling at test site SB1 for testing the envisaged sampling methods. This decision was taken since test site SB1 exhibited a not completely satisfying test performance, similar as SB15 did (compare explanations in Section 5.3.1). Most successful tested actions and methods were later-on applied at all the remaining test sites. Fig. 5.23 and Fig. 5.24 show a series of photos taken during sampling.

Cores from the rock mass were immediately sealed in air-tight sampling boxes. Core material taken from the individual SB seals with individual driving rods remained inside the individually used driving rod which was air-tight sealed on-site right after sampling.

The results of the post-test laboratory analysis of the finally prevailing water content in the samples taken at the four test sites are given in the following sections.

a) Step 1: Coring of a concrete plug

b) Cored concrete plug still in place

c) Step 2: Retrieval of concrete plug

d) Step 3: Retrieval of the packer

e) Retrieved packer

f) Step 4: Coring of seal material

Fig. 5.23 Photos taken during post-test sampling

a) Filled driving rod

b) Seal with a left core borehole

c) Drilling machine shortly before coring an inclined borehole

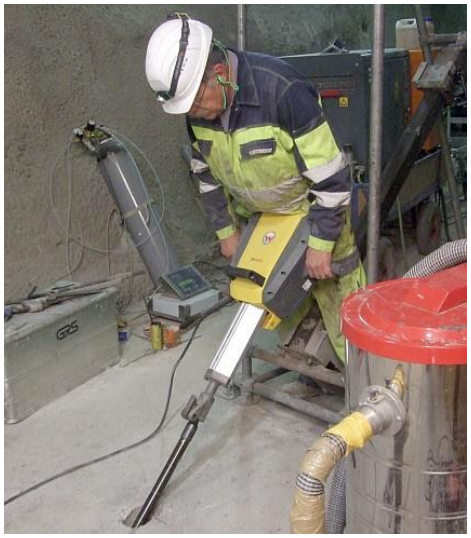

d) Coring of seal material through an inclined borehole

Fig. 5.24 More photos taken during post-test sampling

5.4.1 Post-test results of test SB1

Fig. 5.25 shows the (as-built) set-up of test SB1 and within that drawing the locations of the sampling boreholes and the individual the samples. Fig. 5.26 shows the water content of the samples taken over the seal length from the seal centre with an average water content of 26.6 %. This high water content reflects the comparably low installation density of 1.72 g/cm^3 achieved at this test borehole in comparison to that of 1.91 g/cm^3 achieved in the equally equipped borehole SB2. Although the swelling

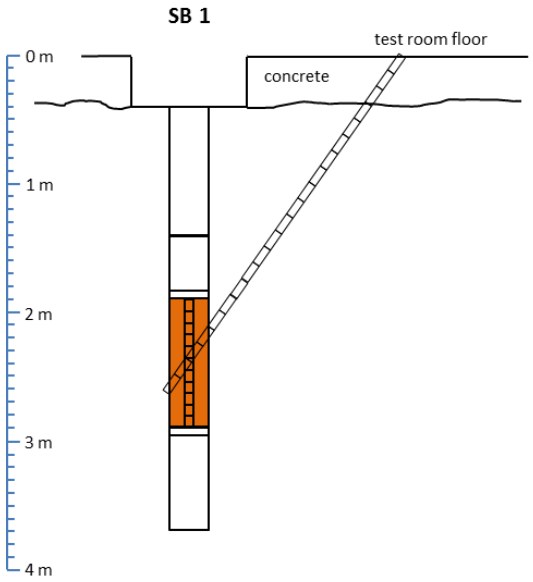

Fig. 5.25 Overview of core boreholes and sample locations at test site SB1

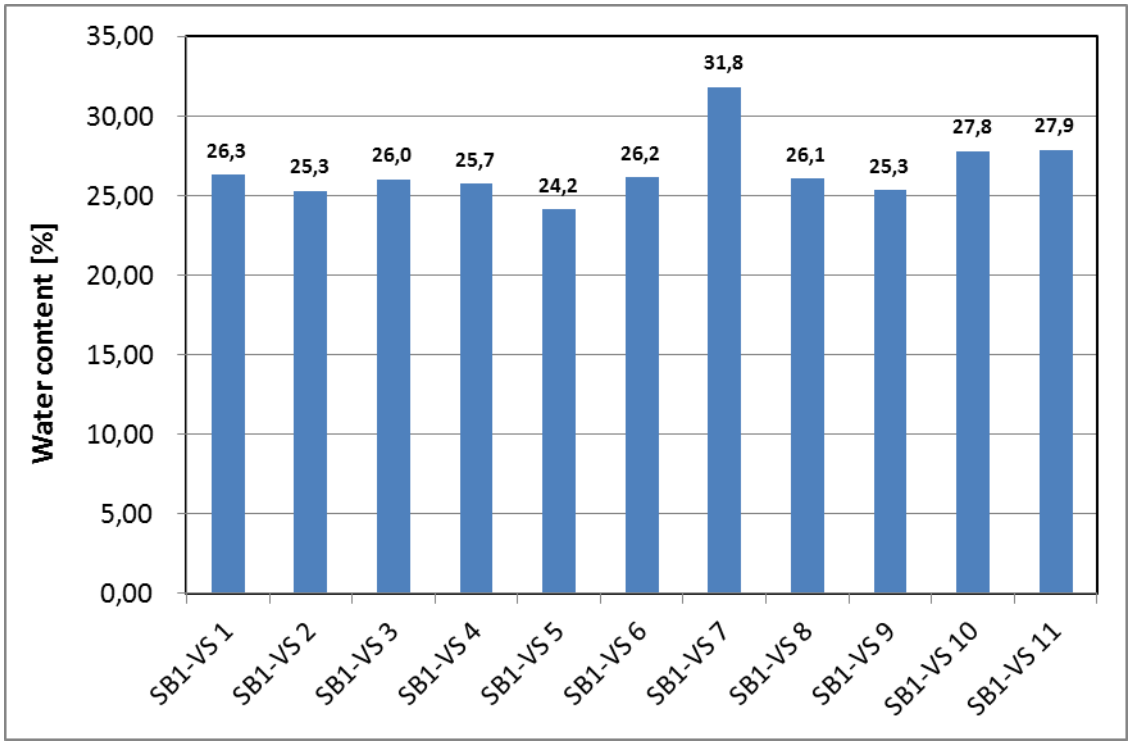

Fig. 5.26 Water content of samples taken from seal centre at test SB1 (left: deepest sample, right: uppermost sample)

pressures measured in the early state of this test showed similar values in the initial test phase (see Fig. 5.4) as observed at test borehole SB2 the bypassing of the injected water along the borehole wall through the excavation damaged zone occurred

after increasing the water injection pressure in the initial phase of this test to about 0.4 MPa (see Section 5.3.1). Unfortunately, this test performance made a reasonable test evaluation impossible.

According to the dry installation density of 1.62 g/cm^3 and the grain densities of the installed clay and sand portions (see data in Tab 2.3 and Tab. 2.4) in this borehole the porosity of the installed material (65/35 sand/bentonite ratio) is calculated to 39.6 %. This value is significantly higher than the porosity of 29 % determined for the same material mixture installed at the mock-up Test 2 and is accordingly in line with the low installation density (see above). The respective water content amounts to about 24.5 % which agrees fairly good with the water content data shown in Fig. 5.26 and thus confirms full saturation of the seal material in this test borehole.

Due to the ventilation over longer periods of time, the average water content of 5.98 % of the clay rock samples taken from the inclined core borehole located outside the borehole BSB1 (see Fig. 5.27) is slightly lower in comparison to the average water content of 7.03 % determined at other test sites in the MTRL /MAZ 08/.

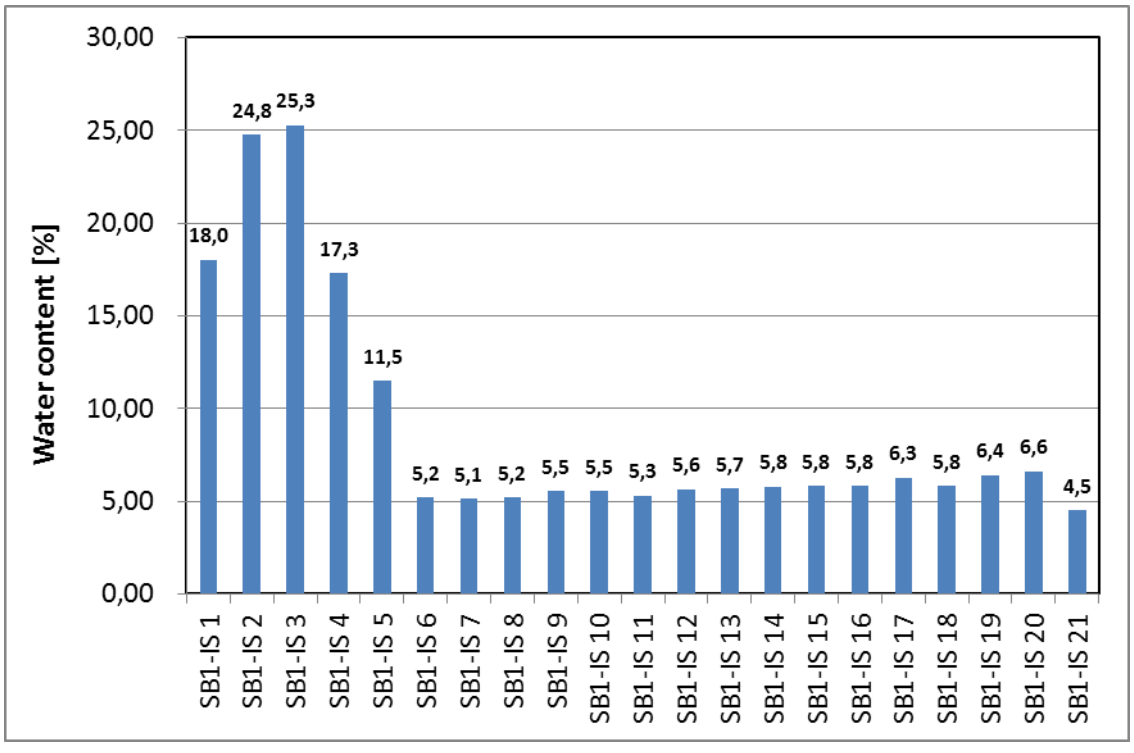

Fig. 5.27 Water content of samples taken from inclined core drilling at test SB1 (left: deepest sample, right: uppermost sample)

5.4.2 Post-test results of test SB15

Fig. 5.28 shows the (as-built) set-up of test SB15 and in this drawing the locations of the two sampling boreholes and the individual samples. Fig. 5.29 shows the water content of the samples taken over the seal length from the seal centre. The water content decreases in both sampling boreholes with decreasing depth, reflecting the fact that the water was injected at the bottom of the seal. The average water content of the seal amounts to 30.1 % which reflects the high porosity of 41 % determined on basis of the low installation density of 1.69 g/cm^3 realised at this test site. The average water content determined for the rock samples taken from the borehole wall which were in contact with the seal material amounts to about 32 % (Fig. 5.30) and is slightly higher than the water content of the seal material itself. This fact might confirm the assumed distinct EDZ prevailing at this test borehole. In addition, the water content determined on basis of the above-mentioned porosity of 41 % would yield a value of only 26 % which does not agree satisfactory with the data shown in Fig. 5.29. The reason for this deviation is not known. A possible explanation could be a transport of seal material out the upper outlet. Such a material transport might have happened in the early testing time when the water injection pressure was increased. At that time the bypassing of water along the seal/rock-interface occurred (see Section 5.3.1) and the acting

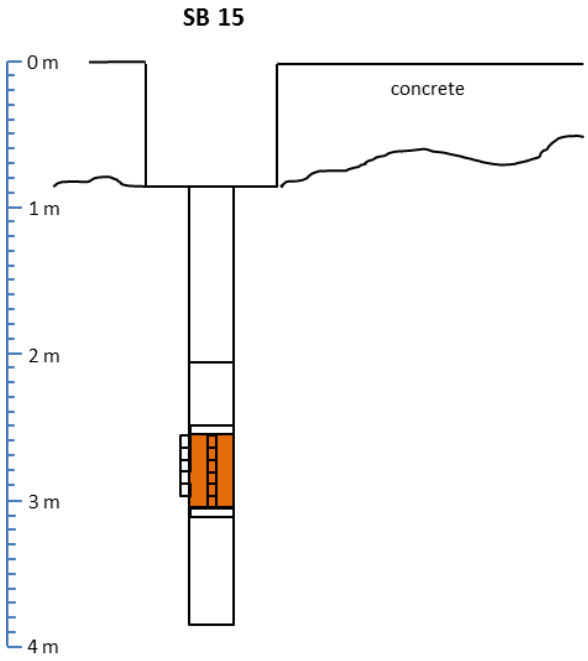

Fig. 5.28 Overview of core boreholes and sample locations at test site SB15

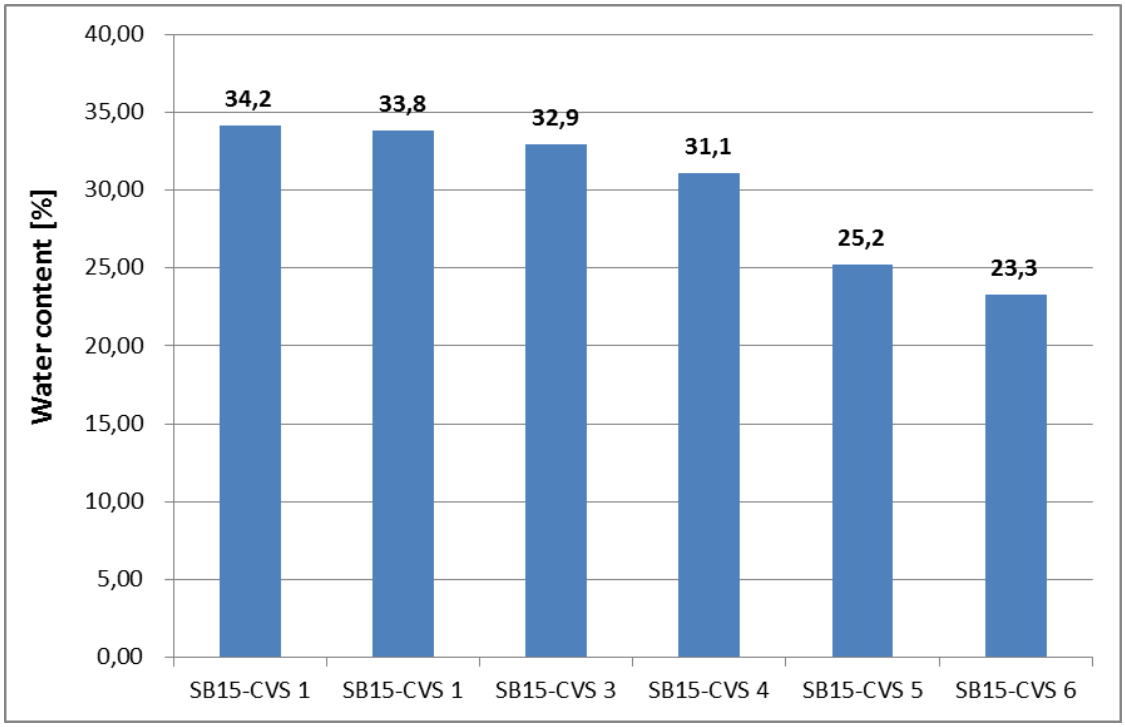

Fig. 5.29 Water content of samples taken from central seal at test SB15 (left: deepest sample, right: uppermost sample)

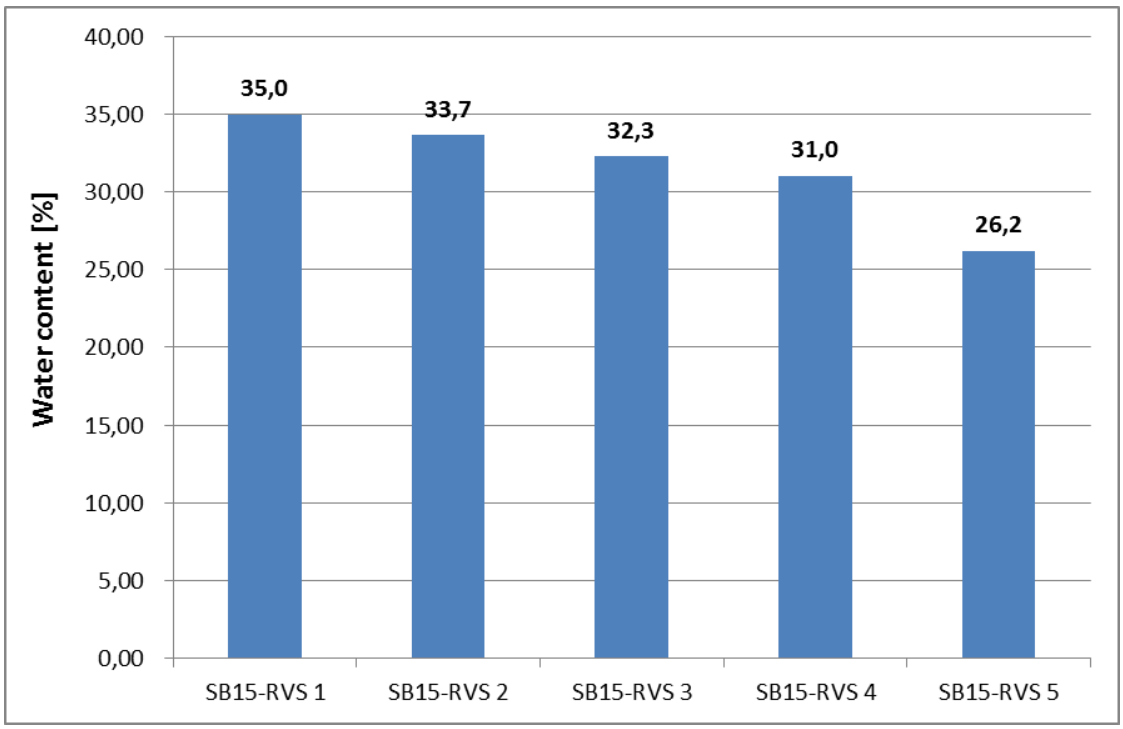

Fig. 5.30 Water content of samples taken from vertical core drilling at the seal/rock-interface of test SB15 (left: deepest sample, right: uppermost sample)

technician reported and outflow of some brown coloured water which could explain this effect. All described effects, the EDZ prevailing at this borehole as well as the likely material transport out of the seal section made a reasonable evaluation of this test impossible, similar as for test SB1.

5.4.3 Post-test results of test SB13

Fig. 5.31 shows the (as-built) set-up of test SB13 and in this drawing the location of the sampling borehole in the seal centre. Fig. 5.32 shows the water content of the samples taken over the seal length. Surprisingly, the water content decreases with increasing depth – against the expected trend, as the water was injected at the bottom of the seal. The average water content of 29.8 % reflects the porosity of 42,7 % determined on basis of the installation density of 1.64 g/cm^3 realised at this test site and is in fairly good agreement with the water content of 28 % determined on basis of the aforementioned material porosity. This fact, as well as the data showing higher water content at the top of the seal, indicates the upcoming saturation of the seal. A water outflow, however, was not detected during the testing period and thus full saturation was obviously not reached in this test. This is also confirmed by swelling pressure measurements with Sensor 1 (red curve in Fig. 5.6) showing a still increasing swelling pressure signal (see also the information about the pressure evolution in Section 5.3.2).

Because of the missing water outflow the test could unfortunately not be evaluated in terms of permeability to water and gas. Anyway, an attempt to determine the gas entry pressure was performed at the end of the testing phase. The gas injection indicated a gas entry pressure above 0.7 MPa (see Section 5.3.2). Theoretically, the swelling pressure is expected to range close to the measured swelling pressure the maximum values of which monitored at about 3 MPa (see Fig. 5.6). The really prevailing gas entry pressure of the actual test set-up, however, could not be determined because of the continuous gas pressure decay (see right side of Fig, 5.6) described in Section 5.3.2. This pressure decay is possibly caused by a preferential gas migration into the EDZ possibly still existing around the fluid injection volume below the SB seal.

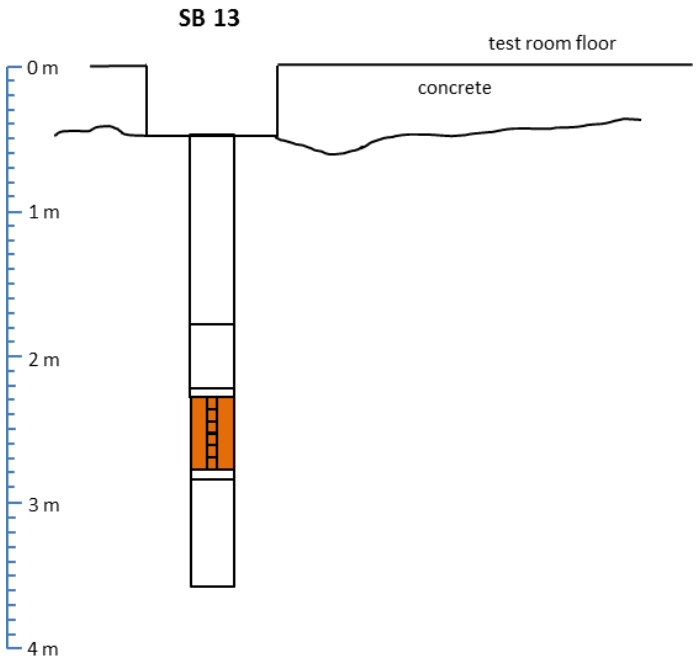

Fig. 5.31 Overview of core boreholes and sample locations at test site SB13

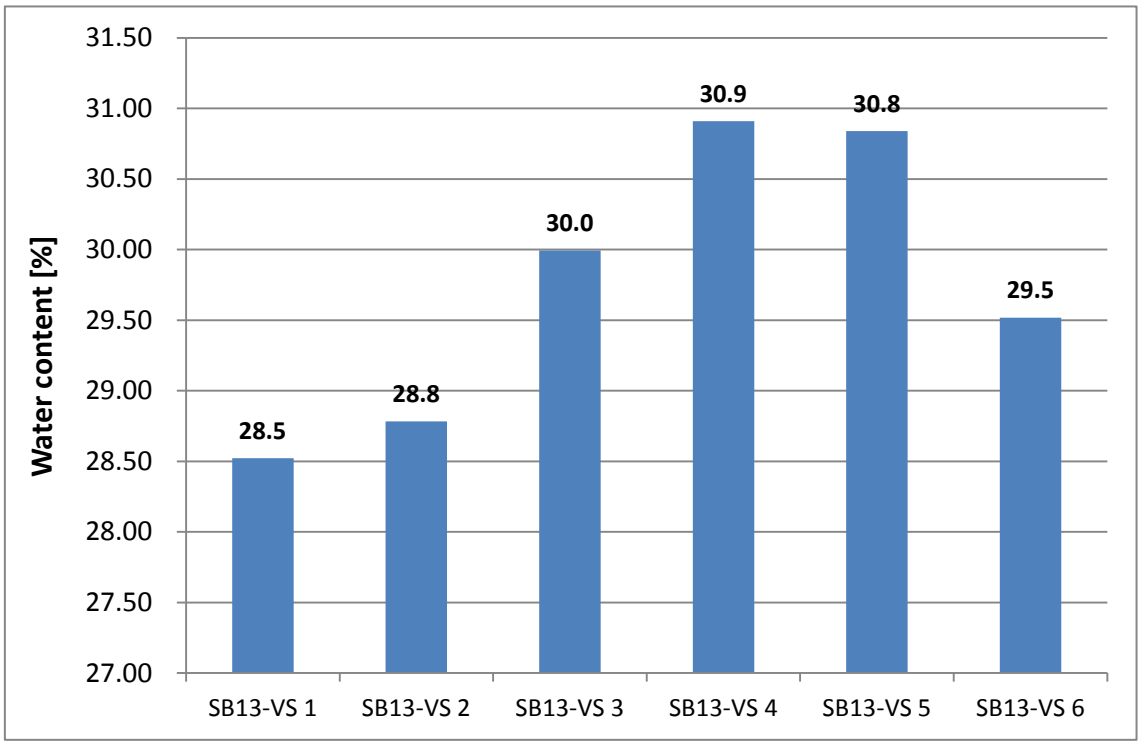

Fig. 5.32 Water content of samples taken from seal centre at test SB13 (left: deepest sample, right: uppermost sample)

5.4.4 Post-test results of test SB2

Fig. 5.33 shows the (as-built) set-up of test SB2 and in this drawing the location of three sampling boreholes in the seal centre as well as in the surrounding rock, parallel and inclined to the test borehole centreline. Fig. 5.34 shows the water content of the samples taken over the seal length averaging at a water content of 19.3 % which is slightly higher than the water content of 18.4 % found in the mock-up post-testsamples. This difference might – among others – be due to the slightly lower installation density and thus higher seal material porosity achieved in the in-situ test.

According to the dry installation density of 1.77 g/cm^3 and the grain densities of the installed clay and sand portions (see data in Tab. 2.3 and Tab. 2.4) in this borehole the porosity of the installed material (65/35 sand/bentonite ratio) is calculated to 29.9 % which agrees very good with the value of 29 % determined for the same material mixture installed at the mock-up Test 2. The content calculated on basis of the porosity of 29.9 % amounts to 16.9 % which is somewhat lower in comparison to the data shown in Fig. 5.34. The reason for this deviation is unclear. Anyway, the data confirm full saturation of the seal at the end of water injection and achievement of the target.

The water content data of the samples taken from the other boreholes at test site SB2 (Fig. 5.35 and Fig. 5.36) mirror the expectations. Samples from that portion of the inclined sampling borehole running through seal material show exactly the same water content of 18.4 % as seen in the mock-up test, but ranging a little bit higher than the water content of 19.3 % determined on the samples taken from the vertical sampling borehole.

Except for three samples, the average water content of the remaining samples taken from the inclined borehole and the second vertical sampling borehole situated at a distance of 0.5 m in the rock ranges around 7.4 %, which agrees fairly good with the average water content of 7.1 % determined at test site SB1.

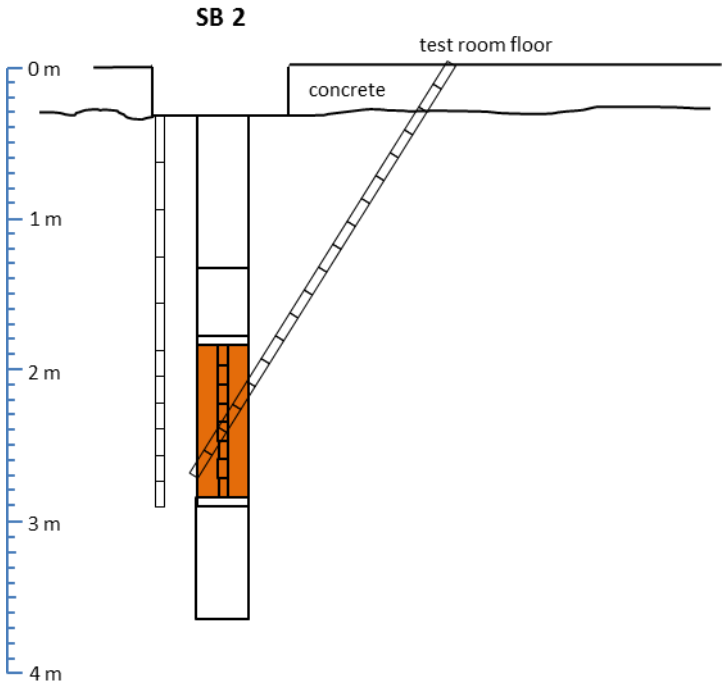

Fig. 5.33 Overview of core boreholes and sample locations at test site SB2

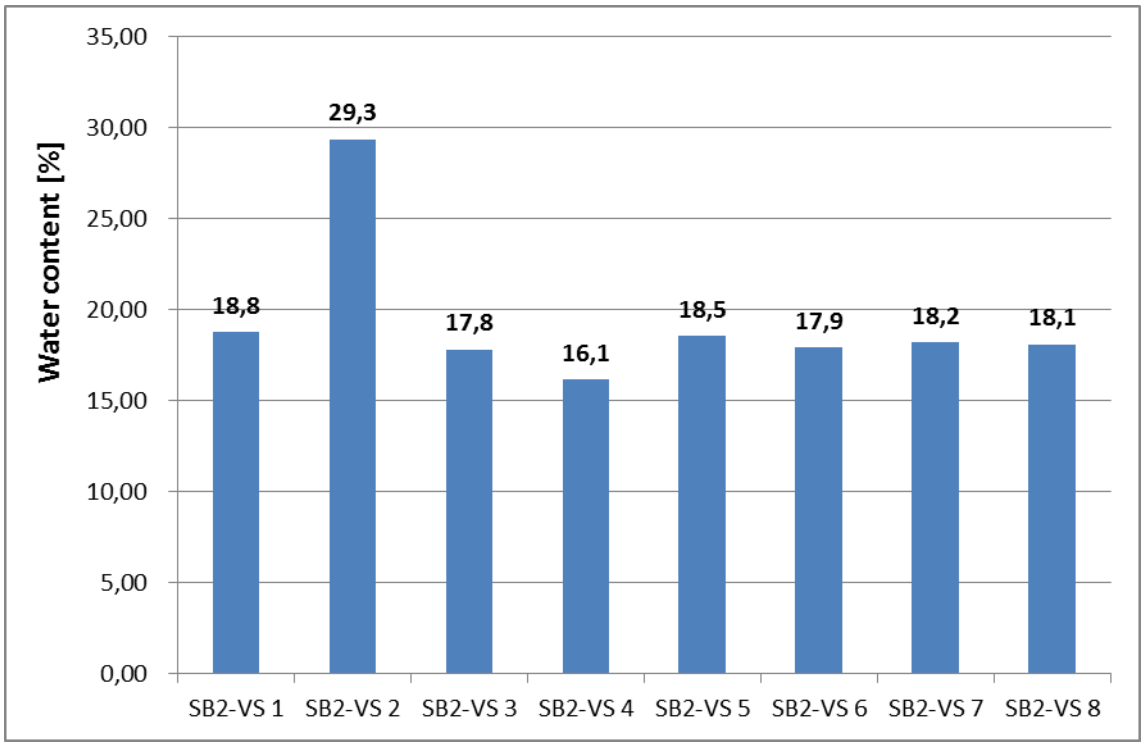

Fig. 5.34 Water content of samples taken from central seal at test SB2 (left: deepest sample, right: uppermost sample)

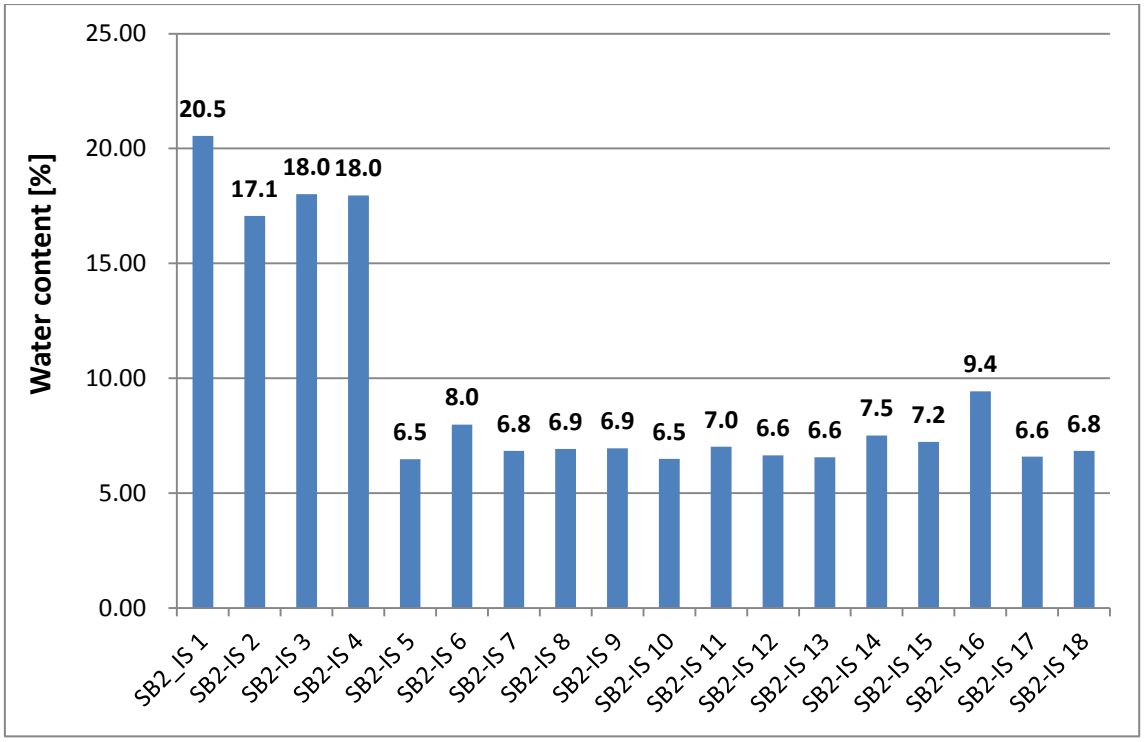

Fig. 5.35 Water content of samples taken from inclined core drilling at test SB2 (left: deepest sample, right: uppermost sample)

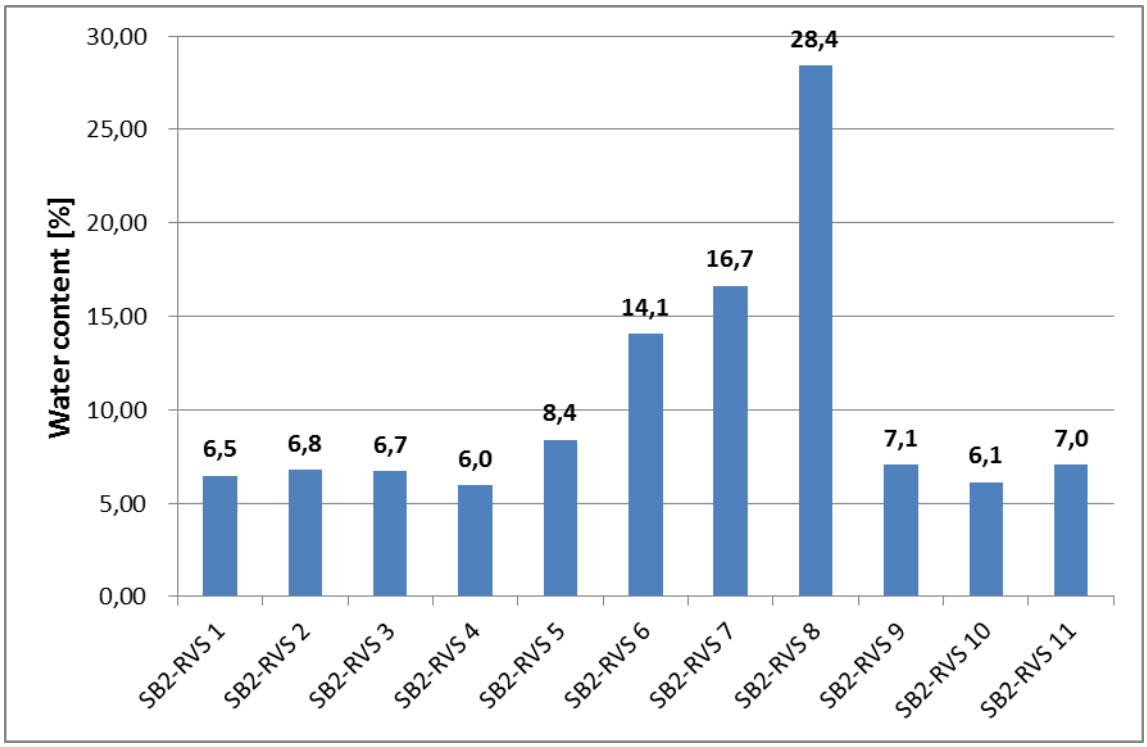

Fig. 5.36 Water content of samples taken from vertical core drilling 0.5 m from centre of test SB2 (left: deepest sample, right: uppermost sample)

The reason for the comparably high water content between 14.1 % and 28.4 % seen at three samples in the second vertical sampling borehole (Fig. 5.35) is not known. The existence of a small fracture connecting the central test borehole BSB1 with the sampling borehole is not excluded because an increasing signal at an adjacent pore-water pressure sensor in borehole BSB09 (see Fig. 5.14) was monitored when the water injection pressure at SB1 was increased in the final test stage (compare Section 5.3.3.2).

5.5 Conclusions drawn from the in-situ experiments

Neglecting the fact that the injection pressure was kept for a considerable period of time at a level being too low for achieving the envisaged water outflow at the top of the SB seals installed in situ, the SB experiment at the MTRL could finally be successfully terminated by applying an improved test procedure in the late testing phase.

The fact that the saturation time needed in the mock-up test exceeded the predicted time by a factor higher than 5 was misleading the in-situ investigators for a considerable period of time. Only when this time period was significantly exceeded in the in-situ experiment a re-examination of the test situation and revised numerical simulations under consideration of actual in-situ measurement data in the late testing stage were done and revealed the improved approach for the successful termination of the SB in-situ experiment.

Especially the results of in-situ test SB1 confirmed the results of the successful and representative mock-up Test 2 and also those results obtained by the early laboratory investigations of the KENTON-project /MIE 03/ on small laboratory-sized samples.

In conclusion it could be shown with the in-situ experiments that the advantageous seal properties of sand/bentonite mixtures can be realised and maintained under in-situ conditions prevailing in a clay repository. By this, the objectives of the SB-project can be considered completely and excellently achieved.

6 Summary and conclusions

The SB project represented a continuation of investigations on the suitability of sand/bentonite mixtures /JOC 00/ /MIE 03/ as optimized sealing material for nuclear repositories containing gas generating radioactive wastes.

As found in the afore-cited projects sand/bentonite mixtures exhibit a high permeability to gas in the unsaturated state, allowing the gases to migrate out of the repository. Even after water uptake from the host rock and compaction due to rock creep, these materials exhibit a comparably low gas entry pressure and thus, high gas pressures will not build-up in the repository, neither in the unsaturated nor in the saturated state.

To test and demonstrate that the advantageous sealing properties of sand/bentonite mixtures can technically be realized and maintained in situ under repository relevant conditions the GRS started the SB-project in January 2003 under consideration of three major project phases: (1) preceding laboratory investigations for selection of suited material mixtures and development of installation/emplacement techniques; (2) large-scale laboratory mock-up testing for the development of suited material installation techniques and determination of time needed to reach full seal saturation; (3) in-situ testing in boreholes under representative in-situ conditions in the Mont Terri Rock Laboratory (MTRL).

The preceding laboratory investigations for the determination of the petrophysical material parameters have been performed on material mixtures containing 35 %, 50 % and 70 % bentonite. The latter one was found unsuitable and the two other-ones were selected for further in-situ testing.

The mock-up test performed in GRS' geoscientific laboratory revealed excellent test results which confirmed the results of the preceding laboratory investigations determined on small-sized material specimens (see Tab. 2.9). A surprising matter was the fact that the time period needed to reach saturation was underestimated by the pre-test modelling (Section 3.5) by a factor of about 5. Instead after 5.5 months saturation was only reached after 29 months.

Two of the three in-situ experiments (one with a 65/35 sand/bentonite mixture and one with a 50/50 sand/bentonite mixture) failed because of a bypassing of the injected water through brittle borehole wall zones. The borehole with pure bentonite pellets which was performed for comparison showed an impressive evolution of the swelling

pressure up to the measuring limits of 3 MPa, but did not reach saturation within the testing period and did also not show any gas entry under the prevailing swelling pressure conditions.

Test SB2 on the contrary showed after the application of an improved testing procedure (see Section 5.3.3) test results of similar excellence as the mock-up test. The main results are given in the Tab. 6.1 in comparison to the results obtained in the preceding laboratory investigations and in the mock-up Test 2.

Tab. 6.1 Overview of laboratory and in-situ test results

Test parameter	**Design values (see Tab. 2.9)**	**Result of laboratory tests**	**Result of SB2 test**
Installation density	1.93 g/cm^3 (see Tab. 2.4)	1.87 – 1.93 g/cm^3	1.91 g/cm^3
Gas permeability under dry conditions	high (> 10^{-15} m^2)	$1.2 \cdot 10^{-13}$ m^2	$3.29 \cdot 10^{-14}$ m^2
Water permeability at full saturation	10^{-18} – 10^{-17} m^2	$5.2 \cdot 10^{-18}$ m^2	$4.2 \cdot 10^{-18}$ m^2
Swelling pressure	< 2 MPa	0.2 – 0.4 MPa	0.15 – 0.19 MPa
Gas entry pressure	< 2 MPa	0.4 – 1.1 MPa	0.45 MPa
Gas permeability after gas break-through	high (> 10^{-18} m^2)	$1.4 \cdot 10^{-17}$ m^2	$9.3 \cdot 10^{-17}$ – $4.1 \cdot 10^{-16}$ m^2

The data given in Tab. 6.1 show that the overall objective of the SB-project "to test and demonstrate that the sealing properties of sand/bentonite mixtures determined in the laboratory can technically be realized and maintained in situ under repository relevant conditions" can be considered as being successfully achieved.

Anyway, there are items to be considered in pursuing R&D activities as follows.

- Discrepancy between saturation time predicted and observed in the mock-up and in-situ experiments.

  Two reasons may be responsible for this: Either the models implemented in the codes used to design and predict the individual tests are not sufficiently representing the physics of the water uptake or the level of uncertainty of the parameter values used in the scoping calculations still needs to be reduced.

- Because of the settling behaviour of granular materials the applicability of sand/bentonite mixtures as sealing materials in horizontal repository drifts needs to be confirmed by additional testing.

- So far, the suitability of sand/bentonite mixtures has been investigated at environmental temperature only. The suitability as sealing material under elevated temperature in disposal cells containing high-level radioactive waste is to be investigated.

And finally there are lessons learnt as follows:

- Model calibration on basis of mock-up test data only was obviously not sufficiently explaining the discrepancy concerning the saturation time of sand/bentonite mixtures.

  Only the consideration of additional information from the in-situ test field such as measuring data of the pore water pressure distribution in the surroundings of the SB-test area enabled representative re-calculation of important data such as adequate water injection pressure to achieve successful termination of the SB experiment.

Acknowledgement

The authors would like to thank the German Federal Ministry of Economics and Technology (BMWi) as well as the European Commission (EC) for the support given to the SB project under contract numbers 02E9894 and FI6W-CT-2003-508851.

Many thanks also to the NAGRA (Nationale Genossenschaft für die Lagerung radioaktiver Abfälle) and especially to Dres. Peter Blümling and Hanspeter Weber for their continuous support and for providing additional funds for the test SB13.

We also would like to thank the Mont Terri Project Management Team for the continuous and most welcomed assistance throughout the entire duration of the SB experiment.

References

/ALO 02/ Alonso, E.E.; Olivella, S.; Delahaye, C. (2002): Gas Migration in Clays. Environmental Geomechanics – Monte Verita 2002, 83-94.

/BOC 08/ Bock, H. (2008): RA Experiment – Updated Review of the Opalinus Clay at the Mont Terri URL based on Laboratory and Field testing. 2008, TR 2008-04.

/BOS 02/ Bossart, P., Meier, P., Moeri, A., Trick, T., Mayor, J.-C. (2002): Geological and hydraulic characterization of the excavation disturbed zone in the Opalinus Clay of the Mont Terri Rock Laboratory, Engineering Geology 66, pp 19 – 38, Elsevier Science B.V.

/DEB 09/ de Bock, Chris, Bosgiraud, J.-M., Breen, B., Johnson, M., Rothfuchs, T., Weber, H., Van Marcke, P., Verstricht, J. (2009): Engineering Studies and Demonstration of Repository Designs (ESDRED Project), European Commission, Contract Number: FI6W-CT-2004-508851, Deliverable 6 Module 1, Work Package 6, Module 1 Final Report.

/HAR 91/ Hartge, K. H., Horn, R. (1991): Einführung in die Bodenphysik. Ferdinant Enke Verlag, Stuttgart, S. 83-84.

/JOC 00/ Jockwer, N., Miehe, R., Müller-Lyda, I. (2000): Untersuchungen zum Zweiphasenfluss und diffusiven Transport in Tonbarrieren und Tongesteinen, Abschlussbericht, FZK-02 E 90170, Gesellschaft für Anlagen- und Reaktorsicherheit (GRS) mbH, Köln, GRS-167.

/MAR 03/ Martin, C.D., Lanyon, G.W., Blümling, P. (2003): Measurement of in-situ stress in weak rocks at Mont Terri Rock Lab. International Journal of Rock Mechanics and Mining Sciences, 40, p.1077 – 1088.

/MAZ 08/ Mazurek, M., Gautschi, A., Marschall, P., Vigneron, G., Lebon, P., Delay,J. (2008): Transferability of geoscientific information from various sources (study sites, underground rock laboratories, natural analogues) to support safety cases for radioactive waste repositories in argillaceous formations. Physics and Chemistry of the Earth, Vol. 33, 95-105.

/MIE 03/ Miehe, R., Kröhn, P., Moog, H. (2003): Hydraulische Kennwerte tonhaltiger Mineralgemische zum Verschluss von Untertagedeponien (KENTON), Gesellschaft für Anlagen- und Reaktorsicherheit (GRS) mbH, Köln, GRS-193.

/MIE 07/ Miehe, R. (2007): Bestimmung der Trockeneinbaudichten in den Bohrlöchern BSB1, BSB2, BSB13, BSB15, SB-Experiment im Mt. Terri Untertagelabor – Prüfbericht, Gesellschaft für Anlagen- und Reaktor-sicherheit (GRS) mbH, Braunschweig.

/MIE 10/ Miehe, R., Czaikowski, O., Wieczorek, K. (2010): BET – Barrier Integrity of the Isolating Rock Zone in Clay Formations, Final Report, Gesellschaft für Anlagen- und Reaktorsicherheit (GRS) mbH, Köln, GRS-261.

/NAG 02/ NAGRA Technical Report 02-06 (2002): Project Opalinus Clay, Models, Codes and Data for safety Assessment – Demonstration of disposal feasability for spent fuel, vitrified high-level waste and long-lived intermediate-level waste (Entsorgungsnachweis), NAGRA National Cooperative for the Disposal of Radioactive Waste.

/OLI 96/ Olivella, S., Gens, A., Carrera, J., Alonso, E. E. (1996): "Numerical formulation for a simulator (Code_Bright) for the coupled analysis of saline media, Engineering Computations, Vol. 13 No. 7, pp. 87 – 112, MCB University Press.

/PEL 99/ Pellegrini, R.; Horseman, S.; Kemp, S.; Rochelle, C.; Boisson, J.-Y.; Lombardi, S.; Bouchet, A.; Parneix, J.-C. (1999): Natural analogues of the thermo-hydro-chemical and thermo-hydro-mechanical response. Final report, EUR19114EN.

/ROD 99/ Rodwell, W.R.; Harris, A.W.; Horseman, S.T.; Lalieux, P.; Müller, W.; Ortiz amaya, L.; Pruess, K. (1999): Gas Migration and Two-Phase Flow through Engineered and Geological Barriers for a Deep Repository for Radioactive Waste. A Joint EC/NEA Status Report, European Commission, EUR19122EN.

/ROT 04/ Rothfuchs, T., Jockwer, N., Miehe, R., Zhang, C.-l. (2004): Self-sealing Barriers of Clay/Mineral Mixtures in a Clay Repository SB Experiment in the Mont Terri Rock Laboratory Final Report of the Pre-Project, Gesellschaft für Anlagen- und Reaktorsicherheit (GRS) mbH, Köln, GRS-212.

/RÜB 04/ Rübel, A., Nosek, U., Müller-Lyda, I., Kröhn, P., Storck, R. (2004): Konzeptioneller Umgang mit Gasen im Endlager, Gesellschaft für Anlagen- und Reaktorsicherheit (GRS) mbH, Köln, GRS-205.

/SEI 09/ Seidler, Wolf (2009): Engineering Studies and Demonstration of Repository Designs (ESDRED Project), European Commission, Contract Number: FI6W-CT-2004-508851, Deliverable D6 of Module 6, WP 4, Final Summary Report and Global Evaluation of the Project.

/SÜD 01/ Süd-Chemie AG (2001): Product information of Calcigel. – Ostenriederstr. 15, D-85368 Moosburg.

/THU 99/ Thury, M., Bossart, P. (1999): Mont Terri Rock Laboratory – Results of the Hydrogeological, Geochemical and Geotechnical Experiments Performed in 1996 and 1997, Landeshydrologie und –geologie, Geologische Berichte Nr. 23.

/UPC 02/ UPC (2002): CODE_BRIGHT, A 3-D program for thermo-hydro-mechanical analysis in geological media, User's Guide.

/VIE 06/ Vietor, T., Blümling, P., Armand, G. (2006): Failure mechanisms of the Opalinus Clay around underground excavations. EUROCK 2006 ISRM regional symposium on multiphysics coupling and long-term behaviour in rock mechanics, May 2006, Liège, Belgium.

/SCH 97/ Schlumberger (1997): Weltest 200 Technical Description, Schlumberger-Geoquest, Logined BV.

/ZHA 04/ Zhang, C.-L., Rothfuchs, T., Moog, H., Dittrich, J., Müller, J. (2004): Experiments and Modelling of Thermo-Hydro-Mechanical and Geochemical Behaviour of the Callovo-Oxfordian Argillite and the Opalinus Clay, Gesellschaft für Anlagen- und Reaktorsicherheit (GRS) mbH, Köln, GRS-202.

List of figures

List of tables

Gesellschaft für Anlagen- und Reaktorsicherheit (GRS) mbH

Schwertnergasse 1
50667 Köln
Telefon +49 221 2068-0
Telefax +49 221 2068-888

Forschungszentrum
85748 Garching b. München
Telefon +49 89 32004-0
Telefax +49 89 32004-300

Kurfürstendamm 200
10719 Berlin
Telefon +49 30 88589-0
Telefax +49 30 88589-111

Theodor-Heuss-Straße 4
38122 Braunschweig
Telefon +49 531 8012-0
Telefax +49 531 8012-200

www.grs.de

ISBN 978-3-939355-81-6